

Aims and Scope: The "Cell Journal (Yakhteh)" is a peer review and monthly English publication of Royan Institute of Iran. The aim of the journal is to disseminate information through publishing the most recent scientific research studies on exclusively Cellular, Molecular and other related topics. **Cell J**, has been certified by the Ministry of Culture and Islamic Guidance since 1999 and also accredited as a scientific and research journal by HBI (Health and Biomedical Information) Journal Accreditation Commission since 2000 which is an open access journal. **This journal holds the membership of the Committee on Publication Ethics (COPE).**

1. Types of articles

The articles in the field of Cellular and Molecular can be considered for publications in **Cell J**. These articles are as below:

A. Original articles

Original articles are scientific reports of the original research studies. The article consists of English Abstract (structured), Introduction, Materials and Methods, Results, Discussion, Conclusion, Acknowledgements, Author's Contributions, and References (**Up to 40**).

B. Review articles

Review articles are the articles written by well experienced authors and those who have excellence in the related fields. The corresponding author of the review article must be one of the authors of at least three published articles appearing in the references. The review article consists of English Abstract (unstructured), Introduction, Conclusion, Author's Contributions, and References (**Up to 70**).

C. Systematic Reviews

Systematic reviews are a type of literature review that collect and critically analyzes multiple research studies or papers. The Systematic reviews consist of English Abstract (unstructured), Introduction, Materials and Methods, Results, Discussion, Conclusion, Acknowledgements, Author's Contributions, and References (**Up to 70**).

D. Short communications

Short communications are articles containing new findings. Submissions should be brief reports of ongoing researches. The short communication consists of English Abstract (unstructured), the body of the manuscript (should not hold heading or sub-heading), Acknowledgements, Author's Contributions, and References (**Up to 30**).

E. Case reports

Case reports are short discussions of a case or case series with unique features not previously described which make an important teaching point or scientific observation. They may describe novel techniques or use equipment, or new information on diseases of importance. It consists of English Abstracts (Unstructured), Introduction, Case Report, Discussion, Acknowledgements, Author's Contributions, and References (**Up to 30**).

F. Editorial

Editorials are articles should be written in relevant and new data of journals' filed by either the editor in chief or the editorial board.

G. Imaging in biology

Images in biology should focus on a single case with an interesting illustration such as a photograph, histological specimen or investigation. Color images are welcomed. The text should be brief and informative.

H. Letter to the editors

Letter to the editors are in response to previously published **Cell J** articles, and may also include interesting cases that do not meet the requirement of being truly exceptional, as well as other brief technical or clinical notes of general interest.

I. Debate

Debates are articles which show a discussion of the positive and negative view of the author concerning all aspect of the issue relevant to scientific research.

2. Submission process

It is recommended to see the guidelines for reporting different kinds of manuscripts. This guide explains how to prepare the

manuscript for submission. Before submitting, we suggest authors to familiarize themselves with **Cell J** format and content by reading the journal via the website (www.celljournal.com). The corresponding author ensures that all authors are included in the author list and agree with its order, and they must be aware of the manuscript submission.

A. Author contributions statements

It is essential for authors to include a statement of responsibility in the manuscript that specifies the contribution of every one of them. This participation must include conception and design of the manuscript, data acquisition or data analysis and interpretation, drafting of the manuscript and/or revising it for critically important intellectual content, revision and final approval of the manuscript and statistical analysis, obtaining funding, administrative, technical, or material support, or supervision. Authors who do not meet the above criteria should be acknowledged in the **Acknowledgments section**.

B. Cover letter and copyright

Each manuscript should be accompanied by a cover letter, signed by all authors specifying the following statement: "The manuscript has been seen and approved by all authors and is not under active consideration for publication. It has neither been accepted for publication nor published in another journal fully or partially (except in abstract form). **Also, no manuscript would be accepted in case it has been pre-printed or submitted to other websites.** I hereby assign the copyright of the enclosed manuscript to **Cell J**." Corresponding author must confirm the proof of the manuscript before online publishing. Also, it is needed to suggest three peer reviewers in the field of their manuscript.

C. Manuscript preparation

Authors whose first language is not English encouraged to consult a native English speaker in order to confirm his manuscripts to American or British (not a mixture) English usage and grammar. It is necessary to mention that we will check the plagiarism of your manuscript by iThenticate Software. The manuscript should be prepared in accordance with the "International Committee of Medical Journal Editors (ICMJE)". Please send your manuscript in two formats word and PDF (including: title, name of all the authors with their degree, abstract, full text, references, tables and figures) and also send tables and figures separately in the site. The abstract and text pages should have consecutive line numbers in the left margin beginning with the title page and continuing through the last page of the written text. Each abbreviation must be defined in the abstract and text when they are mentioned for the first time. Avoid using abbreviation in the title. Please use the international and standard abbreviations and symbols

It should be added that an essential step toward the integration and linking of scientific information reported in published literature is using standardized nomenclature in all fields of science and medicine. Species names must be italicized (*e.g.*, *Homo sapiens*) and also the full genus and species written out in full, both in the title of the manuscript and at the first mention of an organism in a paper.

It is necessary to mention that genes, mutations, genotypes, and alleles must be indicated in italics. Please use the recommended name by consulting the appropriate genetic nomenclature database, *e.g.*, HUGO for human genes. In another words; if it is a human gene, you must write all the letters in capital and italic (*e.g.*, *OCT4*, *c-MYC*). If not, only write the first letter in capital and italic (*e.g.*, *Oct4*, *c-Myc*). **In addition, protein designations are the same as the gene symbol but are not italicized.**

Of note, Cell J will only consider publishing genetic association study papers that are novel and statistically robust. Authors are advised to adhere to the recommendations outlined in the STREGA statement (<http://www.strega-statement.org>). The following criteria must be met for all submissions:

1. Hardy-Weinberg Equilibrium (HWE) calculations must be carried out and reported along with the P-values if applicable [see Namipashaki et al. 2015 (Cell J, Vol 17, N 2, Pages: 187-192) for a discussion].
2. Linkage disequilibrium (LD) structure between SNPs (if multiple SNPs are reported) must be presented.
3. Appropriate multiple testing correction (if multiple independent SNPs are reported) must be included.

Submissions that fail to meet the above criteria will be rejected before being sent out for review.

Each of the following manuscript components should begin in the following sequence:

Authors' names and order of them must be carefully considered (full name(s), highest awarded academic degree(s), email(s), and institutional affiliation(s) of all the authors in English. Also, you must send mobile number and full postal address of the corresponding author).

Changes to Authorship such as addition, deletion or rearrangement of author names must be made only before the manuscript has been accepted in the case of approving by the journal editor. In this case, the corresponding author must explain the reason of changing and confirm them (which has been signed by all authors of the manuscript). If the manuscript has already been published in an online issue, an erratum is needed.

Title is providing the full title of the research (do not use abbreviations in title).

Running title is providing a maximum of 7 words (no more than 50 characters).

Abstract must include Objective, Materials and Methods, Results, and Conclusion (no more than 300 words).

Keywords, three to five, must be supplied by the authors at the foot of the abstract chosen from the Medical Subject Heading (MeSH). Therefore; they must be specific and relevant to the paper.

The following components should be identified after the abstract:

Introduction: The Introduction should provide a brief background to the subject of the paper, explain the importance of the study, and state a precise study question or purpose.

Materials and Methods: It includes the exact methods or observations of experiments. If an apparatus is used, its manufacturer's name and address should be stipulated in parenthesis. If the method is established, give reference but if the method is new, give enough information so that another author can perform it. If a drug is used, its generic name, dose, and route of administration must be given. Standard units of measurements and chemical symbols of elements do not need to be defined.

Statistical analysis: Type of study and statistical methods should be mentioned and specified by any general computer program used.

Ethical considerations: Please state that informed consent was obtained from all human adult participants and from the parents or legal guardians of minors and include the name of the appropriate institutional review board that approved the project. It is necessary to indicate in the text that the maintenance and care of experimental animals complies with National Institutes of Health guidelines for the humane use of laboratory animals, or those of your Institute or agency.

Clinical trial registration: All of the Clinical Trials performing in Iran must be registered in Iranian Registry of Clinical Trials (www.irct.ir). The clinical trials performed abroad, could be considered for publication if they register in a registration site approved by WHO or www.clinicaltrials.gov. If you are reporting phase II or phase III randomized controlled trials, you must refer to the CONSORT Statement for recommendations to facilitate the complete and transparent reporting of trial findings. Reports that do not conform to the CONSORT guidelines may need to be revised before peer-reviewing.

Results: They must be presented in the form of text, tables, and figures. Take care that the text does not repeat data that are presented in tables and/or figures. Only emphasize and summarize the essential features of the main results. Tables and figures must be numbered consecutively as appeared in the text and should be organized in separate pages at the end of the manuscript while their location should be mentioned in the main text.

Tables and figures: If the result of your manuscript is too short, it is better to use the text instead of tables & figures. Tables should have a short descriptive heading above them and also any footnotes. Figure's caption should contain a brief title for the whole figure and continue with a short explanation of each part and also the symbols used (no more than 100 words). All figures must be prepared based on cell journal's guideline in color (no more than 6 Figures and Tables) and also in GIF or JPEG format.

Of Note: Please put the tables & figures of the result in the results section not any other section of the manuscript.

Supplementary materials would be published on the online version of the journal. This material is important to the understanding and interpretation of the report and should not repeat material within the print article. The amount of supplementary material should be limited. Supplementary material should be original and not previously published and will undergo editorial and peer review with the main manuscript. Also, they must be cited in the manuscript text in parentheses, in a similar way as when citing a figure or a table. Provide a caption for each supplementary material submitted.

Discussion: It should emphasize the present findings and the variations or similarities with other researches done by other researchers. The detailed results should not be repeated in the discussion again. It must emphasize the new and important aspects of the study.

Conclusion: It emphasizes the new and important aspects of the study. All conclusions are justified by the results of the study.

Acknowledgements: This part includes a statement thanking those who contributed substantially with work relevant to the study but does not have authorship criteria. It includes those who provided technical help, writing assistance and name of departments that provided only general support. You must mention financial support in the study. Otherwise; write this sentence "There is no financial support in this study".

Conflict of interest: Any conflict of interest (financial or otherwise) and sources of financial support must be listed in the Acknowledgements. It includes providers of supplies and services from a commercial organization. Any commercial affiliation must be disclosed, regardless of providing the funding or not.

References: The references must be written based on the Vancouver style. Thus the references are cited numerically in the text and listed in the bibliography by the order of their appearance. The titles of journals must be abbreviated according to the style

used in the list of Journals Indexed in PubMed. Write surname and initials of all authors when there are six or less. In the case of seven or more authors, the names of the first six authors followed by "et al." must be listed. You can download Endnote file for Journal references style: endnote file

The reference of information must be based on the following order:

Article:

Surname(s) and first letter of name & middle name(s) of author(s) .Manuscript title. Journal title (abbr).publication date (year); Volume & Issue: Page number.

Example: Manicardi GC, Bianchi PG, Pantano S, Azzoni P, Bizzaro D, Bianchi U, et al. Presence of endogenous nicks in DNA of ejaculated human spermatozoa and its relationship to chromomycin A3 accessibility. Biol Reprod. 1995; 52(4): 864-867.

Book:

Surname(s) and first letter of name & middle name(s) of author(s).Book title. Edition. Publication place: publisher name; publication date (year); Page number.

Example: Edelman CL, Mandle CL. Health promotion throughout the lifespan. 2nd ed. ST Louis: Mosby; 1998; 145-163.

Chapter of book:

Surname(s) and first letter of name & middle name(s) of author(s).Chapter title. In: Surname(s) and first letter of name & middle name(s) of editor(s), editors. Book title. Edition. Publication place: publisher name; publication date (year); Page number.

Example: Phillips SJ, Whisnant JP. Hypertension and stroke. In: Laragh JH, Brenner BM, editors. Hypertension: pathophysiology, diagnosis, and management. 2nd ed. New York: Raven Press; 1995; 465-478.

Abstract book:

Example: Amini rad O.The antioxidant effect of pomegranate juice on sperm parameters and fertility potential in mice. Cell J. 2008;10 Suppl 1:38.

Thesis:

Name of author. Thesis title. Degree. City name. University. Publication date (year).

Example: Eftekhari Yazdi P. Comparison of fragment removal and co-culture with Vero cell monolayers on development of human fragmented embryos. Presented for the Ph.D., Tehran. Tarbiyat Modarres University. 2004.

Internet references

Article:

Example: Jahanshahi A, Mirnajafi-Zadeh J, Javan M, Mohammad-Zadeh M, Rohani M. Effect of low-frequency stimulation on adenosineA1 and A2A receptors gene expression in dentate gyrus of perforant path kindled rats. Cell J. 2008; 10 (2): 87-92. Available from: <http://www.celljournal.org>. (20 Oct 2008).

Book:

Example: Anderson SC, Poulsen KB. Anderson's electronic atlas of hematology.[CD-ROM]. Philadelphia: Lippincott Williams & Wilkins; 2002.

D. Proofs are sent by email as PDF files and should be checked and returned within 72 hours of receipt. It is the authors' responsibility to check that all the text and data as contained in the page proofs are correct and suitable for publication. **We are requested to pay particular attention to author's names and affiliations as it is essential that these details be accurate when the article is published.**

E. Pay for publication: Publishing an article in **Cell J** requires Article Processing Charges (APC) that will be billed to the submitting author following the acceptance of an article for publication. For more information please see www.celljournal.org.

F. Ethics of scientific publication: Manuscripts that have been published elsewhere with the same intellectual material will refer to duplicate publication. If authors have used their own previously published work or work that is currently under review, as the basis for a submitted manuscript, they are required to cite the previous work and indicate how their submitted manuscript offers novel contributions beyond those of the previous work. Research and publication misconduct is considered a serious breach of ethics.

The Journal systematically employs iThenticate, plagiarism detection and prevention software designed to ensure the originality of written work before publication. Plagiarism of text from a previously published manuscript by the same or

another author is a serious publication offence. Some parts of text may be used, only where the source of the quoted material is clearly acknowledged.

3. General information

A. You can send your manuscript via online submission system which is available on our website. If the manuscript is not prepared according to the format of **Cell J**, it will be returned to authors.

B. The order of article appearance in the Journal is not demonstrating the scientific characters of the authors.

C. **Cell J** has authority to accept or reject the manuscript.

D. The received manuscript will be evaluated by associate editor. **Cell J** uses a single-blind peer review system and if the manuscript suits the journal criteria, we select the reviewers. If three reviewers pass their judgments on the manuscript, it will be presented to the editorial board of **Cell J**. If the editorial board has a positive judgment about the manuscript, reviewers' comments will be presented to the corresponding author (the identification of the reviewers will not be revealed). The executive member of journal will contact the corresponding author directly within 3-4 weeks by email. If authors do not receive any reply from journal office after the specified time, they can contact journal office. Finally, executive manager will respond promptly to authors' request.

The Final Checklist

The authors must ensure that before submitting the manuscript for publication, they have to consider the following parts:

1. The first page of manuscript should contain title, name of the author/coauthors, their academic qualifications, designation & institutions they are affiliated with, mailing address for future correspondence, email address, phone, and fax number.
2. Text of manuscript and References prepared as stated in the "guide for authors" section.
3. Tables should be on a separate page. Figures must be sent in color and also in JPEG (Jpg) format.
4. Cover Letter should be uploaded with the signature of all authors.
5. An ethical committee letter should be inserted at the end of the cover letter.

The Editor-in-Chief: Ahmad Hosseini, Ph.D.

Cell Journal (Yakhteh)

P.O. Box: 16635-148, Iran

Tel/Fax: + 98-21-22510895

Emails: Celljournal@royaninstitute.org

info@celljournal.org





IN THE NAME OF GOD

Gone But not Forgotten

In the memory of the late Director of Royan Institute,
Founder of Stem Cells Research in Iran and Chairman of
Cell Journal (Yakhteh). May he rest in peace.

Dr. Saeed Kazemi Ashtiani

OWNED:

Royan Institute, Iranian Academic Center for Education Culture and Research (ACECR)

CHAIRMAN:

Hamid Gourabi, Ph.D., (Professor, Royan Institute, Tehran, Iran)

EDITOR IN CHIEF:

Ahmad Hosseini, Ph.D., (Professor, Shahid Beheshti Medical University, Tehran, Iran)

EDITOR ASSOCIATE:

Saeid Abroun, Ph.D., (Professor, Tarbiat Modares University, Tehran, Iran)

EDITORIAL BOARD:

Saeid Abroun, Ph.D., (Professor, Tarbiat Modares University, Tehran, Iran)

Kamran Alimoghadam, M.D., (Associate Professor, Tehran Medical University, Tehran, Iran)

Alireza Asgari, Ph.D., (Professor, Baghyatallah University, Tehran, Iran)

Mohammad Kazem Aghaee Mazaheri, D.D.S., (Assistant Professor, ACECR, Tehran, Iran)

Gila Behzadi, Ph.D., (Professor, Shahid Beheshti Medical University, Tehran, Iran)

Hossein Baharvand, Ph.D., (Professor, Royan Institute, Tehran, Iran)

Mary Familiar, Ph.D., (Senior Lecturer, University of Melbourne, Melbourne, Australia)

Hamid Gourabi, Ph.D., (Professor, Royan Institute, Tehran, Iran)

Jurgen Hescheler, M.D., (Professor, Institute of Neurophysiology of University Zu Koln, Germany)

Ghasem Hosseini Salekdeh, Ph.D., (Assistant Professor, Agricultural Biotechnology Research Institute, Karaj, Iran)

Esmail Jabbari, Ph.D., (Associate Professor, University of South Carolina, Columbia, USA)

Suresh Jesuthasan, Ph.D., (Associate Professor, National University of Singapore, Singapore)

Bahram Kazemi, Ph.D., (Professor, Shahid Beheshti Medical University, Tehran, Iran)

Saadi Khochbin, Ph.D., (Professor, Inserm/Grenoble University, France)

Ali Khademhosseini, Ph.D., (Associate Professor, Harvard Medical School, USA)

Kun Ping Lu, M.D., Ph.D., (Professor, Harvard Medical School, Boston, USA)

Navid Manuchehrabadi, Ph.D., (Angio Dynamics, Marlborough, USA)

Hosseinali Mehrani, Ph.D., (Professor, Baghyatallah University, Tehran, Iran)

Marcos Meseguer, Ph.D., (Clinical Embryology Laboratory IVI Valencia, Valencia, Spain)

Seyed Javad Mowla, Ph.D., (Professor, Tarbiat Modares University, Tehran, Iran)

Mohammad Hossein Nasr Esfahani, Ph.D., (Professor, Royan Institute, Tehran, Iran)

Toru Nakano, M.D., Ph.D., (Professor, Osaka University, Osaka, Japan)

Donald Newgreen, Ph.D., (Professor, Murdoch Children Research Institute, Melbourne, Australia)

Mojtaba Rezazadeh Valojerdi, Ph.D., (Professor, Tarbiat Modares University, Tehran, Iran)

Mohammad Hossein Sanati, Ph.D., (Associate Professor, National Institute for Genetic Engineering and Biotechnology, Tehran, Iran)

Eimei Sato, Ph.D., (Professor, Tohoku University, Sendai, Japan)

Andreas Serra, M.D., (Professor, University of Zurich, Zurich, Switzerland)

Abdolhossein Shahverdi, Ph.D., (Professor, Royan Institute, Tehran, Iran)

Michele Catherine Studer, Ph.D., (Institute of Biology Valrose, IBV University of Nice Sophia-Antipolis, France)

Peter Timashev, Ph.D., (Sechenov University, Moscow, Russia)

Daniela Toniolo, Ph.D., (Head, Unit of Common Disorders, San Raffaele Research Institute, Milano, Italy)

Christian van den Bos, Ph.D., Managing Director MARES Ltd, Greven, Germany

Catherine Verfaillie, Ph.D., (Professor, Katholie Universiteit Leuven, Leuven, Belgium)

Gianpaolo Zerbin, M.D., Ph.D., (San Raffaele Scientific Institute, Italy)

Shubing Zhang, Ph.D., (Associate Professor, Central South University, China)

Daniele Zink, Ph.D., (Institute of Bioengineering and Nanotechnology, Agency for Science Technology & Science, Singapore)

EXECUTIVE MANAGER:

Farideh Malekzadeh, M.Sc., (Royan Institute, Tehran, Iran)

EXECUTIVE BOARD:

Parvaneh Afsharian, Ph.D., (Royan Institute, Tehran, Iran)
Reza Azimi, B.Sc., (Royan Institute, Tehran, Iran)
Reza Omani-Samani, M.D., (Royan Institute, Tehran, Iran)
Elham Amirchaghmaghi, M.D., Ph.D., (Royan Institute, Tehran, Iran)
Leila Daliri, M.Sc., (Royan Institute, Tehran, Iran)
Mahdi Lotfipannah, M.Sc., (Royan Institute, Tehran, Iran)

ENGLISH EDITOR:

Mitra Amiri Khabooshan, Ph.D., (Monash University, Victoria, Australia)
Sima Binaafar, M. Sc., (Royan Institute, Tehran, Iran)
Saman Eghtesad, Ph.D., (Royan Institute, Tehran, Iran)
Jane Elizabeth Ferrie, Ph.D., (University College of London, London, UK)
Vahid Ezzatizadeh, Ph.D., (Royan Institute, Tehran, Iran)
Kiana Kakavand, Ph.D., (University of Melbourne, Melbourne, Australia)
Farnaz Shapouri, Ph.D., (Memphasys Limited, NSW, Australia)
Kim Vagharfard, M.Sc., (Royan Institute, Tehran, Iran)

GRAPHICS:

Laleh Mirza Ali Shirvani, B.Sc., (Royan Institute, Tehran, Iran)

PUBLISHED & SPONSORED BY:

Publication of Royan Institute (ACECR)

Indexed in:

1. Thomson Reuters (ISI)
2. PubMed
3. PubMed Central (PMC)
4. National Library Medicine (NLM)
5. Biosis Preview
6. Index Medicus for the Eastern Mediterranean Region (IMEMR)
7. Regional Information Center for Sciences and Technology (RICeST)
8. Index Copernicus International
9. Cambridge Scientific Abstract (CSA)
10. EMBASE
11. Scopus
12. Cinahl Database
13. Google Scholar
14. Chemical Abstract Service (CAS)
15. Proquest
16. Directory of Open Access Journals (DOAJ)
17. Open Academic Journals Index (OAJI)
18. Directory of Research Journals Indexing (DRJI)
19. Scientific Information Database (SID)
20. Iranmedex
21. Islamic World Science Citation Center (ISC)
22. Magiran
23. Science Library Index
24. Biological Abstracts
25. Essential Science Indicators
26. EuroPub

ACECR**Copyright and license information:**

The **Cell Journal** (^{Yakhteh}) is an open access journal which means the articles are freely available online for any individual author to download and use the providing address. The journal is licensed under a Creative Commons Attribution-Non Commercial 3.0 Unported License which allows the author(s) to hold the copyright without restrictions that is permitting unrestricted use, distribution, and reproduction in any medium provided the original work is properly cited.

Editorial Office Address (Dr. Ahmad Hosseini):

Royan Institute, P.O.Box: 16635-148,
Tehran, Iran
Tel & Fax: (+9821)22510895
Website: www.celljournal.org
Emails: info@celljournal.org
celljournal@royaninstitute.org

Printing Company:

Naghshe e Johar Co.
No. 103, Fajr alley, Tehranpars Street,
Tehran, Iran.



CONTENTS

Systematic Review

- **Determining The Role of MicroRNAs in Self-Renewal, Metastasis and Resistance to Drugs in Human Gastric Cancer Based on Data Mining Approaches: A Systematic Review**

Mahnaz Azimi, Mehdi Totonchi, Marzieh Ebrahimi 1

Original Articles

- **Using Deep Learning Algorithm: The Study of Sperm Head Vacuoles and Its Correlation with Protamine mRNA Ratio**

Fatemeh Ghasemian, Mohammad Hadi Bahadori, Seyede Zahra Hosseini Kolkooh, Maryam Esmacili 7

- **CircRNA-011235 Counteracts The Deleterious Effect of Irradiation Treatment on Bone Mesenchymal Stem Cells by Regulating The miR-741-3p/CDK6 Pathway**

Xianhui Wen, Hebin Xie, Rong Gui, Xinmin Nie, Dongyong Shan, Rong Huang, Hongyu Deng, Junhua Zhang 15

- **The Effect of Endometrial Cell Culture on $\alpha 3$ and $\beta 1$ integrin Genes and Protein Expression in Type 2 Diabetic Rats at The Time of Implantation**

Fatemah Sadat Mostafavi, Abbas Bakhteyari, Parvaneh Nikpour, Nahid Eskandari, Roshanak Aboutorabi 22

- **Effects of Exosomes Derived from Kidney Tubular Cells on Diabetic Nephropathy in Rats**

Fereshtesadat Fakhredini, Esrafil Mansouri, Seyyed Ali Mard, Armita Valizadeh Gorji, Mohammad Rashno, Mahmoud Orazizadeh 28

- **Fabrication and *In Vitro* Evaluation of A Chondroitin Sulphate-Polycaprolactone Composite Nanofibrous Scaffold for Potential Use in Dermal Tissue Engineering**

Mohamad Pezeshki-Modaress, Mohadeseh Akbarzadeh, Dariush Ebrahimibagha, Mojgan Zandi, Tayyeb Ghadimi, Amin Sadeghi, Sarah Rajabi 36

- **The Inhibitory Effect of Sulforaphane on The Proliferation of Acute Myeloid Leukemia Cell Lines through Controlling miR-181a**

Mohsen Koolivand, Maryam Ansari, Soheila Moein, Masoomeh Afsa, Kianoosh Malekzadeh 44

Short Communication

- **Akt1 Decreases Gcn5 Protein Stability through Regulating The Ubiquitin-Proteasome Pathway in Mouse Embryonic Fibroblasts**

Da Som Jeong, Yu Cheon Kim, Ji Hoon Oh, Myoung Hee Kim 51

- **Front page of Cell Journal (Yakhteh): Figure 1, Page: 9**

Determining The Role of MicroRNAs in Self-Renewal, Metastasis and Resistance to Drugs in Human Gastric Cancer Based on Data Mining Approaches: A Systematic Review

Mahnaz Azimi, M.Sc.¹, Mehdi Totonchi, Ph.D.², Marzieh Ebrahimi, Ph.D.^{1,3*}

1. Department of Stem Cells and Developmental Biology, Cell Science Research Center, Royan Institute for Stem Cell Biology and Technology, ACECR, Tehran, Iran
2. Department of Genetics, Reproductive Biomedical Research Centre, Royan Institute for Reproductive Biomedicine, ACECR, Tehran, Iran
3. Department of Regenerative Medicine, Cell Science Research Center, Royan Institute for Stem Cell Biology and Technology, ACECR, Tehran, Iran

*Corresponding Address: P.O.Box: 16635-148, Department of Stem Cells and Developmental Biology, Cell Science Research Center, Royan Institute for Stem Cell Biology and Technology, ACECR, Tehran, Iran
Email: m.ebrahimi@royan-rc.ac.ir

Received: 09/December/2019, Accepted: 09/May/2020

Abstract

Gastric cancer (GC) is one of the leading causes of cancer-related deaths worldwide. The major problems of patients with GC are the lack of proper response to the treatment, drug resistance and metastasis attributed to the presence of a subpopulation of cells inside the tumour that are called cancer stem cells (CSCs). In addition, deregulation of microRNAs (miRNAs) has been reported in different stages of GC. The aim of the present study is to determine and introduce miRNAs that contribute to regulation of stemness, metastasis and drug resistance in GC. A systematic review, we conducted data mining of available datasets and a review of previous studies to select miRNAs that target stemness, epithelial-mesenchymal transition (EMT) and drug resistance. All selected miRNAs were analysed by R software to find a common miRNA target for all three processes. Then, the target prediction of miRNAs and their related signalling pathways were obtained by using bioinformatics tools, ONCO.IO and KEGG databases, respectively. We identified seven miRNAs (miR-34a, miR-23a, miR-27a, miR-30a, miR-19b, miR-107, miR-100) from our searching approach. These miRNAs regulate pathways that contribute to stemness, EMT and drug resistance in GC. Four (miR-34a, miR-23a, miR-30a, and miR-100) had significant interactions with each other and 52 target genes among them, from which *MYC*, *CDK6*, *NOTCH1*, *NOTCH2*, *SIRT1*, *CD44*, *CD24*, and *AXL* were involved in the regulation of several biological processes. These data suggest that the three significant properties can be regulated by common miRNAs (hsa-miR-34a, hsa-miR-23a, hsa-miR-30a and hsa-miR-100). Hence, targeting selected miRNAs or their targets might be helpful to stop tumour growth and metastasis development, and increase tumour sensitivity to chemotherapy agents. This signature can also be assumed for early detection of metastasis or drug resistance. However, there should be additional experimentation to validate these results.

Keywords: Drug Resistance, Gastric Cancer, Metastasis, MicroRNA, Stem Cells

Cell Journal(yakhteh), Vol 24, No 1, January 2022, Pages: 1-6

Citation: Azimi M, Totonchi M, Ebrahimi M. Determining the role of microRNAs in self-renewal, metastasis and resistance to drugs in human gastric cancer based on data mining approaches: a systematic review. Cell J. 2022; 24(1): 1-6. doi: 10.22074/cellj.2022.7173.

This open-access article has been published under the terms of the Creative Commons Attribution Non-Commercial 3.0 (CC BY-NC 3.0).

Introduction

Gastric cancer (GC) ranks as the fifth most common cancer worldwide (1) and the second most common cancer among Iranian men (2). The rate of GC is estimated at 18.7% per 10,000 males and 11.1% per 10,000 females in Iran (3). The major problems of patients with GC include the lack of a proper response to treatment, drug resistance, and metastasis that leads to a rapid increase in mortality among patients. Recently, cancer stem cells (CSCs) are proposed to be a cause for tumour growth, invasion, recurrence, metastasis potential, and resistance to traditional therapies (4). Most treatments have the capability to eliminate cancer cells but cannot eradicate CSCs (5). Despite the advances in different types of gastric adenocarcinoma treatments, the survival rate of patients is not satisfactory. Although there is enhanced detection of GC, the need exists to develop novel detection kits for early detection of GC (6), detect drug

resistance in patients before or after chemotherapy and find those who are at increased risk for metastasis.

microRNAs (miRNAs) are small, non-encoding RNA molecules, 18-24 nucleotides in length. They can bind to the target region of 3'-untranslated regions (3'-UTR) and control gene expressions at the post-transcriptional level by messenger RNA (mRNA) degradation or inhibition of protein translation (7, 8). They are known as oncogenes or tumour suppressors that can target several genes simultaneously (9). miRNAs have a stable structure and more than 50% of the miRNA genes are located in genomic regions associated with cancer (10). Thus, they are considered promising tools for detection of any stage of cancer development and cancer treatment (11). Likewise, miRNAs can control metastasis development through the expressions of a large number of target genes (12), regulation of self-renewal property and resistance to

conventional treatments (13, 14).

Recently, there is a tremendous demand for analysis and interpretation of large volumes of biological data. Hence, bioinformatics studies are analysis tools that help to store, organize, and analyse high-throughput data volumes. Clinical data mining techniques have made remarkable contributions to medical and clinical sciences (15). The overall aim of the present study is to find miRNAs that target stemness, epithelial-mesenchymal transition (EMT) and drug resistance in GC and identify target genes that are effective in this regulation. Understanding the mechanism of regulation by miRNAs, which target three important regulatory pathways in GC, can help with early detection of treatment-resistant patients and those at risk for metastasis following chemotherapy.

Materials and Methods

Search strategy

In this systematic review, we initially designed a systematic review to assess the stemness-regulating miRNAs. Relevant published papers were collected through a PubMed search engine (<https://www.ncbi.nlm.nih.gov/>). Keywords such as "stem cell" or "sphere" or "side population (SP) cell" and "miRNA profile" or "microRNA profile" and "gastric cancer" were used. The duplicated papers or papers without any information about GC stem cells (GCSCs) or miRNAs were excluded.

Next, in order to obtain metastasis-regulating miRNAs, the COREMINE database (<https://www.coremine.com/>), as a text mining algorithm, was used to search keywords that included "metastasis," "gastric cancer", and "miRNA". In the third step, keywords, such as "gastric cancer", "drug resistance", and "miRNA" were chosen in the COREMINE to acquire a list of drug resistance-regulating miRNAs. Finally, R programming language (version 3.6.1) was used for the identification and analysis of drug resistance/metastasis-regulating miRNAs based on the text mining method.

microRNA target

miRNAs have a deregulated expression in various types of cancers and might influence cell signalling pathways. Putative miRNA targets are essential to discover relevant pathways and they were identified by the ONCO.IO database (<https://onco.io/>). The Enrichr database (<https://amp.pharm.mssm.edu/Enrichr/>) was used for further enrichment analysis, along with KEGG 2015 (<https://www.genome.jp/kegg/>) to obtain the top ten significant pathways regulated by the miRNA target genes. The role of each miRNA target, such as proliferation, drug resistance, apoptosis, invasion, and metastasis was identified in cellular processes regulation.

microRNA-target gene network

As described earlier, the function of miRNAs is

determined through their target genes. Hence, we created a regulatory network model to illustrate a better concept for miRNA-gene or miRNA-protein interactions through the ONCO.IO database.

The Ethical Committee of Royan Institute reviewed and approved the study (IR.ACECR.ROYAN.1396.230).

Results

In the present study, based on the Preferred Reporting Items for Systematic Reviews and Meta-Analyses (PRISMA-P) protocols, we reviewed 138 papers after searching in PubMed. In the first screening, 31 papers were excluded because of a lack of relevance in the title and abstract, and low citation rates. In the second screening, 22 papers were irrelevant to GCSCs and miRNAs (Fig.1). We did not include any meta-analyses and review papers in this study. Finally, 21 studies were chosen and assessed, which pertained to 191 miRNAs involved in regulating stemness features of GC (Table S1, See Supplementary Online Information at www.celljournal.org).

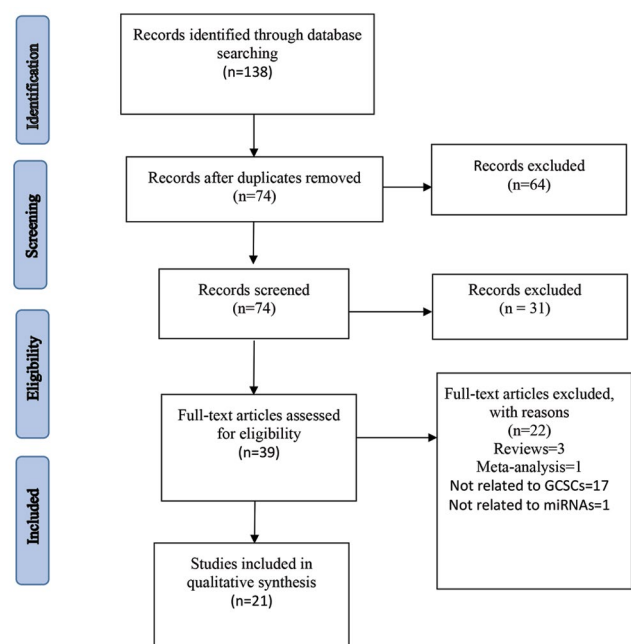


Fig.1: Search strategy flowchart of the systematic study derived from PubMed database following the Preferred Reporting Items for Systematic Reviews and Meta-Analyses (PRISMA-P). GCSC; Gastric cancer stem cell and miRNA; microRNA.

In the second and third steps, 161 and 57 miRNAs were evaluated for metastasis (Table S2, See Supplementary Online Information at www.celljournal.org) and drug resistance properties (Table S3, See Supplementary Online Information at www.celljournal.org) respectively, through the COREMINE database. We determined that there were seven common miRNAs involved in these three properties (miR-34a, miR-23a, miR-27a, miR-30a, miR-19b, miR-107, miR-100) (Fig.2).

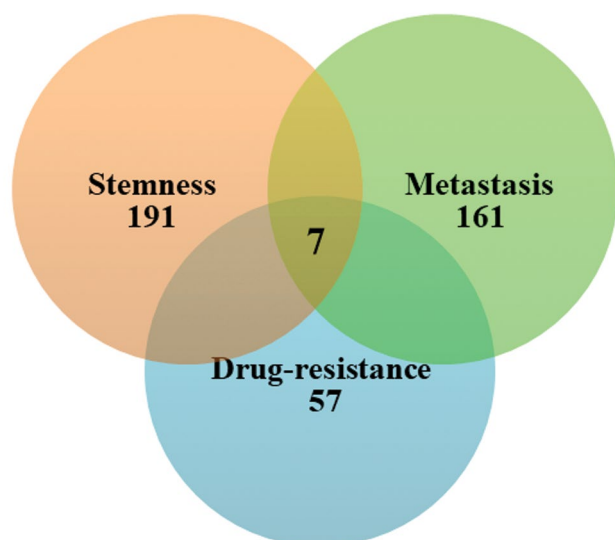


Fig.2: Venn diagram that shows the common microRNAs (miRNAs) in all three pathways.

Investigation of the regulatory network for the microRNA target genes

The ONCO.IO database was used to obtain a regulatory network of seven effective stemness-regulating miRNAs, metastasis, and drug resistance. The results indicated that miR-34a, miR-23a, miR-30a and miR-100 showed significant interactions with each other, and a network of target genes (Fig.3). These target genes have the greatest effect on

regulating biological processes of invasion, proliferation, migration, and apoptosis. Table 1 lists the effects of the miR-34a, miR-23a, miR-30a, and miR-100 targets in regulating these biological processes.

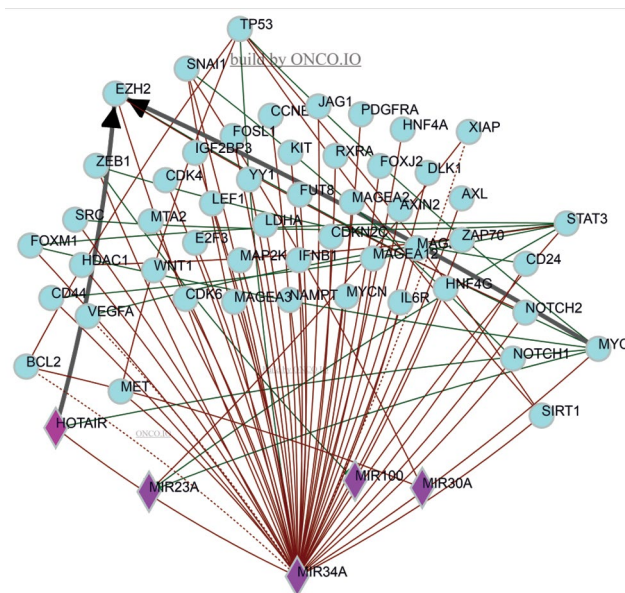


Fig.3: A network of differential expression of four microRNA (miRNA) target genes. Circle and rhombic forms represent target genes and miRNAs, respectively. The red and green arrows indicate inhibitors and activators, respectively. The thick black arrow shows the interaction between two genes.

Table 1: Performance of 52 targeted target genes of four microRNAs (miRNAs) in the regulation of important biological processes. Some of these genes interact with the regulation of several bio-processes

Process	Number	Gene
Invasion	18	<i>SNAIL, MYC, MET, NOTCH1, NOTCH2, CDK6, JAG1, CDK6, STAT3, FOSL1, DLK1, KIT, CD24, SRC, IL6R, HOTAIR, HNF4G, FUT8</i>
Proliferation	15	<i>AXL, MYC, MET, NOTCH1, NOTCH2, CDK6, MAP2K1, SIRT1, DLK1, CD44, HOTAIR, HNF4G, HDAC1, IGF2BP3, EZH2</i>
Migration	10	<i>SNAIL, MYC, MET, YY1, FOSL1, KIT, CD44, CD24, SRC, FUT8</i>
Apoptosis	10	<i>TP53, AXL, MET, CDK6, SIRT1, DLK1, HDAC1, XIAP, IGF2BP3, BCL2</i>
Chemoresistance	6	<i>AXL, SIRT1, MAGEA2, MAGEA3, MAGEA6, MAGEA12</i>
Metastasis	5	<i>YY1, CDK6, NOTCH2, NOTCH1, CD44,</i>
EMT	3	<i>STAT3, IL6R, CD24</i>
Stemness	2	<i>MYC, CD24</i>

EMT; Epithelial-mesenchymal transition.

Table 2: A list of microRNA (miRNA) targets based on relative position

Upstream genes	Downstream genes					
<i>ZEB1</i>	<i>HNF4A</i>	<i>MTA2</i>	<i>MET</i>	<i>MAP2K1</i>	<i>FOSL1</i>	<i>IFNB1</i>
<i>TP53</i>	<i>AXL</i>	<i>WNT1</i>	<i>YY1</i>	<i>AXIN2</i>	<i>MAGEA2</i>	<i>ZAP70</i>
<i>STAT3</i>	<i>MYCN</i>	<i>LDHA</i>	<i>NOTCH1</i>	<i>SIRT1</i>	<i>MAGEA3</i>	<i>DLK1</i>
<i>EZH2</i>	<i>CCNE2</i>	<i>BCL2</i>	<i>JAG1</i>	<i>CDKN2C</i>	<i>FUT8</i>	<i>KIT</i>
<i>HOTAIR</i>	<i>CDK4</i>	<i>XIAP</i>	<i>NOTCH2</i>	<i>PDGFRA</i>	<i>FOXJ2</i>	<i>CD24</i>
<i>SNAIL</i>	<i>E2F3</i>	<i>VEGFA</i>	<i>HDAC1</i>	<i>LEF1</i>	<i>MAGEA6</i>	<i>CD44</i>
	<i>HNF4G</i>	<i>MYC</i>	<i>CDK6</i>	<i>NAMPT</i>	<i>MAGEA12</i>	
	<i>RXRA</i>	<i>IL6R</i>	<i>IGF2BP3</i>	<i>FOXMI</i>	<i>SRC</i>	

Regulation of cell signalling pathways by microRNAs in cancer development

A list of target genes for *miRNAs* (*miR-34a*, *miR-23a*, *miR-30a*, *miR-100*) was obtained using the ONCO.IO database to find signalling pathways regulated by miRNAs. The results demonstrated that 52 genes are regulated by four miRNAs (Table 2). Enrichr database was used to investigate these target genes. Consequently, the KEGG database was used to analyse the functional pathways of four miRNAs. These miRNAs are significantly involved in the top ten pathways that regulate cell signalling, including pathways in cancer, miRNAs in cancer, the PI3K-Akt signalling pathway, hepatitis B, small cell lung cancer, bladder cancer, pancreatic cancer, melanoma, central carbon metabolism in cancer, and the thyroid hormone signalling pathway (Table 3). Pathways with the strongest P values were analysed and it was determined that most of these are cancer-dependent.

Table 3: Targeted signalling pathways by seven selected microRNAs (miRNAs) according to the highest P value

Rank	Signalling pathway	P value
1	Pathways in cancer	8.134e-18
2	miRNAs in cancer	2.612e-18
3	PI3K-Akt signalling pathway	4.343e-12
4	Hepatitis B	4.343e-12
5	Small cell lung cancer	2.711e-11
6	Bladder cancer	2.421e-10
7	Pancreatic cancer	6.671e-9
8	Melanoma	8.983e-9
9	Central carbon metabolism in cancer	6.671e-9
10	Thyroid hormone signalling pathway	8.983e-9

Discussion

miRNAs have a significant effect on regulation of gene expression and they have their own distinct expression patterns in various cancers. Therefore, the identification of miRNA biomarkers might provide tremendous opportunities for the sensitisation of tumour cells to targeted therapeutic agents in order to prevent cancer metastasis (10).

The results of some biological and clinical trials support miRNAs regulation in GC. However, a few systematic studies have focused on novel miRNA candidates that possess all three effective properties in GC development. In this study, miRNAs that regulate stemness, drug resistance, and metastasis features were selected by bioinformatics approaches (database sources and R programming language) and systematic literature reviews. Bioinformatics algorithms show significant potential in medical research. These tools help researchers understand

the biological processes in different disorders and predict disease-prone genes. They also can reduce a considerable amount of search space of datasets and detect the highest statistical significance datasets (15). The integration of miRNA profiles and their targets with computational analysis tools helps to investigate the role of miRNAs in the development of metastatic cancer and their potential role as agents in cancer treatment (16).

Based on the present study, six miRNAs (*miR-100*, *miR-34a*, *miR-23a*, *miR-27a*, *miR-30a*, and *miR-19b*) were obtained that contributed to regulation of stemness, metastasis and drug resistance in GC. These miRNAs can potentially be used to induce the sensitivity of GC cells to chemotherapy. Six of the seven candidate miRNAs (*miR-23a*, *miR-27a*, *miR-30a*, *miR-19b*, *miR-107* and *miR-100*) are overexpressed in GC. Interestingly, all of the predicted miRNAs were previously reported to play pivotal roles in stem cell-like phenotype and drug resistance in GC (17-20). It is proposed that these miRNAs act as an oncomiR, which might have a carcinogenic function. However, many other miRNAs have reduced expressions in various types of cancers and they act as tumour suppressors. Among this set, both *miR-34a* and *miR-100* have low expressions in GC and can inhibit invasion, metastasis and the possibility of tumour relapse (21, 22).

Four miRNAs (*miR-34a*, *miR-23a*, *miR-30a*, *miR-100*) play an important role in interacting with target genes. They regulate important cellular processes as well as signalling pathways. Among the four major miRNAs, *miR-34a* regulates a variety of target genes involved in promoting cell death by (SP-4-2)-diamminedichloroplatinum (cisplatin) with involvement of the PI3K/Akt/survivin signalling pathway (23). Excessive expression of *miR-34a* leads to enhanced sensitivity of GC cells exposed to cisplatin-based chemotherapy. Overexpression of *miR-34a* can inhibit invasion and induce apoptosis by inhibiting the *PI3K/Akt* signalling pathway in the SGC-7901 GC cell line (24, 25). *miR-34a*, by targeting the *NOTCH*, *HMG2* and *BCL2* genes, can control self-renewal and survival of CSCs in GC (17, 26).

miR-23a is located in the *miR-23a~27a~24-2* cluster and its overexpression promotes acute lymphoblastic leukaemia, acute myeloid leukaemia, and pancreatic cancer. It appears to increase significantly in GC compared to normal tissues and is recognized as an oncomiR in tumour malignancy (18). It can also regulate the sensitivity of GC cells to chemotherapy by inhibiting the *ATG12* and *HMGB2* genes, which are associated with autophagocytosis (19). Inhibition of *PTEN* gene by *miR-23a* leads to activation of Akt/ERK and EMT related pathways in GC cells; thereby it causes an induction of proliferation in GC cells and tumour growth in mouse models (27).

miR-30a can act as an oncomiR in GC by regulating the P53-mediated mitochondrial apoptotic pathway (27). It can also reduce the multidrug resistance (MDR) of GC cells and acts as an inhibitor of EMT in other cancer cells (28).

Overexpression of miR-100 can inhibit cell proliferation in GC cells by targeting BMP2 and CXCR7 (29, 30). Moreover, it can promote apoptosis by cisplatin (2 µg/ml) (29). Since both BMP2 and CXCR7 have a role in promoting invasion and tumour metastasis in cancers, miR-100 might regulate the metastasis potential in GC (29, 30).

Enrichment analysis of the miRNA target genes by Enrichr and KEGG showed that the most significant pathways were associated with cancer. The PI3K/Akt signalling pathway has a specific role in gastric adenocarcinoma treatment, as personalized medicine. The role of miRNAs in GCSCs has been shown by regulation of the PI3K/Akt pathway (31, 32).

Conclusion

Overall, the results of systematic literature reviews and data mining showed that the three important properties involved in GC could be regulated by Six miRNAs (miR-100, miR-34a, miR-23a, miR-27a, miR-30a, and miR-19b). Among them, miR-34a, miR-23a, miR-30a and miR-100 were the more relevant in regulating the three features associated with cancer development. Hence, bioinformatics analysis could be a useful approach to predict miRNAs or their targets that could halt tumour growth and metastasis development, and increase tumour sensitivity to chemotherapy agents. Our miRNA signature could be assumed for early detection of metastasis or drug resistance. However, additional studies should be conducted to validate our findings.

Acknowledgements

All authors agree with the contents of the manuscript. This project was supported by the National Institute for Medical Research Development (NIMAD, grant no. 2441). The authors declare that there is no conflict of interest.

Authors' Contributions

M.A.; Analysed the data, designed the manuscript structure, and wrote the manuscript. M.T.; Validation of data and conceived the presented idea. M.E.; Contributed to the study concept and design, and final approval of the manuscript. All authors read and approved the final manuscript.

References

- Rawla P, Barsouk A. Epidemiology of gastric cancer: global trends, risk factors and prevention. *Prz Gastroenterol.* 2019; 14(1): 26-38.
- Pakzad R, Khani Y, Pakzad I, Momenimovahed Z, Mohammadian-Hashejani A, Salehiniya H, et al. Spatial analysis of stomach cancer incidence in Iran. *Asian Pac J Cancer Prev.* 2016; 17(S3): 27-32.
- Kalan Farmanfarma K, Mahdaviifar N, Hassanipour S, Salehiniya H. Epidemiologic study of gastric cancer in Iran: a systematic review. *Clin Exp Gastroenterol.* 2020; 13: 511-542.
- Phi LTH, Sari IN, Yang YG, Lee SH, Jun N, Kim KS, et al. Cancer stem cells (CSCs) in drug resistance and their therapeutic implications in cancer treatment. *Stem Cells Int.* 2018; 2018: 5416923.
- Brown DV, Filiz G, Daniel PM, Hollande F, Dworkin S, Amiridis S, et al. Expression of CD133 and CD44 in glioblastoma stem cells correlates with cell proliferation, phenotype stability and intra-tumor heterogeneity. *PLoS One.* 2017; 12(2): e0172791.
- Takahashi T, Saikawa Y, Kitagawa Y. Gastric cancer: current status of diagnosis and treatment. *Cancers (Basel).* 2013; 5(1): 48-63.
- Fang X, Wei J, He X, An P, Wang H, Jiang L, et al. Landscape of dietary factors associated with risk of gastric cancer: a systematic review and dose-response meta-analysis of prospective cohort studies. *Eur J Cancer.* 2015; 51(18): 2820-2832.
- Gao Y, Feng B, Han S, Zhang K, Chen J, Li C, et al. The roles of microRNA-141 in human cancers: from diagnosis to treatment. *Cell Physiol Biochem.* 2016; 38(2): 427-448.
- Chen CZ. MicroRNAs as oncogenes and tumor suppressors. *N Engl J Med.* 2005; 353(17): 1768-1771.
- Holzheimer RG, Mannick JA. Surgical treatment: evidence-based and problem-oriented. Munich; Zuckschwerdt: 2001.
- Raza U, Zhang JD, Sahin O. MicroRNAs: master regulators of drug resistance, stemness, and metastasis. *J Mol Med (Berl).* 2014; 92(4): 321-336.
- Wei H, Pu K, Liu XG, Li BX, Zhang HS, Wang H, et al. The diagnostic value of circulating microRNAs as a biomarker for gastric cancer: a meta analysis. *Oncol Rep.* 2018; 41(1): 87-102.
- Liu C, Kelnar K, Liu B, Chen X, Calhoun-Davis T, Li H, et al. The microRNA miR-34a inhibits prostate cancer stem cells and metastasis by directly repressing CD44. *Nat Med.* 2011; 17(2): 211-215.
- Magee P, Shi L, Garofalo M. Role of microRNAs in chemoresistance. *Ann Transl Med.* 2015; 3(21): 332.
- Chou SM, Lee TS, Shao YE, Chen IF. Mining the breast cancer pattern using artificial neural networks and multivariate adaptive regression splines. *Exp Syst Appl.* 2004; 27(1): 133-142.
- Banwait JK, Bastola DR. Contribution of bioinformatics prediction in microRNA-based cancer therapeutics. *Adv Drug Deliv Rev.* 2015; 81: 94-103.
- Zhang H, Li S, Yang J, Liu S, Gong X, Yu X. The prognostic value of miR-34a expression in completely resected gastric cancer: tumor recurrence and overall survival. *Int J Clin Exp Med.* 2015; 8(2): 2635-2641.
- Ruggieri V, Russi S, Zoppoli P, Rocca F, Angrisano T, Falco G, et al. The role of MicroRNAs in the regulation of gastric cancer stem cells: a meta-analysis of the current status. *J Clin Med.* 2019; 8(5): 639.
- An Y, Zhang Z, Shang Y, Jiang X, Dong J, Yu P, et al. miR-23b-3p regulates the chemoresistance of gastric cancer cells by targeting ATG12 and HMGB2. *Cell Death Dis.* 2015; 6(5): e1766.
- Li L, Zhang J, Pan Q, Lei C. MicroRNA-23a regulates cell migration and invasion by target PTEN in gastric cancer. *Int J Clin Exp Pathol.* 2016; 9(2): 877-887.
- Li C, Zou J, Zheng G, Chu J. MiR-30a decreases multidrug resistance (MDR) of gastric cancer cells. *Med Sci Monit.* 2016; 0: 0.
- Liu G, Jiang C, Li D, Wang R, Wang W. MiRNA-34a inhibits EGFR-signaling-dependent MMP7 activation in gastric cancer. *Tumor Biol.* 2014; 35(10): 9801-9806.
- Huang D, Duan H, Huang H, Tong X, Han Y, Ru G, et al. Cisplatin resistance in gastric cancer cells is associated with HER2 upregulation-induced epithelial-mesenchymal transition. *Sci Rep.* 2016; 6: 20502.
- Cao W, Yang W, Fan R, Li H, Jiang J, Geng M, et al. miR-34a regulates cisplatin-induced gastric cancer cell death by modulating PI3K/AKT/survivin pathway. *Tumor Biol.* 2014; 35(2): 1287-1295.
- Wang G, Liu G, Ye Y, Fu Y, Zhang X. Upregulation of miR-34a by diallyl disulfide suppresses invasion and induces apoptosis in SGC-7901 cells through inhibition of the PI3K/Akt

- signaling pathway. *Oncol Lett.* 2016; 11(4): 2661-2667.
26. Ji Q, Hao X, Meng Y, Zhang M, DeSano J, Fan D, et al. Restoration of tumor suppressor miR-34 inhibits human p53-mutant gastric cancer tumorspheres. *BMC Cancer.* 2008; 8: 266.
 27. Ma G, Dai W, Sang A, Yang X, Gao C. Upregulation of microRNA-23a/b promotes tumor progression and confers poor prognosis in patients with gastric cancer. *Int J Clin Exp Pathol.* 2014; 7(12): 8833-8840.
 28. Wang J, Jiao Y, Cui L, Jiang L. miR-30 functions as an oncomiR in gastric cancer cells through regulation of P53-mediated mitochondrial apoptotic pathway. *Biosci Biotechnol Biochem.* 2017; 81(1): 119-126.
 29. Peng CW, Yue LX, Zhou YQ, Tang S, Kan C, Xia LM, et al. miR-100-3p inhibits cell proliferation and induces apoptosis in human gastric cancer through targeting to BMPR2. *Cancer Cell Int.* 2019; 19: 354.
 30. Cao Y, Song J, Ge J, Song Z, Chen J, Wu C. MicroRNA-100 suppresses human gastric cancer cell proliferation by targeting CXCR7. *Oncol Lett.* 2018; 15(1): 453-458.
 31. Singh SS, Yap WN, Arfuso F, Kar S, Wang C, Cai W, et al. Targeting the PI3K/Akt signaling pathway in gastric carcinoma: a reality for personalized medicine? *World J Gastroenterol.* 2015; 21(43): 12261-12273.
 32. Hu M, Zhu S, Xiong S, Xue X, Zhou X. MicroRNAs and the PTEN/PI3K/Akt pathway in gastric cancer. *Oncol Rep.* 2019; 41(3): 1439-1454.
-

Using Deep Learning Algorithm: The Study of Sperm Head Vacuoles and Its Correlation with Protamine mRNA Ratio

Fatemeh Ghasemian, Ph.D.^{1*}, Mohammad Hadi Bahadori, Ph.D.², Seyedeh Zahra Hosseini Kolkooh, M.Sc.³,
Maryam Esmaili, B.Sc.³

1. Department of Biology, Faculty of Science, University of Guilan, Rasht, Iran

2. Cellular and Molecular Research Center, Guilan University of Medical Sciences, Rasht, Iran

3. Reproductive Health Research Center (IVF Center), Alzahra Educational and Remedial Center, Guilan University of Medical Sciences, Rasht, Iran

*Corresponding Address: P.O.Box: 41335-1914, Department of Biology, Faculty of Sciences, University of Guilan, Rasht, Iran
Email: ghasemian@guilan.ac.ir

Received: 16/February/2020, Accepted: 15/August/2020

Abstract

Objective: It is necessary to evaluate fertility effective agents to predict assisted reproduction outcomes. This study was designed to examine sperm vacuole characteristics, and its association with sperm chromatin status and protamine-1 (*PRM1*) to protamine-2 (*PRM2*) ratio, to predict assisted pregnancy outcomes.

Materials and Methods: In this experimental study, ninety eight semen samples from infertile men were classified based on Vanderzwalmen's criteria as follows: grade I: no vacuoles; grade II: ≤ 2 small vacuoles; grade III: ≥ 1 large vacuole and grade IV: large vacuole with other abnormalities. The location, frequency and size of vacuoles were assessed using high magnification, a deep learning algorithm, and scanning electron microscopy (SEM). The chromatin integrity, condensation, viability and acrosome integrity, and protamination status were evaluated for vacuolated samples by toluidine blue (TB) staining, aniline blue, triple staining, and CMA3 staining, respectively. Also, *Protamine-1* and *protamine-2* genes expression was analysed by reverse transcription-quantitative polymerase chain reaction (PCR). The assisted reproduction outcomes were also followed for each cycle.

Results: The results show a significant correlation between the vacuole size (III and IV) and abnormal sperm chromatin condensation ($P=0.03$ and $P=0.02$, respectively), and also, protamine-deficient ($P=0.04$ and $P=0.03$, respectively). The percentage of reacting acrosomes was significantly higher in the grades III and IV spermatozoa in comparison with normal group. The vacuolated spermatozoa with grade IV showed a high protamine mRNA ratio (*PRM-2* was underexpressed, $P=0.01$). In the IVF cycles, we observed a negative association between sperm head vacuole and fertilization rate ($P=0.01$). This negative association was also significantly observed in pregnancy and live birth rate in the groups with grade III and IV ($P=0.04$ and $P=0.03$, respectively).

Conclusion: The results of our study highlight the importance sperm parameters such as sperm head vacuole characteristics, particularly those parameters with the potency of reflecting protamine-deficiency and *in vitro* fertilization/ intracytoplasmic sperm injection (IVF/ICSI) outcomes predicting.

Keywords: Algorithm, Human Sperm, Pregnancy, Protamines, Vacuole

Cell Journal (Yakhteh), Vol 24, No 1, January 2022, Pages: 7-14

Citation: Ghasemian F, Bahadori MH, Hosseini Kolkooh SZ, Esmaili M. Using deep learning algorithm: the study of sperm head vacuoles and its correlation with protamine mRNA Ratio. Cell J. 2022; 24(1): 7-14. doi: 10.22074/cellj.2022.7448.

This open-access article has been published under the terms of the Creative Commons Attribution Non-Commercial 3.0 (CC BY-NC 3.0).

Introduction

While normal sperm parameters were found in almost 15% of infertile males, the routine semen analysis is not sufficient to evaluate the male fertility status (1). Nowadays, several assays have been suggested to achieve more details in the male infertility diagnosis (2), which included nucleus assessment (chromatin integrity and condensation, protamination status, aneuploidy), and sperm function assay (1, 2). In addition, the evaluation of the detailed morphology of motile sperm in real-time at a high magnification (up to $\times 6600$) which is called the motile sperm organelle morphology examination (MSOME), is another of these evaluations. In fact, MSOME is seen sperm morphology with more details, which is not provided at $\times 400$ or $\times 200$ magnifications (2).

Although, the origin and nature of vacuole remain unknown, sperm head vacuole has been defined as one of the most important of sperm abnormalities (2). Sperm

morphology, particularly head vacuoles, has a major effect on the assisted reproductive techniques (ARTs) outcomes (3). Therefore, the selection of 'good' spermatozoa prior to intracytoplasmic sperm injection (ICSI) may be a powerful step to obtain better outcomes. The presence of morphologically and morphometrically normal head (2, 4, 5) and lack of vacuoles or less than two small vacuoles is determined a 'good' spermatozoa (6). On the other hand, the classification of spermatozoa has been defined as the following four groups according to the presence or size of vacuoles: grade I: no vacuoles; grade II: ≤ 2 small vacuoles (which occupy $< 4\%$ of the head's area); grade III: more than two small vacuoles or ≥ 1 large vacuole (which occupy between 13% to 50% of the head's surface area); and grade IV: large vacuole with other abnormalities (7). The difference in size and location of sperm-head vacuoles may be associated with chromatin condensation failure as well as nuclear DNA damage (8, 9). So that,

the many studies have indicated the negative impact of spermatozoa' nuclear vacuoles on embryo development, blastocyst rate, and pregnancy outcomes (10-13).

Moreover, replacement of DNA-binding histones by protamines is a most important parameter in the fertilization success (14). Recently, an association between improper protamine mRNA/protein ratio and male infertility has been found. This ratio is known as a suitable biomarker for fertilization success. The relative ratio of protamine-1 to protamine-2 is almost at a 1:1 ratio (15). This relative ratio of protamine-1 to protamine-2 has been reported as a range of 0.5 to 1.4 for normozoospermia specimens (16). The correlation between male infertility and abnormal protamine mRNA ratio has been found (15). However, it should be further investigated whether the protamine mRNA ratio is impacted by vacuolated spermatozoa percentage, and correlated with fertilization, embryo development and pregnancy rates during *in vitro* fertilization (IVF) or ICSI cycles. Therefore, the sperm genomic quality and its association with assisted reproductive outcomes has been located as a one of the most important goals in recent years.

However, it is not clear whether vacuoles influence assisted reproductive outcomes (e.g., fertilization rate, embryo development, and pregnancy rate). Therefore, we used deep learning algorithm (17) to select the 'good' spermatozoa. And also, we tried to investigate relations among vacuole(s) and the protamine-1 to protamine-2 mRNA ratio and assisted reproductive outcomes. In this study, we used a novel deep learning algorithm in combined with high magnification and SEM images to visualize sperm's vacuoles and its association to chromatin status, protamine mRNA ratio, and the sperm fertility potential. Also, we compared the protamine-1 to protamine-2 mRNA ratio among spermatozoa with different vacuole grades. In addition, the acrosome reaction, chromatin condensation and integrity, protamination status, and fertilizing capacity of semen samples with different degrees of vacuolated spermatozoa were studied during ICSI/IVF cycles. To the best of our knowledge, this is the first study to provide empirical evidence for this issue.

Materials and Methods

Participants

A total of 309 specimens was collected from fertile and infertile men (age 22-38 years) who visited in Alzahra hospital (IVF center), Rasht, Iran, between May 2018 to September 2019. This experimental study was approved by the Guilan University of Medical Sciences committee (IR.GUMS.REC.1397.154). In addition, the informed consent was obtained from all the volunteer participants in the present study. The couples who received ICSI or IVF services with an ICSI or IVF failure history were invited to this study. They were excluded based on their spermocytogram, and woman age. The semen samples were collected via masturbation after three to four days of sexual abstinence. The semen samples were analyzed

according to the World Health Organization (WHO) criteria (18). The semen parameters such as pH, volume, motility, morphology, concentration, viability were assessed. The vacuolated semen samples were included in this study (n=98). Also, female factor infertility, maternal age >40 years, and less than three oocytes made our exclusion criteria. The couples with male factor infertility (e.g., severe teratozoospermia, asthenozoospermia, and oligoasthenoteratozoospermia) were also excluded from this study to remove effects of other sperm parameters on sperm quality and ART outcomes.

Totally, ninety-eight semen samples were included in this study. The vacuolated sperm categorization and selection during ICSI cycles were performed with both high magnification ($\times 1000$) and a novel deep learning algorithm (17) as real-time ($\times 400$). Also, a part of semen sample ($\sim 100 \mu\text{l}$) was prepared for scanning electron microscopy (SEM) to view and determine the percentage of sperm's vacuoles in more detail. Based on information obtained from evaluations, the semen samples were categorized into four groups according to Vanderzwalmen's criteria: grade I: no vacuoles (normal/control group); grade II: ≤ 2 small vacuoles (which occupy $< 4\%$ of the head's area); grade III: more than two small vacuoles or ≥ 1 large vacuole (which occupy between 13 to 50% of the head's surface area); and grade IV: large vacuole with other abnormalities (7).

Assay using a novel deep learning algorithm

Using deep learning algorithm, sperm morphology, especially vacuole was analyzed. This algorithm was performed with a high accuracy (94.65%) to detect sperm's vacuoles. In addition, this method worked very fast and categorized sperm images in real-time. Therefore, the classification of spermatozoa was done using this algorithm in line with the results of high magnification ($\times 1000$) and SEM images.

In this way, for detecting abnormalities in the vacuole, Javadi and Mirroshandel (17) have proposed a novel deep learning approach. They have trained a deep convolutional neural network on mini-batches generated from the training set. The size of a mini-batches in this study is 64, which is a common value. Mini-batch means you only take a subset of all your training data during model construction. Also, they have proposed oversampling and data augmentation in order to overcome the problem of low count of training samples and class imbalance (i.e., the sperms number with abnormal vacuole in our training data is smaller than the number of normal sperms). This network consists of 24 convolutions, three pooling, and two fully-connected layers. The overall trainable parameters of the model are 5,637,649. The implementation of the model was done using TensorFlow and Keras.

Scanning electron microscopy

For correct measurement of sperm vacuole, each semen samples were evaluated by SEM to observe the smallest

details. The semen samples were washed by using sucrose density gradient centrifugation at 3000 rpm for 10 minutes at RT temperature, and then, fixed in Karnovsky solution for 30 minutes at 4°C. Then, the samples were treated with 1% osmium tetroxide (OT20816-12-0, Merck, Germany) for 30 minutes as a post fixation step. Afterwards, the ascending degrees of ethanol (50, 70, 80, 90, 96%, and absolute alcohol) (E64-17-5, Hamontebmarkazi, Iran) were used to dehydrate. The drying was performed at a critical point (Balzers CPD-010). The specimens coated with gold (MED-010, BALZERS, USA) were examined in a Philips FEM 515 scanning electron microscope (Philips SEM 515, F.E.I. Company, Netherlands).

Sperm chromatin assays

Toluidine blue stain

The abnormality in the sperm chromatin structure was distinguished using toluidine blue (TB) staining. In this way, the air-dried smears (~100 µl semen samples) on silane-coated slides (SL002-72, BioMarq, India) were fixed in 96% ethanol-acetone solution (CAS 67-64-1, Merck, Germany) (1:1) at 4°C for 1 hour. To hydrolysis, slides were put in 0.1 N HCl (109060, Merck Millipore, China) at 4°C for 5 minutes, then were washed. The staining was done with 0.05% TB (in 50% McIlvaine's citrate phosphate buffer, pH=3.5) (T92-31-9, Merck, Germany) for 5 minutes at room temperature (RT). On average, 100 sperms were evaluated in each slide using a light microscope. The observation of light blue or deep violet/purple heads is the sign of existence normal or abnormal chromatin structure, respectively (Fig. 1A).

Aniline blue stain

The adhesion between lysine residues of histones and aniline blue (AB) stain were detected the abnormal condensation of sperm chromatin. Briefly, the smears (~100 µl semen samples) were fixed in the 4% formalin (50-00-0, Junsei Chemical, Tokyo, Japan). After washing, the slides were stained with 5% AB (AB 229660250, Sigma-Aldrich Co., St. Louis, MO, USA) in a solution of 4% acetic acid (pH=3.5) (A64-19-7, Merck, Germany) for 5 minutes at RT. On average, 100 spermatozoa in each slide were observed under a light microscope. The sperms with dark-blue or colorless heads were considered as abnormal and normal chromatin condensation, respectively (Fig. 1B).

Acrosome reaction assessment

The acrosome status (reacted acrosome and intact acrosome) was evaluated using triple staining. In brief, sperms (~100 µl semen samples) were put in 2% trypan blue (1:1) (T10282, Sigma, Germany), incubated at 37°C for 15 minutes, and centrifuged at 600 × g for 5-10 minutes. Then, the pellet was washed and diluted in the Ham's F10 solution to obtain a clear/ pale blue mixture. In the next step, the washed sperms were fixed using glutaraldehyde (3% glutaraldehyde in 0.1 M cacodylate buffer at pH=7.4)

(G111-30-8, Sigma, China) for 30 to 60 minutes, and were centrifuged at 6000×g for 5 minutes. The pellet was stained with Bismark brown Y (10114-58-6, Sigma, Germany) at 40°C for 5 minutes. Then, Rose Bengal stain (100467, Merck, Germany) was added at 24°C for 20-45 minutes. The smears were prepared from stained sperms, washed (in water), dehydrated (in an ascending degree of alcohol), and cleared in xylene (108633, Merck Millipore, China). At the end, almost 100 sperms in each slide were examined under a light microscope. Four staining templates were seen as follows: i. Dead sperm and intact acrosome as dark-blue post-acrosomal regions and pink acrosomes, respectively, ii. Dead sperm and degenerated acrosome as dark-blue post-acrosomal regions and blue/white acrosomes, respectively, iii. Alive sperm and intact acrosome as light brown post-acrosomal regions and pink acrosomes, respectively, and iv. Alive sperm and degenerated acrosome as light brown post-acrosomal regions and blue/white acrosomes, respectively (Fig. 1C).

Chromomycin A3 stain

The degree of sperm protamination was determined by chromomycin A3 (CMA3) staining (89158-860, Sigma, Germany) (Fig. 1D) as a detector of guanosine-cytosine-rich sequence. All air-dried smears (~100 µl semen samples) were fixed in the methanol/glacial acetic acid (3:1) for 20 minutes at 4°C. Then, the slides were treated for 20 minutes with 100 µl of CMA3 solution (0.25 mg/ml CMA3 in McIlvaine's buffer, containing 10 µm MgCl₂). The sperms with dull yellow staining (CMA3 negative) and bright yellow fluorescence (CMA3 positive) were considered as normal and abnormal chromatin protamination, respectively.

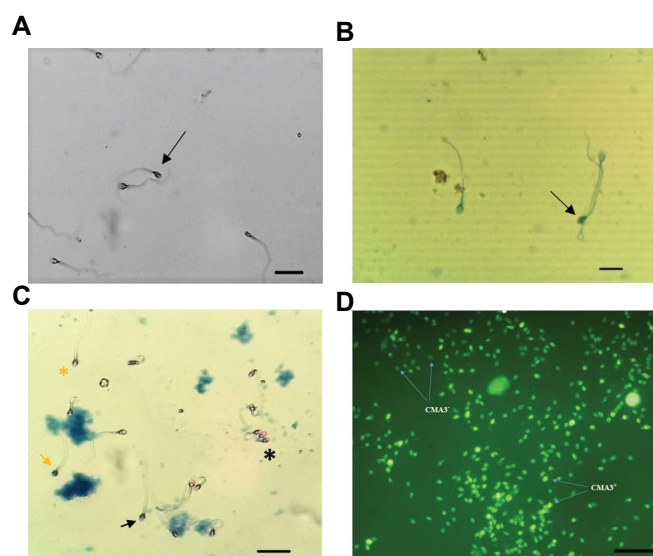


Fig.1: Sperm chromatin assays. **A.** Sperm cell heads with abnormal chromatin structure were deep violet (arrow) following toluidine blue staining. **B.** Sperm cell heads with abnormal chromatin condensation were dark blue (arrow) following aniline blue staining. **C.** The status of sperm acrosome reaction and viability was observed as following: dead sperm with an intact acrosome (black arrow), dead sperm without an acrosome (yellow arrow), live sperm with an intact acrosome (black star), and live sperm without an acrosome (yellow star) (scale bar: 10 µm). **D.** Spermatozoa stained with CMA3 was with dull yellow/normal chromatin (CMA3⁻) and bright yellow/abnormal chromatin (CMA3⁺) (scale bar: 100 µm).

RNA extraction and first strand cDNA synthesis

RNA extraction was performed using the RNeasy Mini kit (74104, Roche Molecular Biochemicals, Mannheim, Germany) and stored at -80°C . The first strand cDNA synthesis was done the cDNA kit (4368813, Thermo Scientific, EU), according to the manufacturer's protocol at 42°C for 60 minutes, and stored at -20°C .

Real-time reverse transcription-quantitative polymerase chain reaction

Reverse transcription-quantitative polymerase chain reaction (RT-qPCR) was done to quantify mRNA transcript levels of *protamine-1* (*PRM1*) and *protamine-2* (*PRM2*) genes. The primer pairs of

PRM1-

F: 5'-ACTAGATGCACAGAATAGCAA-3'
R: 5'-GTGGCATTGTCCTTAGCAG-3'

PRM2-

F: 5'-CAGCCTCAATCCAGAACCTCC-3'
R: 5'-CTCGCGTTCATGGTCTTGTC-3'

GAPDH-

F: 5'-CAAGGTCATCCATGACAACCTTTG-3'
R: 5'-GTCCACCACCCTGTTGCTGTAG-3' (housekeeping)

genes were designed by Oligo 7. The analyzing gene expression was conducted by real time thermal cycler (Applied Biosystems, Foster City, USA) and QuantiTect SYBR Green RT-PCR kit (204243, Applied Biosystems, Germany) was also used for amplifying the reference and the target genes (5 μl cDNA per sample) in the same run. The conditions were 95°C for 5 minutes (holding step), 95°C for 15 seconds, 58°C for 30 seconds, and 72°C for 15 seconds (cycling, step), which was followed by a melt curve step at 95°C for 15 seconds, 60°C for 1 minutes, and 95°C for 15 seconds. All PCR amplifications were carried out in triplicate and mean values were calculated. Determining of relative quantitation for target genes was performed using $\Delta\Delta\text{CT}$ method.

Intracytoplasmic sperm injection and *in vitro* fertilization laboratory procedures

Semen samples were collected via masturbation on the oocyte retrieval day. A period of three to four days of the ejaculatory abstinence was considered. Follow of liquefaction, semen samples were washed by density gradient centrifugation method (90 and 45% SpermGrade; 10099, Vitrolife, Sweden). The evaluation of semen parameters was performed according to the World Health Organization (18) criteria. These parameters including volume, motility, concentration, morphology, and pH can be mentioned. The washed semen samples were incubated at 37°C in a 5% CO_2 atmosphere up to three to four hours before ICSI or IVF procedures performance. Treatment procedure (ICSI/IVF) was selected based on the sperm concentration, morphology, motility, infertility etiology,

the patient's history, and female age.

A first selection of motile spermatozoa in the polyvinyl pyrrolidone (PVP, 10111, Vitrolife, Sweden) drop was performed at $\times 400$ magnification during an ICSI cycle. Photo-documented was analyzed using a novel deep learning algorithm as real-time and used for the grading. The best spermatozoa selected was immobilized and injected for conventional ICSI at $\times 200$ and $\times 400$ magnifications (2). The injected oocytes were incubated. The selected spermatozoa were also assessed at $\times 1000$ magnification (under a Hoffman modulation contrast) in line with deep learning algorithm's results.

Then, the analysis of fertilization was done by observing of two pronuclei in 16-18 hours after ICSI or IVF. In addition, the evaluation of embryo development rate and embryo transfer (ET) was performed at four to five days after fertilization.

Standardization of results

The sample coefficients of variation (CV) were recorded during primary experiments. Then, intra-assay variations were distinguished by assessment 100 sperms on 5 different microscopic fields (total 500 sperms) from the same semen samples which were prepared for AB, TB, CMA3, and triple staining. The CV for inter-assay and intra-assay were determined by using: (standard derivation/the mean value) $\times 100$ formula.

Statistical analysis

The relationship between vacuolization grade and other semen parameters was analyzed by using correlation coefficient and Student's t test analysis. Fisher's exact test was used to assess the statistical correlation of vacuolization grade with clinical variables (ART outcomes). The categorized protamine-1 to protamine-2 ratios were analyzed by using the Bonferroni-adjusted Mann-Whitney U-test. Statistical analysis was done using SPSS 20 software (SPSS, IBM, Armonk, NY, USA) and the values with $P < 0.05$ were considered significant. In addition, to evaluate the effect of each feature/factor of vacuole (size, location and frequency) on the sperm parameters and ART outcomes, we used different modules of WEKA software (www.cs.waikato.ac.nz/~ml/weka) including correlation, attribute, Eval and Ranker.

Results

Grouping of vacuolated spermatozoa

The classification of spermatozoa was done by using a novel deep learning algorithm. The results of this algorithm were similar to the results of high magnification ($\times 1000$). In addition, scanning electron microscope (SEM) images showed more details of vacuole (size, location, and frequency) in the semen samples of each patient (Fig.2). Therefore, samples grouping was performed very precise based on the novel deep learning algorithm, high magnification ($\times 1000$), and the SEM images.

Vacuolization and sperm parameters

The results of AB staining showed significant abnormal condensation rate of chromatin in the grade IV ($P=0.02$) in comparison with the control group (grade I). There was no significant difference in the viability and abnormality of the DNA structure of vacuolated spermatozoa among different grades ($P=0.15$, Table 1).

The presence of bright yellow fluorescence (CMA3-positive) was observed more frequently in the spermatozoa with a large nuclear vacuole (LNV) (grade III: 2336/4200; 55.6% vs. grade IV: 621/1500; 41.4%) than other groups. Therefore, a higher percentage of sperm protamine deficiencies in the vacuolated spermatozoa with grade III ($P=0.04$) and IV ($P=0.03$) was detected. Also, the presence of more than one small nuclear vacuole showed more abnormal chromatin protamination in comparison with large non-nuclear vacuole ($P=0.03$). The percentage of reacted acrosomes (blue/white) was significantly higher in the non-nuclear vacuoles spermatozoa (grade III and IV) in comparison with other groups ($P=0.04$ and $P=0.03$, respectively). In addition, there was no significant difference in the sperms viability rate among these different groups ($P=0.25$).

The protamine mRNA ratio in the vacuolated spermatozoa

As seen in Figure 3, the assessment of *PRM1* gene expression showed a significant difference in the grade III (median 0.4457 ± 0.03 , $P=0.03$) in comparison with the control group (group I, normal semen samples). In addition, comparison between grade IV and control group showed a significant difference in the *PRM1* gene expression ($P=0.0001$). While, there is no significant difference in the *PRM1* gene expression in the grade II (median 0.83184) in compared to the control group (median 1.0201 ± 0.06 , $P=0.35$, Fig.3). In addition, the analysis of *PRM2* gene expression showed significant differences among grade II (0.6623 , $P=0.01$), grade III (median 0.60262 ± 0.007 , $P=0.0001$), and grade IV (median 0.2772 ± 0.012 , $P=0.0001$) in comparison with the control group (median 1.001 ± 0.04 , grade I).

The protamine mRNA ratio was evaluated among different vacuolization grades in the fertile and infertile men. Vacuolated spermatozoa from infertile men with grade IV (median 3.40006 ± 1.81 , $P=0.008$) displayed a significant difference in the protamine mRNA ratio in comparison with the control group (median 1.02 ± 0.81 m, $P=0.004$).

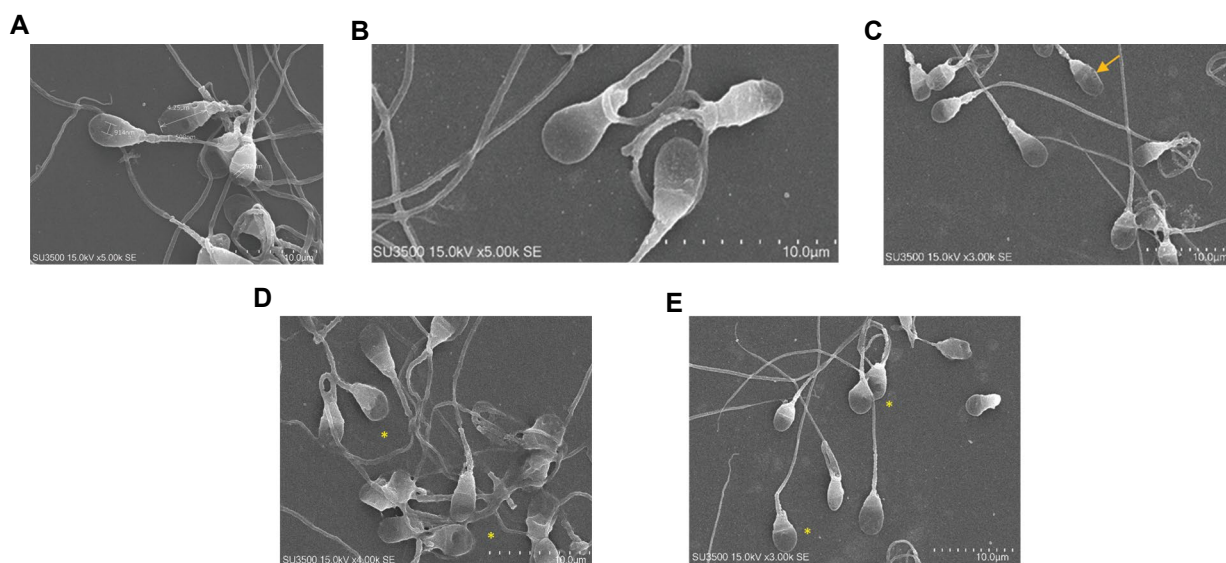


Fig.2: Evaluation of sperm morphology using the scanning electron microscope. **A.** The presence of small and large vacuoles and its location in the nuclear or non-nuclear position is clear. **B.** Grade I: without vacuoles, **C.** Grade II: with ≤ 2 small vacuoles (arrows), **D.** Grade III: more than two small vacuoles or ≥ 1 large vacuole (Stars), and **E.** Grade IV: with large vacuole (stars).

Table 1: Vacuolization and sperm parameters

Vacuole grade	N	Protamination status (%)	Spont. A.R. (%)	Condensation status (%)	Chromatin integrity (%)	Viability (%)	<i>PRM1</i> : <i>PRM2</i>
I	27	28.3 ± 2.9	15.1 ± 1.9	22.7 ± 2.1	23.7 ± 2.4	65.45 ± 10.08	1.01917
II	24	32.4 ± 2.6	19.8 ± 2.1	29.5 ± 2.2	26.8 ± 2.5	59.9 ± 9.81	1.1149
III	23	$36.1 \pm 3.2^*$	$27.16 \pm 2.4^*$	32.4 ± 3.2	28.9 ± 3.1	59.02 ± 9.07	0.7397
IV	24	$41.3 \pm 3.4^{**}$	$29.9 \pm 2.7^*$	$38.6 \pm 3.6^*$	29.7 ± 3.2	55.14 ± 9.14	3.400**

There is a significant difference between chromatin protamine-deficient (CMA3), spontaneously reacted acrosomes and abnormal chromatin condensation (AB staining) in the spermatozoa with grade III and IV in comparison with the control group (grade I). The χ^2 test was used to analysis differences among the groups. Data are expressed as mean \pm SD and percentage (%). *; $P=0.04$, **; $P=0.03$, and Spont. A.R.; Spontaneously acrosome reaction.

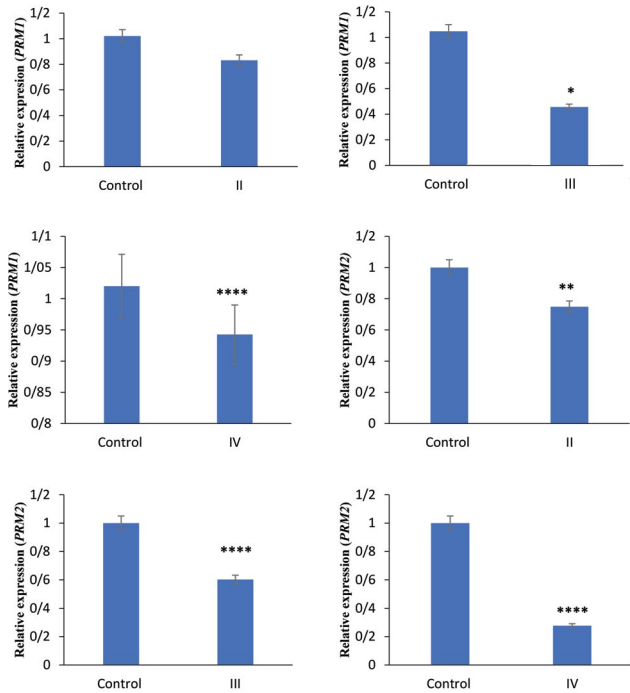


Fig.3: The *PRM1* and *PRM2* gene expression of vacuolated spermatozoa. A significant difference was seen in the *PRM1* gene expression (underexpression) of grade III (P=0.03) and grade IV (P=0.0001) of spermatozoa in comparison with the control group (grade I). Also, there is a significant difference in the *PRM2* gene expression (over-expression) among different grades of spermatozoa in comparison to the control group (grade I): II (P=0.01), III (P=0.0001), and IV (P=0.0001), respectively. *, P<0.05, **, P<0.01, and ****, P<0.0001.

Vacuolated spermatozoa and *in vitro* fertilization/ intracytoplasmic sperm injection outcomes

The results of the influences of different grading of

sperm vacuolization and normal sperm on the clinical outcomes are shown in the Table 2. In the IVF cycles, a decrease in the fertilization rate was observed in the cases who received sperms of grade III (39.6%, P=0.018) and IV (32.4%, P=0.012) in compared to the control group (70.3%). However, no significant difference was seen in the fertilization rate in the ICSI cycles (III, 60.52 and IV, 57.2%) in comparison with the control group (65.1%, P=0.12). Increased levels of sperm vacuoles were also associated with a decreased rate of embryo development in comparison with the control group. So that, development rate in the ICSI cycles was significantly decreased in the grades of III=51.33% (P=0.04), and IV=49.17% (P=0.02), in compared to grade I=57%. While, declined embryo development rate was recorded in the IVF cycles as following: grades III=55.01 and IV=56% (P=0.04). The increased percentage of vacuolated sperms was correlated with the decreased chance of an embryo developing to the blastocysts stage. In this way, the rate of successful pregnancy was significantly decreased in the groups with vacuolated sperms (III and IV) under IVF treatment (28.57 and 21.42%, P=0.04 and P=0.019, respectively) in compared to the control (grade I) group, while this outcome was also significant in the ICSI group (III and IV grades: 33.3 and 20%, P=0.02 and P=0.011, respectively).

Factors ranking

Another important experiment was measuring of the effect of different aspects of vacuole on the male fertility (Table 3). The effect of vacuole location (nuclear) weighed more than the effect of other parameters on pregnancy.

Table 2: The effect of different vacuolization grade on the ART outcomes

Vacuole grade of sperm	ART technique	Fertilization rate (%)	Cleavage rate (%)	Clinical pregnancy rate P/ET (%)	Live birth LB/IE (%)
I	ICSI	65.1	57	5/12 (41.66)	3/5 (60)
	IVF	70.3	68.1	7/15 (46.66)	4/7 (57.1)
II	ICSI	53.26	55.31	4/11 (36.36)	2/4 (50)
	IVF	60.03	62.32	5/13 (38.46)	3/5 (60)
III	ICSI	60.52	51.33*	3/9 (33.33)*	1/3 (33.3)*
	IVF	39.6**	55.01*	4/14 (28.57)*	1/4 (25)*
IV	ICSI	57.2	49.17*	3/10 (30)**	1/3 (33.3)*
	IVF	32.4**	56*	3/14 (21.42)**	1/3 (33.3)*

There is a significant difference between ART outcomes and grades of spermatozoa (III and IV). The χ^2 test was used to analysis differences among the groups. Data are expressed as mean \pm SD and percentage (%). *, P<0.05, **, P<0.01, ART; Assisted reproductive technique, ICSI; Intracytoplasmic sperm injection, IVF; *In vitro* fertilization, P; Positive cycle, ET; Embryo transfer, LB; Live birth, and IE; Implanted embryo.

Table 3: The effect of different features of vacuoles on male fertility potential

Feature	Protamination status	Protamine ratio	Chromatin condensation	Acrosome reaction	Fertilization	Pregnancy
Nuclear location	0.0812	0.0752	0.0537	0.0529	0.0832	0.0875*
Number	0.0689	0.0543	0.0312	0.0241	0.0776	0.07601
Size	0.0567	0.0487	0.0192	0.0138	0.0617	0.0651

*; The effects of nuclear location weighed more than the effects of other features on pregnancy. The WEKA test was used to analysis differences among the groups.

Discussion

A novel insight was provided in this study that how vacuolization affects sperm fertility potential. It is a better predictor of IVF/ICSI outcomes following evaluation of sperm by using high magnification, deep learning algorithm, and SEM images. The results of this study show that variations in vacuole parameters including higher size, greater frequency, and nuclear location were associated with protamine-deficient sperms as well as CMA3 positive and aberrant *PRM1* and *PRM2* gene expression. In addition, the presence of non-nuclear vacuole leads to increased immature acrosome reaction and decreases the fertilization rate under IVF cycles.

Although, limitations of routine semen analysis have been reported, this is performed as a common evaluation in many clinical practices (19). This conventional semen analysis does not recognize the subtle abnormalities in the male genome, DNA structure and condensation (2). The abnormalities in chromatin structure and condensation is known to be correlated with numerous indicators of assisted reproductive outcomes, including fertilization rate, embryo development rate and quality, pregnancy and spontaneous miscarriage (19-21). Although, it has been determined that human sperms have a highly dynamic and key roles in the embryonic development, the utility of more detail analysis of sperm is still a matter of debate (22, 23). In the present study, the predictive value of vacuolated sperm testing was distinguished between potentially pregnant and not potentially pregnant couples who were undertaken IVF or ICSI cycles. As mentioned above, these poor outcomes may have related to abnormalities of chromatin condensation and sperm protamination (CMA3 positive) with aberrant *PRM1* and *PRM2* gene expression. While, the cause of abnormal sperm chromatin condensation is still unclear. The results of this study suggest a direct correlation between sperm nuclear vacuolization and abnormalities in the sperm chromatin packaging. It seems that the contribution of the immune seminal cells, mature sperms and immature germ cells lead to the production of reactive oxygen species that can cause vacuolated head in the sperms (22). It has been also reported that poor chromatin condensation and aneuploidy could be observed in the spermatozoa with large vacuoles (24).

In this study, the protamine mRNA ratio of infertile men

was 0.739 ± 0.212 and 3.400 ± 1.281 in the vacuolated spermatozoa with grades III and IV, respectively. While, the protamine mRNA ratio has been reported in the previous studies as follows: 0.83 ± 0.05 (n=50) (25), 1.3 ± 0.1 (n=12) (26) and 0.98 ± 0.02 (n=77) (16), a range of 0.54 to 1.43 of the protamine ratio has been reported in normozoospermic men (16). The ratio of 1.06 ± 0.60 versus 10.68 ± 33.72 was also seen in the normozoospermia semen samples versus teratozoospermia ones (15). Therefore, present study outcomes indicated that vacuolization affects negatively the protamine ratio in the infertile men. So that, a low protamine ratio was seen in the vacuolated spermatozoa with grade III (protamine-1 was underexpressed). Also, a high protamine ratio was observed in the vacuolated spermatozoa with grade IV (normal expression of protamine-1 and underexpression of protamine-2). Aoki et al. (27) reported *PRM1* under expression and *PRM2* overexpression in the infertile patients with a low protamine ratio. On the other hand, in the patients with a high protamine ratio, *PRM2* was underexpressed and *PRM1* has a normal expression. Numerous studies also indicated a significant aberrant of protamine ratio in infertile men (28, 29) and our result is in line with them.

Moreover, it is widely accepted that there is a correlation between sperm quality and infertility (22). In addition, our study results indicate this correlation between sperm quality and fertility potential. In this way, the embryos resulting from morphologically abnormal sperm lead to significantly lower pregnancy rates (2). The correlation between spermatozoa with large nuclear vacuoles and ICSI outcomes has been reported (24). While the origin and consequences of vacuoles of sperm head are also a problem of controversy. Therefore, the association among different sizes, locations, and frequencies of vacuole with chromatin status, IVF/ICSI outcomes, and weight of each feature (size, location, and frequency of vacuoles) on pregnancy rate are essential that this study considered them.

Kacem et al. (30) showed that a large sperm head vacuole could originate from spermatogenesis damaging, abnormal maturation or modifications during the acrosome reaction. Our results are consistent with the results of this study. So that, the immature acrosome reaction was greater in the spermatozoa of grade III and grade IV, therefore, the fertilization rate was decreased in these groups.

Conclusion

The results of this study indicate that the semen samples from infertile men are characterized by a higher ratio of vacuolization grades, although, there are categorized in normozoospermia samples. This frequency of vacuolization may be correlated to abnormal chromatin condensation, greater sperm protamine deficiencies, declined *PRM1* and *PRM2* gene expression, and a high protamine mRNA ratio. Also, tracing the IVF/ICSI outcomes showed that the poor fertilization rate during (IVF cycles), embryo quality, and declined clinical pregnancy rate may have related to the abnormal maturation and sperm head vacuoles. Therefore, it seems the evaluation of the semen sample vacuole status, as a definite parameter before starting treatment cycles, may be a useful tool for selecting the best treatment cycle (IVF or ICSI) in ART plan.

Acknowledgements

We thank Ms. Mirzanezhad for her skillful technical assistance (Genetic Laboratory, University of Guilan, Rasht, Iran). This research did not receive any specific grant from funding agencies in the public, commercial, or not-for-profit sectors. The authors have no conflict of interest to disclose.

Authors' Contribution

F.G., M.H.B.; The design of the study, experiment conductors, interpretation, and manuscript drafting and reviewing. S.Z.H.K, M.E.; *In vitro* experiment performance, critical reagents provider, statistical analysis and contribution of patient data. All authors read and approved the final manuscript.

References

- Colaco S, Sakkas D. Paternal factors contributing to embryo quality. *J Assist Reprod Genet.* 2018; 35(11): 1953-1968.
- Zanetti BF, Braga DPAF, Provenza RR, Figueira RCS, Iaconelli A Jr, Borges E Jr. Sperm morphological normality under high magnification is correlated to male infertility and predicts embryo development. *Andrology.* 2018; 6(3): 420-427.
- Zhu WJ. Transmission electron microscopy analysis of the origin and incidence of sperm intranuclear cytoplasmic retention in fertile and teratozoospermia men. *Andrology.* 2018; 6(2): 317-324.
- Gao Y, Zhang X, Xiong S, Han W, Liu J, Huang G. Motile sperm organelle morphology examination (MSOME) can predict outcomes of conventional in vitro fertilization: a prospective pilot diagnostic study. *Hum Fertil (Camb).* 2015; 18(4): 258-264.
- Pocate-Cheriet K, Heilikman I, Porcher R, Barraud-Lange V, Sermondade N, Herbemont C, et al. Predicting the clinical outcome of ICSI by sperm head vacuole examination. *Syst Biol Reprod Med.* 2017; 63(1): 29-36.
- Zhu WJ, Li J. A simple sperm nuclear vacuole assay with propidium iodide. *Andrologia.* 2015; 47(7): 779-785.
- Vanderzwalmen P, Hiemer A, Rubner P, Bach M, Neyer A, Stecher A, et al. Blastocyst development after sperm selection at high magnification is associated with size and number of nuclear vacuoles. *Reprod Biomed Online.* 2008; 17(5): 617-627.
- Boitrelle F, Ferfour F, Petit JM, Segretain D, Tourain C, Bergere M, et al. Large human sperm vacuoles observed in motile spermatozoa under high magnification: nuclear thumbprints linked to failure of chromatin condensation. *Hum Reprod.* 2011; 26(7): 1650-1658.
- Franco JG Jr, Mauri AL, Petersen CG, Massaro FC, Silva LF, Felipe V, et al. Large nuclear vacuoles are indicative of abnormal chromatin packaging in human spermatozoa. *Int J Androl.* 2012; 35(1): 46-51.
- Berkovitz A, Eltes F, Ellenbogen A, Peer S, Feldberg D, Bartoov B. Does the presence of nuclear vacuoles in human sperm selected for ICSI affect pregnancy outcome? *Hum Reprod.* 2006; 21(7): 1787-1790.
- Vanderzwalmen P, Hiemer A, Rubner P, Bach M, Neyer A, Stecher A, et al. Blastocyst development after sperm selection at high magnification is associated with size and number of nuclear vacuoles. *Reprod Biomed Online.* 2008; 17(5): 617-627.
- Knez K, Tomazevic T, Zorn B, Vrtacnik-Bokal E, Virant-Klun I. Intracytoplasmic morphologically selected sperm injection improves development and quality of preimplantation embryos in teratozoospermia patients. *Reprod Biomed Online.* 2012; 25(2): 168-179.
- Boitrelle F, Albert M, Petit JM, Ferfour F, Wainer R, Bergere M, et al. Small human sperm vacuoles observed under high magnification are pocket-like nuclear concavities linked to chromatin condensation failure. *Reprod Biomed Online.* 2013; 27(2): 201-211.
- Marchiani S, Tamburrino L, Benini F, Fanfani L, Dolce R, Rastrelli G, et al. Chromatin protamination and catsper expression in spermatozoa predict clinical outcomes after assisted reproduction programs. *Sci Rep.* 2017; 7(1): 15122.
- Savadi-Shiraz E, Edalatkhah H, Talebi S, Heidari-Vala H, Zandemami M, Pahlavan S, et al. Quantification of sperm specific mRNA transcripts (PRM1, PRM2, and TNP2) in teratozoospermia and normozoospermia: new correlations between mRNA content and morphology of sperm. *Mol Reprod Dev.* 2015; 82(1): 26-35.
- Nanassy L, Liu L, Griffin J, Carrell DT. The clinical utility of the protamine 1/protamine 2 ratio in sperm. *Protein Pept Lett.* 2011; 18(8): 772-777.
- Javadi S, Mirroshandel SA. A novel deep learning method for automatic assessment of human sperm images. *Comput Biol Med.* 2019; 109: 182-194.
- World Health Organization. WHO laboratory manual for the examination and processing of human semen. 5th ed. Geneva: WHO Press; 2010.
- Oleszczuk K, Giwercman A, Bungum M. Sperm chromatin structure assay in prediction of in vitro fertilization outcome. *Andrology.* 2016; 4(2): 290-296.
- Tello-Mora P, Hernández-Cadena L, Pedraza J, López-Bayghen E, Quintanilla-Vega B. Acrosome reaction and chromatin integrity as additional parameters of semen analysis to predict fertilization and blastocyst rates. *Reprod Biol Endocrinol.* 2018; 16(1): 102.
- Oldenhof H, Schütze S, Wolkers WF, Sieme H. Fourier transform infrared spectroscopic analysis of sperm chromatin structure and DNA stability. *Andrology.* 2016; 4(3): 430-441.
- López G, Lafuente R, Checa MA, Carreras R, Brassesco M. Diagnostic value of sperm DNA fragmentation and sperm high-magnification for predicting outcome of assisted reproduction treatment. *Asian J Androl.* 2013; 15(6): 790-794.
- Cassuto NG, Hazout A, Hammoud I, Balet R, Bouret D, Barak Y, et al. Correlation between DNA defect and sperm-head morphology. *Reprod Biomed Online.* 2012; 24(2): 211-218.
- Perdrix A, Travers A, Chelli MH, Escalier D, Do Rego JL, Milazzo JP, et al. Assessment of acrosome and nuclear abnormalities in human spermatozoa with large vacuoles. *Hum Reprod.* 2011; 26(1): 47-58.
- Carrell DT, Liu L. Altered protamine 2 expression is uncommon in donors of known fertility, but common among men with poor fertilizing capacity, and may reflect other abnormalities of spermiogenesis. *J Androl.* 2001; 22(4): 604-610.
- de Mateo S, Gázquez C, Guimerà M, Balasch J, Meistrich ML, Ballescà JL, et al. Protamine 2 precursors (Pre-P2), protamine 1 to protamine 2 ratio (P1/P2), and assisted reproduction outcome. *Fertil Steril.* 2009; 91(3): 715-722.
- Aoki VW, Liu L, Jones KP, Hatasaka HH, Gibson M, Peterson CM, et al. Sperm protamine 1/protamine 2 ratios are related to in vitro fertilization pregnancy rates and predictive of fertilization ability. *Fertil Steril.* 2006; 86(5): 1408-1415.
- Rogenhofer N, Ott J, Pilatz A, Wolf J, Thaler CJ, Windischbauer L, et al. Unexplained recurrent miscarriages are associated with an aberrant sperm protamine mRNA content. *Hum Reprod.* 2017; 32(8): 1574-1582.
- Moghbelinejad S, Najafipour R, Hashjin AS. Comparison of protamine 1 to protamine 2 mRNA ratio and YBX2 gene mRNA content in testicular tissue of fertile and azoospermic men. *Int J Fertil Steril.* 2015; 9(3): 338-345.
- Kacem O, Sifer C, Barraud-Lange V, Ducot B, De Ziegler D, Poirot C, et al. Sperm nuclear vacuoles, as assessed by motile sperm organellar morphological examination, are mostly of acrosomal origin. *Reprod Biomed Online.* 2010; 20(1): 132-137.

***CircRNA-011235* Counteracts The Deleterious Effect of Irradiation Treatment on Bone Mesenchymal Stem Cells by Regulating The *miR-741-3p/CDK6* Pathway**

Xianhui Wen, M.D.¹, Hebin Xie, M.D.², Rong Gui, Ph.D.¹, Xinmin Nie, Ph.D.³, Dongyong Shan, M.D.⁴,

Rong Huang, M.D.¹, Hongyu Deng, M.D.⁴, Junhua Zhang, M.D.^{1*}

1. Department of Blood Transfusion, The Third Xiangya Hospital of Central South University, Changsha, China

2. Research and Teaching Department, Changsha Central Hospital, Changsha, Hunan, China

3. The Third Xiangya Hospital of Central South University, Changsha, China

4. Hunan Cancer Hospital and The Affiliated Cancer Hospital of Xiangya School of Medicine, Central South University, Changsha, China

*Corresponding Address: Department of Blood Transfusion, The Third Xiangya Hospital of Central South University, Changsha, China

Email: jhzhangjunhua@163.com

Received: 01/July/2020, Accepted: 24/October/2020

Abstract

Objective: The present work was aimed at uncovering the effect of *circRNA-011235* (*circ-011235*) on irradiation-induced bone mesenchymal stem cells (BMSCs) injury and its regulatory mechanism, with a view to establish a scientific basis for its possible medical applications.

Materials and Methods: In this experimental study, after irradiation with different doses (0, 2, 4, 6 GY), the relative expression levels of *circ-011235*, *miR-741-3p*, and cyclin-dependent kinases 6 (*CDK6*) were detected in the BMSCs, using the real time-quantitative polymerase chain reaction (RT-qPCR). The overexpression effects of *circ-011235* and *CDK6* on the cell proliferation in irradiation-treated BMSCs were measured by the Cell Counting Kit-8 (CCK8) assay. And also, their effects on the cell cycle were evaluated by flow cytometry. RT-qPCR and immunoblotting were performed to detect the effects of *pcDNA-circ-011235* and *pcDNA-CDK6* on the expression of *cyclin D1* and cyclin-dependent kinases 4 (*CDK4*) at the gene and protein levels, respectively.

Results: Irradiation treatment elevated the expression of *circ-011235* and *CDK6*, but reduced *miR-741-3p* expression in the BMSCs with a dose-dependent effect. The proliferation of BMSCs was significantly inhibited in the irradiation treatment group, while the overexpression of *circ-011235* and *CDK6* effectively attenuated this inhibition. Also, overexpression of *circ-011235* and *CDK6* elevated the expression of *cyclin D1* in irradiation-treated BMSCs, but had no significant effect on the *CDK4* expression.

Conclusion: Our results demonstrated that *circ-011235* up-regulated the expression of *cyclin D1* via *miR-741-3p/CDK6* signal pathway, thereby promoting cell cycle progression and proliferation of irradiation-treated BMSCs. This finding suggested *circ-011235/ miR-741-3p/CDK6* pathway exerted a protective role in the response to irradiation and will be a potential new target for future research on the mechanism involved in the resistance of BMSCs to radiation.

Keywords: Bone Mesenchymal Stem Cell, CDK6, Cell Cycle, Irradiation

Cell Journal(yakhteh), Vol 24, No 1, January 2022, Pages: 15-21

Citation: c *CircRNA-011235* counteracts the deleterious effect of irradiation treatment on bone mesenchymal stem cells by regulating the *miR-741-3p/CDK6* pathway. Cell J. 2022; 24(1): 15-21. doi: 10.22074/cellj.2022.7697.

This open-access article has been published under the terms of the Creative Commons Attribution Non-Commercial 3.0 (CC BY-NC 3.0).

Introduction

Bone marrow transplantation (BMT) remains the fundamental treatment for various hematological malignancies, aplastic anemia, severe thalassemia, and some congenital immune deficiency or metabolic diseases (1). Total body irradiation (TBI) is one of the most important pretreatment methods for BMT in the patients with leukemia (2). While TBI pretreatment induces bone mesenchymal stem cells (BMSCs) injury, BMT may seriously interfere with the implantation and transplantation of hematopoietic stem cells (HSCs). Also, TBI pretreatment will inevitably cause other normal cells damages as well as body tissue cells in the bone marrow, and consequently, destroy the hematopoietic system (3). When the body is exposed to irradiation, a series of adaptive stress responses are triggered to repair the damage and reduce the effects of injury (4). At present, the damage mechanism in these patients before BMT

radiotherapy is not fully understood. Further study on the regulatory mechanism of irradiation stress and elucidation of the molecular mechanism of irradiation biological effect will lay a theoretical foundation for the protection and treatment of irradiation injury in the TBI treated patients.

CircRNAs are a particular type of non-coding RNAs characterized by a closed ring lacking a 5' cap and a 3' end poly (A) features. They regulate gene expression in the eukaryotes via RNA-RNA interaction at post-transcriptional levels (5). Some circRNAs are molecular sponges of their target miRNAs, which can chelate and inhibit miRNAs activity (6). The interaction between circRNAs and miRNAs implicated in numerous processes suggests their critical regulatory roles in these processes (7, 8). In our previous studies, we found that *circ-011235* and *circ-016901* are significantly up-regulated in the

mice BMSCs follow of TBI irradiation. Bioinformatics analysis, we concluded that *circRNA-011235* (*circ-011235*) can be acted as a *miR-741-3p* sponge (9). Previous studies showed that *miR-741-3p* can be used as a biomarker for non-alcoholic fatty liver disease (10) and attention-deficit/hyperactivity disorder (11). However, there are limited studies concerning *circ-011235* and *miR-741-3p* and irradiation-induced BMSCs injury.

The cell cycle is a process tightly regulated by cyclins and cyclin-dependent kinases (CDKs) (12). CDK6, a catalytic subunit of the CDK complex, drives the G1 phase process and G1/S transition of the cell cycle. CDK6 activity first appeared in the mid-G1 phase, which is precisely controlled by many regulatory subunits such as family members of inhibitor of cyclin-dependent kinase 4 (*INK4*) and D-type cyclins. Cyclin D1 plays an essential regulatory role in the cell cycle and is a key regulatory protein of the G1 phase (13). *Cyclin D1* overexpression may lead to an uncontrolled cell proliferation (14). Studies have shown that CDK4 and CDK6 form a complex with cyclin D1 to promote G1-S phase transformation via promoting the phosphorylation of tumor suppressor retinoblastoma (Rb) and formation of CDK2/Cyclin E complex (15).

Here, we attempted to explore the potential role of *circ-011235* in the proliferation of BMSC following irradiation injury. And also, we investigated the irradiation-induced self-protection mechanism of *circ-011235* in the cell cycle regulation, which may provide novel clinical targets for protecting BMSCs from radiation damage.

Materials and Methods

Ethical consideration

In this experimental study, all animal procedures complied with the guidelines permitted by the Animal Care and Use Committee of XiangYa School of Medicine (No. 2019-S534).

Isolation, culture and identification of bone mesenchymal stem cells

Twenty healthy 2-month-old male BALB/c mice (21 ± 3 g) were provided from the XiangYa School of Medicine of Central South University, China.

Isolation, culture and identification of BMSCs from femurs and tibias were performed as described in our previous study (9). Briefly, after exposure to CO₂, the femurs and tibias of euthanized mice were separated and freshly isolated bone marrow cells were washed and then, cultured in the Dulbecco's Modified Eagle's medium (DMEM, Cat No. 12634010, ThermoFisher Scientific, Shanghai, China) containing 10% fetal bovine serum (FBS, Cat No. 10099133C, ThermoFisher Scientific, Shanghai, China) and incubated at 37°C in 5% CO₂ for 24 hours. The DMEM was replaced every three days. Using CytoFLEX V2-B2-R0 Flow Cytometer (model No. C09752, Beckman Coulter, Miami, FL, USA), the

cells were sorted with FITC-labeled CD34, CD45, CD90 and Sca-1 after obtaining 80% confluency. Isolated cells that were identified to be CD34(-), CD45(-), CD90(+) and Sca-1(+) were considered as BMSCs and used in subsequent experiments.

Radiation treatment

A cell suspension of BMSCs was prepared by trypsinization with 0.25% trypsin (Cat No. 25300120, ThermoFisher Scientific, Shanghai, China), and the cell density was maintained at 2×10⁶ cells/mL. Subsequently, the BMSCs were exposed to different doses of irradiation (0, 2, 4, 6 Gy) for 6 hours by using 6 MV X-rays of a 137 Cs-γ source (Sangyo Kagaku, Japan) at an irradiation rate of 0.4 Gy/minutes and a distance of 100 cm from the source.

Circ-011235 siRNA interference assay

Small interfering RNA (siRNA) targeting *circ-011235* (*siRNA-011235*) and scrambled siRNA negative control (*siNC*) were commercially available from KangChen Bio-tech (Shanghai, China). Using the Lipofectamine 2000 kit (Cat No. 11-668-500, Invitrogen, Carlsbad, CA, USA), BMSCs in the logarithmic phase were transfected with *siRNA-011235* and *siNC*, according to the protocols provided by the manufacturer. Briefly, the siRNAs were mixed for 20 min with Lipofectamine 2000 to prepare the Lipofectamine 2000/siRNA complexes. Meanwhile, the BMSCs were incubated with DMEM medium at 37°C for 24 hours in 96-well plates. After that, the medium was refreshed and Lipofectamine 2000/siRNA complexes were added dropwise to the BMSCs while gently shaking the plate. Next, after incubation in 5% CO₂ incubator for 5 hours, the transfection efficiency was examined by Reverse-transcription quantitative polymerase chain reaction (RT-qPCR).

Dual luciferase reporter assay

The potential negative regulatory relationship between *circ-011235* and *miR-741-3p* was found by Bioinformatics analysis. Also, predicted databases, Targetscan and miRBase, were used to identify a binding site between the *CDK6* gene and *miR-741-3p*. The respective fragments of *circ-011235* and *CDK6* harboring *miR-741-3p* binding sites, *miR-741-3p* mimic, and miRNA negative control (mimic control) were synthesized by GenePharma (Shanghai, China). Subsequently, the fragments were subcloned into the *psiCHECK-2 Renilla* (Cat No. C8021, Promega, Madison, WI, USA) luciferase reporter vector following the manufacturer's instructions. BMSCs were cotransfected with *circ-011235/CDK6* wild type (WT) vectors or *circ-011235/CDK6* mutated (MUT) vectors with *miR-741-3p* mimic via the Lipofectamine 2000 (Cat No. 11-668-500, Invitrogen, Carlsbad, CA, USA) transfection approach. The Dual-Luciferase Reporter Assay System (Promega, Madison, WI, USA) was employed for assessing renilla luciferase activity.

Circ-011235 and CDK6 overexpression assay

Sequences of *circ-011235* and *CDK6* gene were synthesized by KangChen Bio-tech (Shanghai, China) and cloned into the expression vector *pcDNA3.1* (Cat No. V79020, Invitrogen, Carlsbad, CA, USA) to generate the overexpression recombinant plasmids *pcDNA-circ-011235* and *pcDNA-CDK6*, and the empty vector *pcDNA3.1* was used as a negative control. The recombinant plasmids were identified by RT-qPCR and DNA sequencing. Then, recombinant plasmids were transfected into the logarithmic phase BMSCs by Lipofectamine 2000 kit (Cat No. 11-668-500, Invitrogen, Carlsbad, CA, USA) based on the manufacturer's protocol. RT-qPCR was performed to detect the transfection efficiency 48 hours after transfection.

Cell proliferation assay

Following of 6 GY of irradiation treatment, transfected cells were cultured in 96-well plates and the cell concentration was maintained at 5×10^3 cells/well. The cell proliferation at 12, 24, 36 and 48 hours after seeding was evaluated using the CCK8 assay (Cat No. GK10001, Glpbio, Montclair, CA, USA). In brief, we added 10 μ L CCK8 solution to each sample and incubated for 2 hours. Subsequently, the absorbance was detected by the spectrophotometric approach at 450 nm wavelength.

Cell cycle analysis

Twenty four hours after transfection, BMSCs were harvested by centrifugation at 1200 rpm for 5 minutes. The number of BMSCs was calculated using a haemocytometer, and the final density of cells was maintained at 1×10^6 cells/mL with phosphate buffer saline (PBS, Cat No. C791P76, Thomas Scientific, Swedesboro, NJ, USA). Subsequently, the cells were fixed with 70% ethanol (3 mL) at 4°C overnight, and collected by centrifugation at 1200 rpm for 5 minutes. Next, 200 μ L of RNase (Cat No. AM2288, ThermoFisher Scientific, Shanghai, China) was added, followed by incubation at 37 °C for 30 minutes. Afterwards, 800 μ L of propidium iodide (PI, 20 mg/mL, Cat No. P1304MP, ThermoFisher Scientific, Shanghai, China) was added, followed by incubation for 30 minutes at 25°C in the dark. The distribution of cells was detected by flow cytometry (Beckman, Los Angeles, CA, USA).

Real time-quantitative polymerase chain reaction

After transfection, total RNA of BMSCs was extracted by TRIzol Reagent (Cat No. 15596018, ThermoFisher Scientific, Shanghai, China), based on the manufacturer's directives. The isolated total RNA (20 ng/ μ L) was employed to synthesize the cDNA by reverse transcription using the GoScript reverse transcriptase (Promega, Charbonnières-les-Bains, France). For *circ-011235*, the RNase R digestion reaction was performed at a ratio of 3U enzyme/1 μ g RNA before reverse transcription. The cDNA library was amplified using the Gene Amp PCR System 9700 (Applied Biosystems, Foster City, CA, USA). The reaction was started at 95°C for

2 minutes and then subjected to 40 cycles of 95°C for 10 seconds and 60 °C for 60 seconds. The primer sequences were synthetically produced by KangChen Bio-tech (Shanghai, China). The primer sequences were displayed in Table 1. The $2^{-\Delta\Delta Ct}$ formula was applied to measure the relative expression of *circ-011235*, *miR-741-3p*, *CDK6* and *CDK4* (16).

Table 1: The primer sequences used in this study

Gene	Primer sequence (5'-3')
<i>GADPH</i>	F: CACTGAGCAAGAGAGGCCCTAT R: GCAGCGAACTTTATTGATGGTATT
<i>circ-011235</i>	F: AACAAAGGACCGAACTAAGAGG R: TGTATCCACCAGAATTACTCCC
<i>miR-741-3p</i>	F: TGGATGCCACGCTATGTAGAT R: GCGACGAGCAAAAAGCTTGT
<i>CDK6</i>	F: GCTGACCAGCAGTAC GAATG R: GCACACATCAAACAACCTGACC
<i>cyclin D1</i>	F: TGTTCGTGGCCTCTAAGATGAAG R: AGGTTCCACTTGAGCTT GTTCAC
<i>CDK4</i>	F: TTGCATCGTTCACCGAGATC R: CTGGTAGCTGTAGATTCTGGCCA

Protein extraction, purification and western blotting

Radio-immunoprecipitation assay (RIPA) lysis buffer (Cat No. 20-188, Merck, Shanghai, China) was used to extract the total cellular RNA while this contains an inhibitor cocktail mixture of phosphatase and protease (Cat No. ab201119, Abcam, Waltham, MA, USA). Next, protein concentration of the collected supernatant was measured by Pierce BCA assay kit (Cat No. 23225, ThermoFisher Scientific, Rockford, IL, USA). The extracted proteins were transferred to polyvinylidene fluoride (PVDF) membranes (Cat No. IPVH00010, Merck, Shanghai, China) after purification on 10% SDS-PAGE (Cat No. MT-46040CI, Fisher Scientific, Loughborough, USA), and then, 5% skim milk (Cat No. 100518-0201, Medallion Milk Co., Winnipeg, MB, USA) was used to block the membranes. Next, the membranes were reacted with our primary antibodies at 4°C overnight. Our primary antibodies were included : CDK4 (1:1000; Cat No. 12790, Cell Signaling Technology, Beverly, MA, USA), cyclin D1 (1:1000; Cat No. 55506, Cell Signaling Technology, Beverly, MA, USA) and GAPDH (1:2000; Cat No. 5174, Cell Signaling Technology, Beverly, MA, USA). Then, the membranes were incubated at 37°C for 60 min with the HRP-labeled secondary antibody (1:2000; Cat No. 7074, Cell Signaling Technology, Beverly, MA, USA). Subsequently, a chemiluminescence imaging system (model No. GeneGnome XRQ, Syngene, Cambridge, UK) was used to examine the immunoblot signals of the target proteins, and GAPDH was chosen as a housekeeping endogenous

control for these proteins. The analysis of protein bands was performed using the software Image J (National Institutes of Health, Bethesda, MD, USA).

Statistical analysis

The results were analysed by SPSS 28.0.1 software (IBM, Armonk, NY, USA). All data were presented as mean \pm standard deviation (SD). All data were analyzed using one-way or two-way analysis of variance (ANOVA) followed by Turkey's Post Hoc multiple comparison test to detect the differences among the groups. Pearson correlation analysis was achieved using the R package Hmisc. Also, $P < 0.05$ was considered for statistical significance.

Results

Irradiation increased the expression of *circ-011235* and *CDK6*

To examine the relationship between the expression of *circ-011235*, *miR-741-3p* and *CDK6*, the correlation of their expression levels in the BMSCs treated with irradiation was analyzed. It was found that the irradiation treatment increased the expression of *circ-011235* and *CDK6* in the BMSCs in comparison with the control group (0 GY) ($P < 0.01$, Fig.1A, B) but decreased the expression of *miR-741-3p* ($P < 0.01$, Fig.1C); there was a significant dose-dependent effect (2 GY < 4 GY < 6 GY) in the irradiation treated BMSCs. The Pearson correlation analysis found a strong correlation between *circ-011235* and *CDK6* ($r = 0.99$, $P < 0.05$, Fig.1D). Additionally, *miR-741-3p* expression was negatively interrelated with the expression levels of *circ-011235* ($r = -0.98$, $P < 0.05$) and *CDK6* ($r = -0.97$, $P < 0.05$, Fig.1D).

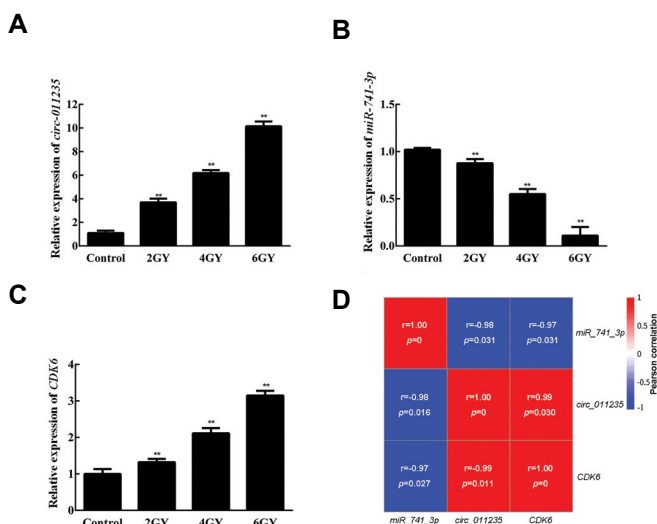


Fig.1: RT-qPCR detection of gene expression in the BMSCs after irradiation treatment with different doses (0, 2, 4, 6 GY). **A.** Relative expression of *circ-011235*. **B.** Relative expression of *miR-741-3p*. **C.** Relative mRNA expression of *CDK6* in the BMSCs. **D.** Pearson correlation analysis of the correlation among *circ-011235*, *miR-741-3p*, and *CDK6* in the BMSCs after irradiation treatment. Data were represented by mean \pm SD. Independent experiments were replicated three times, **, $P < 0.01$, vs. the control group, RT-PCR; Real time-quantitative polymerase chain reaction, and BMSCs; Bone mesenchymal stem cells.

Circ-011235 regulated *miR-741-3p*/*CDK6* pathway in irradiation-treated bone mesenchymal stem cells

Using online databases, IntaRNA, TargetScan, and miRBase, we observed that *miR-741-3p* have a potential binding site for *circ-011235* (Fig.2A), and a unique binding site with 7 base pairs between 3'-UTR of *CDK6* gene and *miR-741-3p* (Fig.2B). The results showed that *circ-011235* siRNA significantly up-regulated the expression of *miR-741-3p*, but down-regulated the expression of *CDK6* ($P < 0.01$, Fig.2C, D). The transfection efficiency of *miR-741-3p* mimic was examined using RT-qPCR, and the results indicated that *miR-741-3p* overexpression significantly upregulated the expression of *miR-741-3p* ($P < 0.01$, Fig.2E). In addition, *miR-741-3p* overexpression significantly decreased luciferase activity in the *WT-circ-011235* and *WT-CDK6* transfected cells ($P < 0.01$) but there was no significant effect on luciferase activity in the *MUT-circ-011235* and *MUT-CDK6* transfected cells ($P > 0.05$, Fig.2F, G).

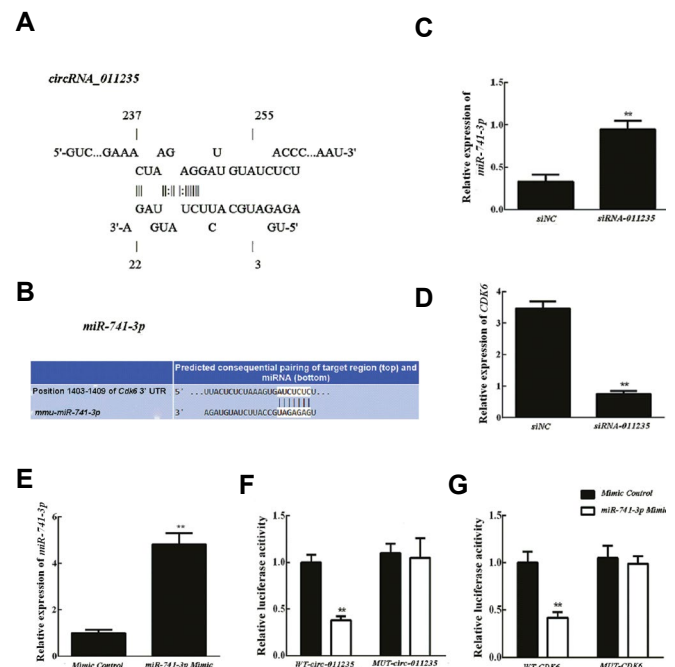


Fig.2: *Circ-011235*/*miR-741-3p*/*CDK6* signal pathway. **A.** IntaRNA prediction of *miR-741-3p* as a target for *circ-011235*. **B.** TargetScan prediction of 3'-UTR of *CDK6* gene as a target for *miR-741-3p*. **C.** *Circ-011235* silencing upregulates the *miR-741-3p* expression in the BMSCs. **D.** *Circ-011235* silencing decreases the *CDK6* expression in the BMSCs. **E.** Evaluation by RT-qPCR of the transfection efficiency of *miR-741-3p* mimic. **F.** Luciferase reporter assay illustrating the interactions between *circ-011235* and *miR-741-3p*. **G.** Luciferase reporter assay illustrating the interactions between *CDK6* and *miR-741-3p* in the BMSCs. Data were represented by mean \pm SD. Independent experiments were replicated three times, **, $P < 0.01$, vs. the control group, RT-PCR; Real time-quantitative polymerase chain reaction, and BMSCs; Bone mesenchymal stem cells.

Overexpression of *circ-011235* and *CDK6* increased the irradiation-treated bone mesenchymal stem cells proliferation

To investigate the transfection efficiency of *pcDNA-circ-011235* and *pcDNA-CDK6*, we detected the expression levels of *circ-011235* and *CDK6* in

BMSCs. The results showed that *pcDNA-circ-011235* significantly up-regulated *circ-011235* in comparison with the control group ($P < 0.01$, Fig.3A), and *pcDNA-CDK6* treatment led to the similar results for the *CDK6* cell (Fig.3B). Furthermore, we also examined the overexpression effect of *circ-011235* and *CDK6* on the proliferation after exposure to 6 Gy irradiation. It was found that irradiation treatment hindered the proliferation of BMSCs compared with the control group ($P < 0.01$); however, overexpression of *circ-011235* or *CDK6* significantly reversed this inhibitory effect after 24 hours seeding (Fig.3C).

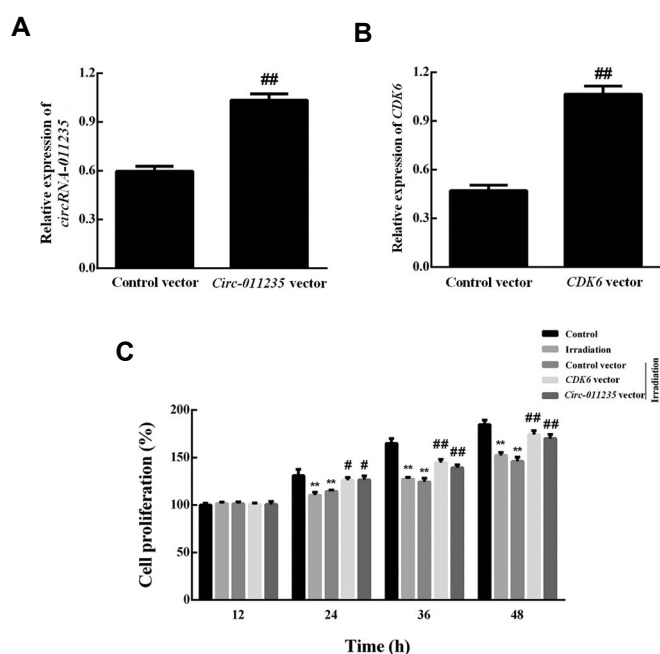


Fig.3: Effect of *circ-011235* and *CDK6* on the proliferation of irradiation-treated BMSCs. **A.** RT-qPCR detection of transfection efficiency of *pcDNA-circ-011235*. **B.** RT-qPCR detection of transfection efficiency of *pcDNA-CDK6*. **C.** CCK-8 assay detection of the effects of *pcDNA-circ-011235* and *pcDNA-CDK6* on the proliferation of irradiation-treated BMSCs. Values were represented by the mean \pm SD. Separated experiments were repeated three times. **, $P < 0.01$, vs. the control group, #, $P < 0.05$, ###, $P < 0.01$, vs. the irradiation treatment group and control vector group, RT-PCR; Real time-quantitative polymerase chain reaction, BMSCs; Bone mesenchymal stem cells, and h; Hour.

Overexpression of *circ-011235* and *CDK6* affected the cell cycle of irradiation-treated bone mesenchymal stem cells

To investigate the overexpression effect of *circ-011235* and *CDK6* on cell proliferation, cell cycle analysis was performed. When compared with the control group, the results showed that irradiation treatment significantly increased the percentage of cells in the G1 phase ($P < 0.01$), while the proportion of cells in the S phase was significantly declined ($P < 0.01$, Fig.4A). However, compared with the irradiation-treated group, *circ-011235* overexpression significantly reduced the percentage of cells in the G1 phase and elevated the percentage of cells in the S phase ($P < 0.01$, Fig.4A). Similar results were found with the *CDK6* overexpression.

Also, the expression analysis of cyclin D1 showed that cyclin D1 was significantly up-regulated in the *circ-011235* overexpression group and *CDK6* overexpression group compared to the irradiation-treated group ($P < 0.01$), while there was no significant change in *CDK4* expression (Fig.4B-D).

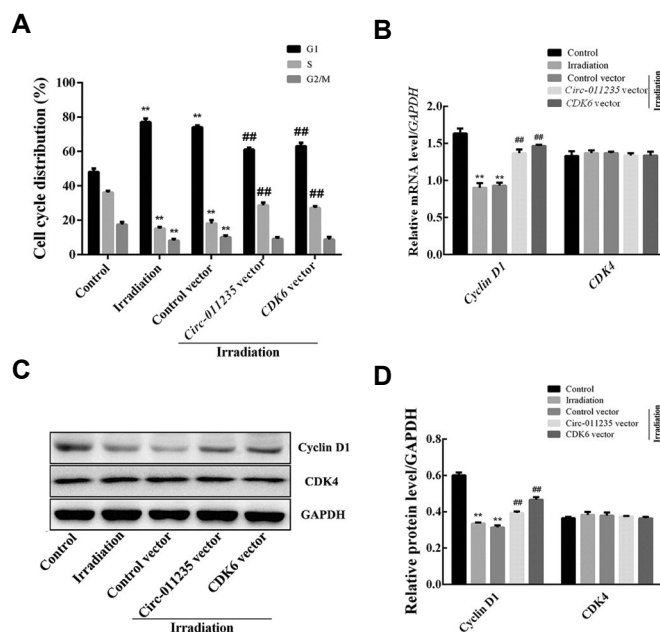


Fig.4: Effects of *circ-011235* and *CDK6* on the cell cycle in the irradiation-treated BMSCs. **A.** Flow cytometry analysis of the effects of *pcDNA-circ-011235* and *pcDNA-CDK6* on the cell cycle in the irradiation-treated BMSCs. **B.** RT-qPCR detection of the expression of *cyclin D1* and *CDK4* at the gene level. **C.** Western blot detection of the expression of *cyclin D1* and *CDK4* at the protein levels. **D.** Densitometry analysis of western blot bands of the expression of cyclin D1 and CDK4. Data were represented by mean \pm SD. Separate experiments were replicated three times, **, $P < 0.01$, vs. the control group, ##, $P < 0.01$, vs. the irradiation treatment group and control vector group, RT-PCR; Real time-quantitative polymerase chain reaction, and BMSCs; Bone mesenchymal stem cells.

Discussion

HSC transplantation has been achieved a huge success in the treatment of blood system diseases and is currently known as a most effective cell replacement therapy. TBI is one of the necessary pretreatments for HSC transplantation (17). Whether the injury of TBI to BMSCs affects the hematopoietic function of HSCs. Although, its regulatory mechanism is not fully known, rational treatment plans will direct to high efficiency and low toxicity in the clinical phase.

The hematopoietic support of BMSCs mainly regulates the survival, self-renewal, migration and differentiation of hematopoietic stem or progenitor cells through intercellular interactions and secretion of growth factors, chemical factors, and extracellular matrix (18). Co-infusion of HSCs and MSCs heterogeneity have been observed to promote hematopoietic reconstruction (19). BMSCs with low immunogenicity and immunomodulation can avoid and alleviate host immune responses, induce the formation of specific immune tolerance, and promote the transplantation of HSCs. It repairs tissue injury

caused by pre-transplant pretreatment, which can reduce the incidence of severe GVHD and transplant-related mortality (20). Compared with HSCs, BMSCs are highly resistant to irradiation and can survive acute exposure (21), which is an important hematopoietic support cell for hematopoietic recovery after irradiation. The study of irradiation-induced injury in the BMSCs has significant implications to improve the HSCs transplantation survival rate. In the present study, the expression of *circ-011235*, *miR-741-3p*, and *CDK6* was dose-dependent after irradiation for 6 h, indicating that irradiation can change the molecular profile of BMSCs.

Studies have shown that non-coding RNAs such as circRNAs and miRNAs act as gene expression regulators and have been confirmed to be involved in the regulation of the cell proliferation such as cancer cells (22). CircRNA contains miRNA response elements, which act as a competitive endogenous RNA to compete binding site between miRNA and its target gene, thereby may be acted as a eliminating agent against the inhibitory effect of miRNA on their target gene (23). In this study, our results showed that *circ-011235* increases the cell proliferation and progresses cell cycle of irradiation-treated BMSCs by down-regulating *miR-741-3p* expression and up-regulating *CDK6* expression. This suggests that *circ-011235* derepresses *CDK6* gene by acting as a sponge of *miR-741-3p* to counteract the irradiation-induced damage of BMSCs. This is the first study to explore the role and function of *circ-011235* and *miR-741-3p* in the irradiation-induced BMSCs injury.

As an oncogene, *CDK6* can promote the cell proliferation and play a regulatory role in the occurrence and development of various cancers, such as bladder cancer, glioma, and medulloblastoma (24). Cyclin D-associated kinases inhibitors such as CDK4 and CDK6 can be used as a potential cancer therapeutic targets. The function and regulation mechanism of *CDK6* in the BMSCs are still not clearly explained. CDK6, together with CDK4, acts as a switching signal in the G1 phase that, directing cells towards the S phase (25). CDK6 is an important driving factor in the shift of the cell cycle from G1 to S stage. However, a previous study showed that the cell cycle is regulated by complex regulatory pathways, and CDK6 is not necessary for the proliferation of every cell type (26). In addition, CDK4 or CDK2 are protein kinases that compensate the effects of CDK6. Moreover, CDK6 is primarily associated with cyclins proteins such as cyclins D1, D2, and D3 (27). The positive activation of CDK6 can be achieved by phosphorylation of the 177th conserved threonine residue by CDK activated kinase (CAK) (28). In addition, Kaposi's sarcoma-associated herpesvirus can phosphorylate and overactive CDK6, and cause uncontrolled cell proliferation (29). In the present study, our results demonstrated that *circ-011235* and *CDK6* were activated by irradiation and their expression associated with a dose-dependent increase effect. Similarly, a previous study in mice found that the cell viability was reduced by ultraviolet light C

(UVC) treatment, but loss of *Runx2* could counteract UVC induced cell death by increasing the expression of cyclins and related CDK activities (30). Moreover, Zou et al. (31) showed that the Cell Division Cycle 25A (*CDC25A*), an activator of G1 CDKs in the nucleus, could inhibit the oxidant-triggered gamma irradiation induced apoptosis via diminishing the activation of the oxidative stress kinase cascades. Furthermore, the complex of cyclin D1 with CDK4 and CDK6 is involved in the regulation of the cell cycle, which phosphorylates the Rb protein, thereby promoting the cell cycle from G1 to S stage (32). Previous studies showed that CDK6 activity elevates in the cultured mouse astrocytes without alteration of CDK4 activity (33). Also, we found that overexpressions of *circ-011235* and *CDK6* both promoted the proliferation and cell cycle through increasing the expression of cyclin D1 in the irradiation treated BMSCs, which suggested its vital role in the self-protection mechanism of BMSCs in response to irradiation. We did not same results in the overexpression of CDK4.

Finally, our study presents some limitations. In cell cycle analysis, only cyclin D1 and CDK4 protein and mRNA expression were detected, and further cyclins such as cyclin E, CDK2, and p27 kipl are required to increase the confidence of our findings. Moreover, animal experiments are needed to explore the potential role of *circ-011235*, *miR-741-3p*, and *CDK6*. However, further measurement methods are still needed to confirm our findings.

Conclusions

In this study, we uncovered the regulatory function of *circ-011235* on the cell cycle in the irradiation-treated BMSCs. Our results showed that *circ-011235* increases the irradiation-treated BMSCs proliferation and promotes cell cycle progression through down-regulating *miR-741-3p* and up-regulating *CDK6*. Also, *Circ-011235* and *CDK6* overexpression could effectively reverse the inhibitory effect of irradiation on the proliferation and cell cycle arrest of the BMSCs through promoting the expression of cyclin D1. This is the first study to demonstrate the protective role of *circ-011235/miR-741-3p/CDK6* axis, especially *circ-011235* and *miR-741-3p*, against irradiation-induced damage of BMSCs. The *circ-011235/miR-741-3p/CDK6* axis may be a probable therapeutic target in the clinical application of TBI-induced BMSCs injury.

Acknowledgments

The authors wish to thank all his collaborators for this work. We thank Hunan Natural Science Foundation for their kind supporting. This study was supported by the Hunan Natural Science Foundation (2018JJ3791). All data generated or analyzed during this study are included in this published article. The authors declare that they have no competing interests.

Authors' Contributions

X.W., H.X., R.G., X.N., D.S., R.H., H.D.; Experiment performance, data collection and interpretation. X.W., H.X., R.G., X.N., D.S., R.H., H.D., J.Z.; Study design, data collection, evaluation, participation in manuscript preparation, data analysis and manuscript drafting. All authors read and approved the final manuscript.

References

- Borel C, Ahmad I, Ceballos P, Desbrosses Y, Hamzy F, Ravinet A, et al. Hematopoietic stem cell transplantation ocular complications: guidelines from the Francophone Society of Bone Marrow Transplantation and Cellular Therapy (SFGM-TC). *Bull Cancer*. 2020; 107(12S): S116-S121.
- Gieger TL, Nolan MW, Roback DM, Suter SE. Implementation of total body photon irradiation as part of an institutional bone marrow transplant program for the treatment of canine lymphoma and leukemias. *Vet Radiol Ultrasound*. 2019; 60(5): 586-593.
- Wang Y, Zhang J, Li J, Gui R, Nie X, Huang R. CircRNA_014511 affects the radiosensitivity of bone marrow mesenchymal stem cells by binding to miR-29b-2-5p. *Bosn J Basic Med Sci*. 2019; 19(2): 155-163.
- Bianchi ME, Crippa MP, Manfredi AA, Mezzapelle R, Rovere Querini P, Venereau E. High-mobility group box 1 protein orchestrates responses to tissue damage via inflammation, innate and adaptive immunity, and tissue repair. *Immunol Rev*. 2017; 280(1): 74-82.
- Chan JJ, Tay Y. Noncoding RNA:RNA regulatory networks in cancer. *Int J Mol Sci*. 2018; 19(5): 1310.
- Xiong DD, Dang YW, Lin P, Wen DY, He RQ, Luo DZ, et al. A circRNA-miRNA-mRNA network identification for exploring underlying pathogenesis and therapy strategy of hepatocellular carcinoma. *J Transl Med*. 2018; 16(1): 220.
- Lin X, Chen Y. Identification of potentially functional circrna-mirna-mrna regulatory network in hepatocellular carcinoma by integrated microarray analysis. *Med Sci Monit Basic Res*. 2018; 24: 70-78.
- Zhang Q, Zhang W, Nogales-Cadenas R, Lin JR, Cai Y, Zhang ZD. From gene expression to disease phenotypes: network-based approaches to study complex human diseases. Dordrecht: Springer; 2016.
- Zhang J, Jiang J, Huang R, Wang Y, Nie X, Gui R. Circular RNA expression profiles are significantly altered in mice bone marrow stromal cells after total body irradiation. *Leuk Res*. 2018; 70: 67-73.
- Nie J, Li CP, Li JH, Chen X, Zhong X. Analysis of nonalcoholic fatty liver disease microRNA expression spectra in rat liver tissues. *Mol Med Rep*. 2018; 18(3): 2669-2680.
- Tian T, Zhang Y, Wu T, Yang L, Chen C, Li N, et al. miRNA profiling in the hippocampus of attention-deficit/hyperactivity disorder rats. *J Cell Biochem*. 2019; 120(3): 3621-3629.
- Pack LR, Daigh LH, Meyer T. Putting the brakes on the cell cycle: mechanisms of cellular growth arrest. *Curr Opin Cell Biol*. 2019; 60: 106-113.
- Dong P, Zhang C, Parker BT, You L, Mathey-Prevot B. Cyclin D/CDK4/6 activity controls G1 length in mammalian cells. *PLoS One*. 2018; 13(1): e0185637.
- Fu X, Feng Y. QKI-5 suppresses cyclin D1 expression and proliferation of oral squamous cell carcinoma cells via MAPK signalling pathway. *Int J Oral Maxillofac Surg*. 2015; 44(5): 562-567.
- VanArsdale T, Boshoff C, Arndt KT, Abraham RT. Molecular pathways: targeting the cyclin D-CDK4/6 axis for cancer treatment. *Clin Cancer Res*. 2015; 21(13): 2905-2910.
- Said R, Garcia-Mayea Y, Trabelsi N, Setti Boubaker N, Mir C, Blel A, et al. Expression patterns and bioinformatic analysis of miR-1260a and miR-1274a in prostate cancer tunisian patients. *Mol Biol Rep*. 2018; 45(6): 2345-2358.
- Davis NL, Stewart CE, Moss AD, Woltersdorf WW, Hunt LP, Elson RA, et al. Growth hormone deficiency after childhood bone marrow transplantation with total body irradiation: interaction with adiposity and age. *Clin Endocrinol (Oxf)*. 2015; 83(4): 508-517.
- Lin L, Lin H, Bai S, Zheng L, Zhang X. Bone marrow mesenchymal stem cells (BMSCs) improved functional recovery of spinal cord injury partly by promoting axonal regeneration. *Neurochem Int*. 2018; 115: 80-84.
- Mohammadi S, Nikbakht M, Sajjadi SM, Rad F, Chahardouli B, Sabour Takanlu J, et al. Reciprocal interactions of leukemic cells with bone marrow stromal cells promote enrichment of leukemic stem cell compartments in response to curcumin and daunorubicin. *Asian Pac J Cancer Prev*. 2017; 18(3): 831-840.
- von der Heide EK, Neumann M, Vosberg S, James AR, Schroeder MP, Ortiz-Tanchez J, et al. Molecular alterations in bone marrow mesenchymal stromal cells derived from acute myeloid leukemia patients. *Leukemia*. 2017; 31(5): 1069-1078.
- Xiang Y, Wu C, Wu J, Quan W, Cheng C, Zhou J, et al. In vitro expansion affects the response of human bone marrow stromal cells to irradiation. *Stem Cell Res Ther*. 2019; 10(1): 82.
- Kristensen LS, Hansen TB, Venø MT, Kjems J. Circular RNAs in cancer: opportunities and challenges in the field. *Oncogene*. 2018; 37(5):555-565.
- Zhong Y, Du Y, Yang X, Mo Y, Fan C, Xiong F, et al. Circular RNAs function as ceRNAs to regulate and control human cancer progression. *Mol Cancer*. 2018; 17(1): 79.
- Li X, Gong X, Chen J, Zhang J, Sun J, Guo M. miR-340 inhibits glioblastoma cell proliferation by suppressing CDK6, cyclin-D1 and cyclin-D2. *Biochem Biophys Res Commun*. 2015; 460(3): 670-677.
- Molina A, Pituello F. Playing with the cell cycle to build the spinal cord. *Dev Biol*. 2017; 432(1):14-23.
- Satyanarayana A, Kaldis P. Mammalian cell-cycle regulation: several Cdk, numerous cyclins and diverse compensatory mechanisms. *Oncogene*. 2009; 28(33): 2925-2939.
- Malumbres M, Sotillo R, Santamaría D, Galán J, Cerezo A, Ortega S, et al. Mammalian cells cycle without the D-type cyclin-dependent kinases Cdk4 and Cdk6. *Cell*. 2004; 118(4): 493-504.
- He H, Xu J, Xie W, Guo QL, Jiang FL, Liu Y. Reduced state transition barrier of CDK6 from open to closed state induced by Thr177 phosphorylation and its implication in binding modes of inhibitors. *Biochim Biophys Acta Gen Subj*. 2018; 1862(3): 501-512.
- Kaldis P. The N-terminal peptide of the Kaposi's sarcoma-associated herpesvirus (KSHV)-cyclin determines substrate specificity. *J Biol Chem*. 2005; 280(12): 11165-11174.
- Kilbey A, Blyth K, Wotton S, Terry A, Jenkins A, Bell M, et al. Runx2 disruption promotes immortalization and confers resistance to oncogene-induced senescence in primary murine fibroblasts. *Cancer Res*. 2007; 67(23): 11263-11271.
- Zou X, Tsutsui T, Ray D, Blomquist JF, Ichijo H, Ucker DS, et al. The cell cycle-regulatory CDC25A phosphatase inhibits apoptosis signal-regulating kinase 1. *Mol Cell Biol*. 2001; 21(14): 4818-4828.
- Romero-Pozuelo J, Figlia G, Kaya O, Martin-Villalba A, Teleman AA. Cdk4 and Cdk6 couple the cell-cycle machinery to cell growth via mTORC1. *Cell Rep*. 2020; 31(2): 107504.
- Sammons SL, Topping DL, Blackwell KL. HR+, HER2- advanced breast cancer and CDK4/6 inhibitors: mode of action, clinical activity, and safety profiles. *Curr Cancer Drug Targets*. 2017; 17(7): 637-649.

The Effect of Endometrial Cell Culture on $\alpha 3$ and $\beta 1$ integrin Genes and Protein Expression in Type 2 Diabetic Rats at The Time of Implantation

Fatemah Sadat Mostafavi, M.D, Ph.D.¹, Abbas Bakhteyari, Ph.D.¹, Parvaneh Nikpour, Ph.D.^{2,3}, Nahid Eskandari, Ph.D.⁴, Roshanak Aboutorabi, Ph.D.^{1*}

1. Department of Anatomical Sciences, Faculty of Medicine, Isfahan University of Medical Sciences, Isfahan, Iran

2. Department of Genetics and Molecular Biology, Faculty of Medicine, Isfahan University of Medical Sciences, Isfahan, Iran

3. Child Growth and Development Research Center, Research Institute for Primordial Prevention of Non-Communicable Disease, Isfahan University of Medical Sciences, Isfahan, Iran

4. Department of Immunology, Faculty of Medicine, Isfahan University of Medical Sciences, Isfahan, Iran

*Corresponding Address: P.O.Box: 8174673461, Department of Anatomical Sciences, Faculty of Medicine, Isfahan University of Medical Sciences, Isfahan, Iran

Email: aboutorabi.r@gmail.com

Received: 18/March/2020, Accepted: 19/July/2020

Abstract

Objective: Given the prevalence of fertility problems in couples and the defect in embryo implantation as well as the low success rate of assisted reproductive techniques, it is necessary to investigate the causes of this phenomenon. Type 2 diabetes mellitus (T2DM) is a metabolic disease with multiple effects on various organs as well as the endometrium. In this study, the effects of endometrial cell culture on the expression of $\alpha 3$ and $\beta 1$ integrin genes and protein in type 2 diabetic rats were investigated.

Materials and Methods: In this experimental study, 35 female rats were divided into five groups: control, sham, diabetic, Pioglitazone-treated and Metformin-treated groups. First, rats were maintained in diabetic condition for 4 weeks. Then, treatment was performed for the next four weeks. Four weeks after induction of diabetes, rats were sacrificed at the time of embryo implantation. The uterus was removed. Endometrial cells were isolated and cultured for 7 days. Immunocytochemistry staining was used to confirm endometrial cells. Expression of $\alpha 3$ and $\beta 1$ integrin genes was determined by real-time polymerase chain reaction (PCR) technique and the $\alpha 3\beta 1$ protein content measured using Western blot both before and after endometrial cell culture.

Result: The expression level of $\alpha 3$ integrin gene in the Pioglitazone-treated group compared with metformin-treated group was significantly decreased ($P < 0.001$). The same result was observed in $\beta 1$ integrin gene expression ($P = 0.004$). Also, the $\alpha 3\beta 1$ protein level increased in all diabetic groups, but its reduction was significantly greater in pioglitazone-treated group ($P = 0.004$).

Conclusion: T2DM altered the expression of $\alpha 3$ and $\beta 1$ integrin genes and related proteins, which endometrial cell culture regulated this disorder. According to these results, may be the endometrial cell culture can reduce the adverse effects of diabetes on $\alpha 3$ and $\beta 1$ integrin expression at the level of gene and protein, in endometrial cells.

Keywords: Cell Culture, Diabetes Mellitus, Implantation, Integrin Alpha1, Integrin Beta3

Cell Journal (Yakhteh), Vol 24, No 1, January 2022, Pages: 22-27

Citation: Mostafavi FS, Bakhteyari A, Nikpour P, Eskandari N, Aboutorabi R. The effect of endometrial cell culture on $\alpha 3$ and $\beta 1$ integrin genes and protein expression in type 2 diabetic rats at the time of implantation. Cell J. 2022; 24(1): 22-27. doi: 10.22074/cellj.2022.7445.

This open-access article has been published under the terms of the Creative Commons Attribution Non-Commercial 3.0 (CC BY-NC 3.0).

Introduction

Diabetes mellitus can be associated with infertility problems so that fertility rates in women with diabetes are lower than in healthy women (1). In diabetic rats, the uterus is become atrophied, sexual activity reduced and the function of hypothalamic-pituitary-ovarian axis weakened. In addition, ovarian function is impaired and ovulation rates decreased (2). According to statistics, the rate of abortion and fetal loss at the window of embryo implantation in diabetic women is 9 times higher than healthy and non-diabetic women (3).

Adhesion molecules play an important role in the embryo implantation process in the endometrium (4). The expression of endometrial integrins at the level of gene and protein is varied in different species of animals, and not even one species itself have the same cycle at

different times. The expression of these heterodimeric glycoproteins is closely related to the tissue maturation (5). For example, in humans and primates, it has been shown that the expression of integrin genes such as $\alpha 3\beta 1$, $\alpha v\beta 3$, $\alpha 4\beta 1$ and $\alpha 1\beta 1$ during the reproductive cycle is affected by ovarian hormones (6). In patients with infertility problems integrins genes and proteins expression significantly changed during implantation (7). Lacking $\beta 1$ integrins in mice lead to implantation failure in the uterine wall and the blastocysts cannot attach to the uterine endometrial cells and penetrate the underlying tissue (8). Despite advances in various techniques of infertility treatment in recent years, the rate of implantation and pregnancy following assisted reproductive technique (ART) is very low (9). The co-culture method is one of the most important techniques for optimizing the conditions of culture in order to obtain embryos with better quality

(10). There is ample evidence to suggest that the use of co-culture system versus conventional and traditional embryo culture systems results in the production of high quality embryos as well as higher pregnancy rates (11). Various cells, such as oviduct, endometrial and granulosa cells have been used to co-culture with the embryo (12). Several studies have pointed to the efficacy of employing one's own endometrial cells in the co-culture system improves fetal quality as well as increases implantation rates in individuals with recurrent failure after *in vitro* fertilization (IVF) techniques (13).

Among different blood glucose regulatory drugs that are used in Type 2 diabetes mellitus (T2DM) treatment, Metformin is the most frequent. The primary function of this drug is reduction of hepatic glucose production (14). Also, Pioglitazone is an insulin-sensitizing agent regulator which can reduce insulin resistance in liver, muscle and adipose tissue and improve glucose and lipid metabolism (15).

The result of our previous work revealed that $\alpha 3$ and $\beta 1$ integrin protein will be changed in diabetic condition which could affect the fertility status. Treatment with Pioglitazone and Metformin improved the level of $\alpha 3$ and $\beta 1$ integrin protein while Pioglitazone was more effective (16).

The hypothesis is this: in women with recurrent IVF failure and diabetic condition, cytokines such as tumour necrosis factor α (TNF α), various molecules including adhesion proteins and the large family of integrins were affected (17, 18). Follow our previous work, we investigated the impression of diabetes on the fetal implantation in uterine endometrium. In this study, we evaluated genes and protein expression of intergrin $\alpha 3\beta 1$ and also, the effect of two common drugs in the treatment of diabetes (Metformin and Pioglitazone) in this regard.

Material and Methods

This experimental study was performed at the Central Laboratory of Isfahan University of Medical Sciences under Ethical Committee permission (IR.MUI.REC.1394.1.184). In this study, 35 adult female Wistar rats weighing 175 to 225 g and 6 to 8 weeks old were randomly divided into five groups of 7 rats in each group). The first group was the control group, with no intervention, the second group was the sham group which received only drugs solvent (normal saline) by orogastric gavage, the third group was type 2 diabetic model rats (T2DM rats), the fourth group was Metformin-treated (100 mg/kg/day by orogastric gavage) T2DM rats and the fifth group was Pioglitazone-treated (20 mg/kg/day by orogastric gavage) T2DM rats.

T2DM was induced by nicotine amide (NA) at a dose of 200 mg/kg and streptozotocin (STZ, Sigma-Aldrich, Germany) at a dose of 65 mg/kg. Three days later, fasting blood sugar (FBS) was measured using a glucometer (HemoCue Glucose 201+, Sweden). Also, blood glucose levels above 250 mg/dl were considered as a T2DM

model. The animals in all groups were kept in diabetic condition for four weeks. Treatment begun during the next 4 weeks. On 3rd day of the eighth week, animals were mated with male rats. In the next morning all rats were checked. Observation of sperm in the vaginal smears was the indication for the first gestational day and 4 days later it was implantation time (19), in which the endometrial biopsy was also performed (Fig.1).

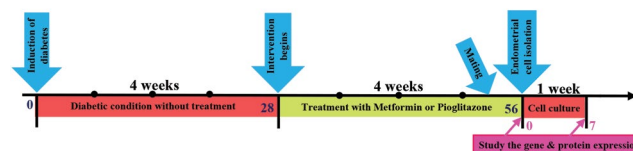


Fig. 1: This study performance: from diabetes induction till tissue sampling and cell culture. The total study time was 9 weeks: diabetic condition=4 weeks, drugs treatment=4 weeks and cell culture=one week. Genes and protein expression was studied at days zero and 7 of the cell culture.

Endometrial cell isolation

Validated method was used for endometrial cells isolation of rat uterus (20). At the end of the eighth week (56th day) of the study and 4 days after the observation of sperm in the vaginal smears, rats in all groups were sacrificed by intraperitoneal injection of ketamine hydrochloride (50 mg/kg, Alfasan, Woerden, Netherlands) and xylazine hydrochloride (Alfasan, Woerden, Netherlands, 7 mg/kg, Fig.1). Their uterine horns were dissected and the endometrium was removed in a sterile condition. The endometrial samples were washed with Hanks' balanced salt solution (Sigma-Aldrich, St. Louis, MO, USA), then chopped into several fragments and kept in the sterile micro tubes. The endometrium of one uterine horn was used directly for molecular experiments, and another was used for cell isolation and culture, followed by molecular experiments on day 7.

The isolated cells in the all groups were maintained in DMEM F-12 (1:1, Sigma-Aldrich, St. Louis, MO, USA) containing fetal calf serum (FCS, 10%, Sigma-Aldrich, St. Louis, MO, USA), penicillin (-Aldrich, St. Louis, MO, USA) and streptomycin (Sigma-Aldrich, St. Louis, MO, USA). The cells were then transferred to special culture flasks. Initial incubation was carried out for 2 hours at 37°C with 5% carbon dioxide concentration. Then, every three days, the cell culture medium changed.

Immunocytochemistry assay

Using immunocytochemistry staining, isolated epithelial cells were identified based on response to the Cytokeratin-19 antigen, a marker of epithelial cells. After centrifugation and removing the culture medium, paraformaldehyde 4% (Sigma-Aldrich, St. Louis, MO, USA) was used to fix the cells and then, kept at room temperature for 30-60 minutes. Primary antibody, anti-Cytokeratin-19 (1:300; Abcam, Cambridge, MA, USA) was added to the cell (1: 300), incubated for 2 hours at

4°C and then, at room temperature overnight. Secondary antibody FITC-conjugated (1:500; Abcam, Cambridge, MA, USA) was added to the cells at a concentration of 1: 1000 and kept at room temperature for 2 hours. DAPI (1:1000, Sigma, USA), at a concentration of 1: 1000 for 2 min, was used to stain the nuclei. Finally, the cells were examined by fluorescent microscopy.

Real-time polymerase chain reaction technique

Gene expression was evaluated on days 0 and 7th of the cell culture. RNA extraction from endometrial cells was performed according to the manufacturer's guideline of RNX solution (Qiagen, Germany) (17). NCBI and Ensembl sites and Gene Runner software (<http://www.generunner.net>) were used to design primers (Table 1). These primers were then blasted to ensure their specificity. Finally, expression of the target genes was measured using real time polymerase chain reaction (PCR) technique. The expression level of each target gene was calculated as $2^{-\Delta\Delta C_t}$, as previously described.

Table 1: Sequences of the real time-polymerase chain reaction primer sets

Gene	Primer sequence (5'-3')
<i>β-actin</i>	F: GCCTTCCTTCCTGGGTATG R: AGGAGCCAGGGCAGTAATC
<i>Itg α3</i>	F: AGCAGCCTCAGCAGATAATC R: GGAGGATATTGATGACAGGTC
<i>Itg β1</i>	F: TACTTCAGACTTCCGCATTG R: GCTGCTGACCAACAAGTTC

Western blot

The western blot technique was performed to measure the amount of α3 and β1 integrin proteins. After electrophoresis, the separated proteins were blotted onto a nitrocellulose membrane (AR0135-02, Boster, USA) Incubation was then performed with a primary antibody solution against rabbit anti-rat α3 and β1 integrin antibody (Bs-1057R, Bioss, London) in appropriate dilution for 2 hours. at room temperature with gentle shaking. Then, incubation in the secondary antibody solution against the primary antibody (mouse anti-rabbit IgG -HRP secondary antibody) (P1308; Applygen Technologies, China) with 1:1000 dilution for 1.5 hours at room temperature with gentle shaking was done.

According to the Bio-Rad kit protocol (170-5060, Bio Rad, USA), the nitrocellulose membrane was coated with an Emission Chemo luminescence (ECL) solution (solution 1 and 2 at a ratio of 1:1) (sc-2048, Santa Cruz Biotechnology, USA), which is actually a substrate of horseradish peroxidase (HRP) enzyme (P8375, Sigma-Aldrich, Germany) for 1 minute. Finally, the western blot bands were evaluated and analyzed by device software.

Statistical analysis of data

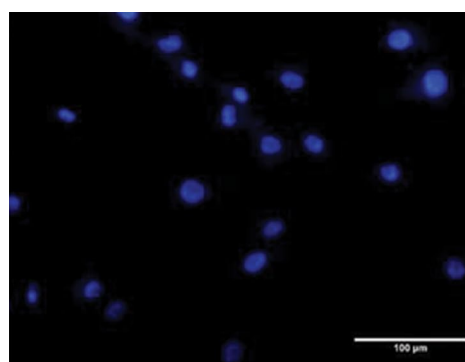
Statistical analysis was carried out with SPSS 20 software (University of Stanford, USA). Using one-way analysis of variance (ANOVA), the results were analyzed. And also, the Bonferroni post hoc test was applied for multiple comparisons. The results were presented as mean ± SEM and the level less than 0.05 was considered significant.

Results

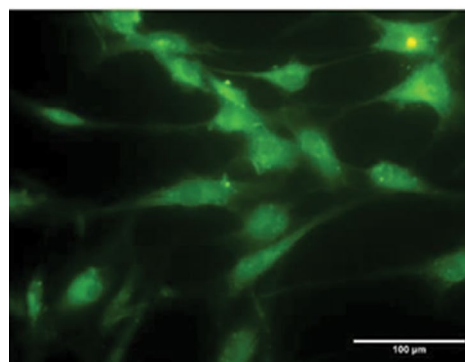
Immunocytochemistry assay

More than 80% of the isolated cells were endometrial cells (Fig.2).

A



B



C

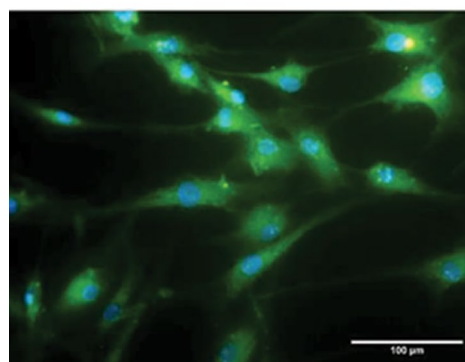


Fig.2: Immunocytochemistry before treatment. **A.** Cell nuclei that are blue with DAPI. **B.** The cell wall appears bright green by antibody conjugated with FITC. **C.** The merged images of A and B represent cells expressing the cytokeratin 19 marker (scale bar: 100 μm).

α3 integrin gene expression

On day zero (Fig.3, black columns) the rate of the

expression of the $\alpha 3$ integrin gene in the diabetic group showed a significant increase in comparison with the control group ($P < 0.001$). After treatment with Metformin, $\alpha 3$ integrin gene's expression increased and was significant compared to the diabetic group ($P = 0.009$). However, the expression of this gene decreased significantly after treatment with Pioglitazone compared to the diabetic group ($P < 0.001$) and also Metformin treated group ($P < 0.001$). Also, $\alpha 3$ integrin gene expression on day 7 after endometrial culture (Fig.3, white columns) had a similar pattern to the day zero although, it was so close. And also, there was no significant difference between any of the groups ($P > 0.05$). In comparing $\alpha 3$ gene expression between days zero and seven, it was observed that diabetic group ($P = 0.006$) and Metformin-treated group ($P < 0.001$) had a significant decrease on day 7 while, Pioglitazone-treated group showed a significant increase ($P = 0.022$).

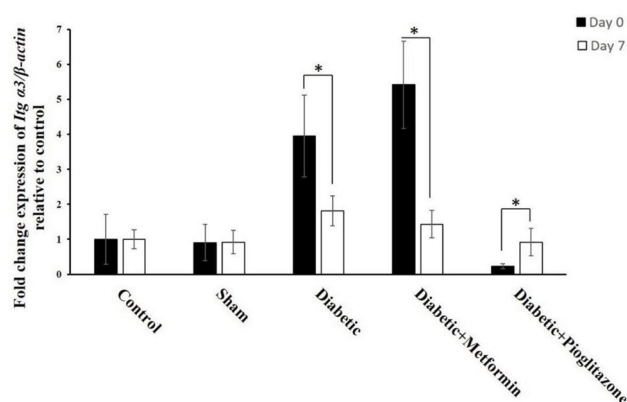


Fig.3: The level of $\alpha 3$ integrin gene expression in the isolated endometrial cells on days 0 and 7th after cell culture at the time of embryo implantation. *, $P < 0.05$.

$\beta 1$ integrin gene expression

The expression of $\beta 1$ integrin gene on the day zero (Fig.4, black columns) showed a significant increase rate in the diabetic group in comparison with the control group ($P < 0.001$). The expression of this gene decreased significantly after treatment with Metformin ($P = 0.008$) and Pioglitazone ($P < 0.001$) compared to the diabetic group. Moreover, the reduction rate was significantly higher in the Pioglitazone-treated group than in the Metformin-treated group ($P = 0.004$). $\beta 1$ integrin gene expression on the day 7 after culture (Fig.4, white columns) had a similar pattern to the day zero. There was no significant difference among all groups ($P > 0.05$) except the diabetic group, that this group had a significant difference with the control ($P < 0.001$), Metformin-treated ($P = 0.008$) and Pioglitazone-treated ($P < 0.001$) groups. In comparing $\beta 1$ gene expression between days zero and seven, the diabetic group ($P = 0.006$), Metformin-treated group ($P < 0.001$) and Pioglitazone-treated group had a significant decrease on day 7.

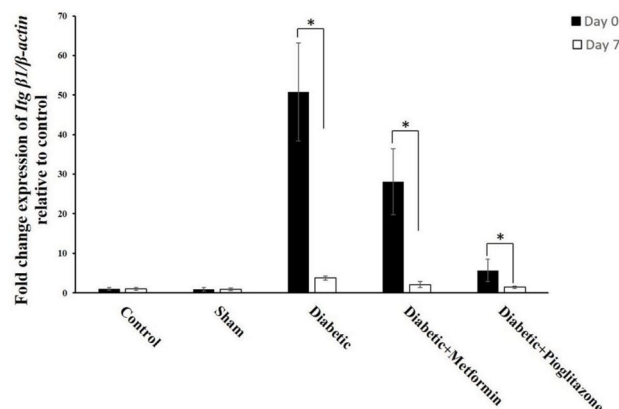


Fig.4: The level of $\beta 1$ integrin gene expression in the isolated endometrial cells on days 0 and 7 after cell culture at the time of embryo implantation. *, $P < 0.05$.

$\alpha 3$ and $\beta 1$ integrin protein expression

At the time of the implantation (day zero) (Fig.5, black columns), the amount of $\alpha 3\beta 1$ integrin protein in the diabetes group increased significantly compared with the control group ($P < 0.001$). However, the amount of this protein in the treatment groups with Metformin ($P = 0.026$) and Pioglitazone ($P < 0.001$) has been significantly reduced. In addition, there was a significant difference between the two treatment groups ($P = 0.033$) and the protein content of $\alpha 3$ and $\beta 1$ integrin in the Pioglitazone treatment group was lower than in the Metformin treatment group. After 7 days endometrial culture (Fig.5, white columns), there was no significant difference between any of the groups ($P > 0.05$) in $\alpha 3$ and $\beta 1$ integrin protein expression, but, protein expression in the different groups, including diabetic ($P < 0.001$), Metformin-treated ($P = 0.003$) and Pioglitazone-treated ($P = 0.024$) was significantly decreased in comparison with the day of implantation.

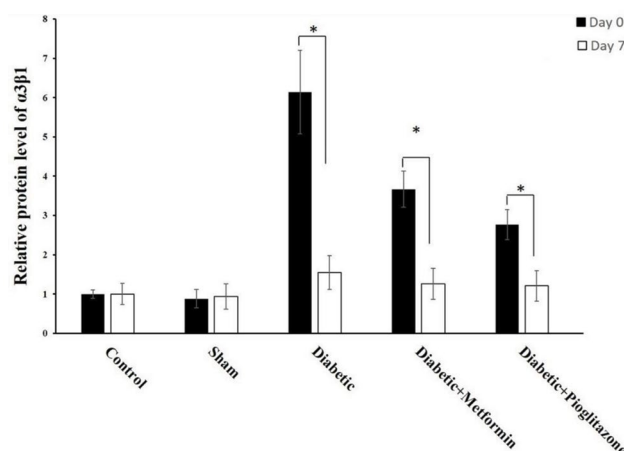


Fig.5: Comparison of $\alpha 3$ and $\beta 1$ integrin protein levels in isolated endometrial cells on days 0 and 7 after cell culture at the time of embryo implantation. *, $P < 0.05$.

Discussion

Nowadays, in developed countries, 7% of all births are due to assisted reproductive methods (21). Despite

advances in the modern infertility therapies, their success rate is still low. Also, in some patients the infertility cause is unknown (22). Increased blood glucose level (hyperglycemia) could have a detrimental effect on oocyte, embryo and the mother's endometrium at the time of embryo implantation. The complications of type 2 diabetes on the fetus are similar to the complications of type 1 diabetes, which can increase the rate of miscarriage and the rate of fetal abnormalities (23). Maternal hyperglycemia affects the integrins molecules that are involved in the process of apoptosis, proliferation, migration, differentiation of embryonic cells and leads to several complications, although the exact mechanism of hyperglycemic effect on the embryo at implantation is still unclear (24).

In the present study, we worked on the effect of diabetes on the expression of genes and protein of $\alpha 3\beta 1$ integrin. Our results revealed that the expression rate increased significantly in diabetic rats. After 7 days of endometrial cell culture in the laboratory, we encountered with a decrease expression even in the diabetic group. The significant reduction was observed in the treated groups, Metformin and Pioglitazone, in comparison with the control group. Briefly, this rate was higher in the Pioglitazone treated group.

Adhesion molecules, specially the integrin family, play an important role in the endometrial receptivity and pregnancy onset (25). Alteration in the endometrium expression of some integrins, were observed by Bakhteyari et al. (17) in the implantation failure cases. Bakhteyari et al. (18) showed that diabetes mellitus may alter integrin gene expression in the many tissues and organs such as reproductive system. Here, our study showed diabetes associated with an increase in the expression of $\alpha 3$ and $\beta 1$ integrin genes and protein in endometrial cells.

Due to the location of $\alpha 3$ and $\beta 1$ integrin protein in the basolateral part of the endometrial cells, it is likely that increasing the expression will increase the connection of these cells to each other, which can prevent the embryo from penetrating and implanting in the uterine endometrium. In addition, increased expression of integrins in other cells, such as platelets, causes plaque buildup and clots at the site of embryo implantation, which can impede embryo implantation and prevent blood flow between the placenta and mother tissue, leading to disruption in implantation process (16).

In a study in 2000 scientist showed that integrins expression increases during the endometrial receptivity phase (26). They proved that the pattern of endometrial integrins expression, indicates their hormonal regulation (27). Also, they revealed integrins in the endometrium play an essential role in the process of pregnancy and implantation and are known as a means of attaching the fetus to the mother tissue (28). Numerous studies of integrins in various tissues have shown that diabetes and hyperglycemia alter the expression of integrins (28) which in the present study it was proved too. Also, Rutherford et

al. (29) showed that changes in the integrins expression can reduce the female fertility rate, which in various ways probably result from a decrease in the uterine endometrium ability to accept blastocyst. The results of the both studies are in line with our study that diabetes causes significant changes in the expression of $\alpha 3$ and $\beta 1$ integrin protein and genes. Moreover, by keeping endometrial cells for 7 days in an environment outside the body of diabetic animals, we observed that even in rats who did not receive drug treatment, the expression of these integrins decreased significantly.

So far, little research has been done on the diabetes effects on the integrins expression in the endometrial tissue. On the other hand, there is no study about the effects of anti-diabetic drugs, such Metformin, and specially Pioglitazone. Although, there are studies on organs other than the reproductive system, particularly, endometrium (30, 31). Also, there is no study on diabetes and endometrial cell culture.

The results of the present study showed that the separation and culture of endometrial cells in diabetic rats by itself could reduce the expression of genes and protein of $\alpha 3$ and $\beta 1$ integrin, which had increased during diabetic condition. Therefore, there was no significant difference between the level of the expression in the diabetes group and the control group. So, if diabetic patients had several embryo implantation failures in the assisted reproductive techniques, it could be assumed this culturing procedure will improve the success rate of implantation and pregnancy. However, in order to graft these cells to the maternal endometrium, the endometrial cell culture needs biological scaffolds i.e., fibrin, alginate and etc. Eventually, the embryo along with the endometrial cells and scaffold will be located and grafted to the mother's uterus. During the present study, we have taken the first step in this direction. And certainly, obtain the favorable outcomes requires further studies and follow-up.

Conclusion

Based on the results of this study, diabetes can increase the expression of genes and protein of $\alpha 3$ and $\beta 1$ integrin during implantation of blastocyst in the uterus endometrial tissue. This protein can increase the connection among endometrial cells. This strong connection does not allow the complete and perfect blastocyst invasion into the endometrial tissue. Between two drugs which were tried in this study, Pioglitazone had a more beneficial and further regulating effect on the expression of $\alpha 3$ and $\beta 1$ integrin genes and protein compared with Metformin.

Acknowledgements

The authors would like to acknowledge the financial support of Isfahan University of Medical Sciences (project number 194184). The authors declare that they have no conflict of interest.

Authors' Contributions

R.A.; Contributed to conception and design. P.N., N.E.; Contributed to data and statistical analysis, interpretation of data and manuscript revision. A.B.; Contributed to all experimental works. F.S.M.; Contributed to data collection and interpretation, and manuscript writing. All authors read and approved the final manuscript.

References

- Szaboova R, Devendra S. Infertility in a young woman with Type 2 diabetes. *London J Prim Care (Abingdon)*. 2015; 7(3): 55-57.
- Ge ZJ, Liang XW, Guo L, Liang QX, Luo SM, Wang YP, et al. Maternal diabetes causes alterations of DNA methylation statuses of some imprinted genes in murine oocytes. *Biol Reprod*. 2013; 88(5): 117.
- Albaghdadi AJH, Kan FWK. Endometrial receptivity defects and impaired implantation in diabetic NOD mice. *Biol Reprod*. 2012; 87(2): 30.
- Simopoulou M, Nikolopoulou E, Dimakakos A, Charalabopoulos K, Koutsilieris M. Cell adhesion molecules and in vitro fertilization. *In Vivo*. 2014; 28(5): 683-690.
- Kim SM, Kim JS. A review of mechanisms of implantation. *Dev Reprod*. 2017; 21(4): 351-359.
- Singh H, Aplin JD. Adhesion molecules in endometrial epithelium: tissue integrity and embryo implantation. *J Anat*. 2009; 215(1): 3-13.
- Su R-W, Fazleabas AT. Implantation and establishment of pregnancy in human and nonhuman primates. *Adv Anat Embryol Cell Biol*. 2015; 216: 189-213.
- Chen G, Xin A, Liu Y, Shi C, Chen J, Tang X, et al. Integrins $\beta 1$ and $\beta 3$ are biomarkers of uterine condition for embryo transfer. *J Transl Med*. 2016; 14(1): 303.
- Jie Z, Yiling D, Ling Y. Association of assisted reproductive technology with adverse pregnancy outcomes. *Iran J Reprod Med*. 2015; 13(3): 169-180.
- Swain JE, Carrell D, Cobo A, Meseguer M, Rubio C, Smith GD. Optimizing the culture environment and embryo manipulation to help maintain embryo developmental potential. *Fertil Steril*. 2016; 105(3): 571-587.
- Dominguez F, Gadea B, Mercader A, Esteban FJ, Pellicer A, Simón C. Embryologic outcome and secretome profile of implanted blastocysts obtained after coculture in human endometrial epithelial cells versus the sequential system. *Fertil Steril*. 2010; 93(3): 774-782. e1.
- Vithoulkas A, Levanduski M, Goudas VT, Illmensee K. Co-culture of human embryos with autologous cumulus cell clusters and its beneficial impact of secreted growth factors on preimplantation development as compared to standard embryo culture in assisted reproductive technologies (ART). *Middle East Fertil Soc J*. 2017; 22(4): 317-322.
- Eyheremendy V, Raffo FGE, Papayannis M, Barnes J, Granados C, Blaquier J. Beneficial effect of autologous endometrial cell coculture in patients with repeated implantation failure. *Fertil Steril*. 2010; 93(3): 769-773.
- He L, Wondisford FE. Metformin action: concentrations matter. *Cell Metab*. 2015; 21(2): 159-162.
- Zou C, Hu H. Use of pioglitazone in the treatment of diabetes: effect on cardiovascular risk. *Vasc Health Risk Manag*. 2013; 9: 429-433.
- Zarrin Y, Bakhteyari A, Nikpour P, Mostafavi FS, Eskandari N, Matinfar M, et al. A study on the presence of osteopontin and $\alpha 3\beta 1$ integrin in the endometrium of diabetic rats at the time of embryo implantation. *J Reprod Infertil*. 2020; 21(2): 87-93.
- Bakhteyari A, Zarrin Y, Nikpour P, Hosseiny ZS, Mostafavi FS, Eskandari N, et al. Diabetes mellitus increased integrins gene expression in rat endometrium at the time of embryo implantation. *Int J Reprod Biomed*. 2019; 17(6): 395-404.
- Bakhteyari A, Nikpour P, Mostafavi FS, Eskandari N, Matinfar M, Soleimani Asl S, et al. Impact of metformin and pioglitazone on serum level of tumor necrosis factor-alpha and lipid profiles during implantation window in diabetic rats. *Int J Fertil Steril*. 2019; 13(2): 148-153.
- Spósito DR, Santos AR. Histochemical study of early embryo implantation in rats. *Int J Morphol*. 2011; 29(1): 187-192.
- Bläuer M, Heinonen PK, Martikainen PM, Tomas E, Ylikomi T. A novel organotypic culture model for normal human endometrium: regulation of epithelial cell proliferation by estradiol and medroxyprogesterone acetate. *Hum Reprod*. 2005; 20(4): 864-871.
- Kushnir VA, Barad DH, Albertini DF, Darmon SK, Gleicher N. Systematic review of worldwide trends in assisted reproductive technology 2004-2013. *Reprod Biol Endocrinol*. 2017; 15(1): 6.
- Pandian Z, Bhattacharya S, Nikolaou D, Vale L, Templeton A. In vitro fertilisation for unexplained subfertility. *Cochrane Database Syst Rev*. 2002; (2): CD003357.
- Zhao J, Hakvoort TBM, Willemsen AM, Jongejan A, Sokolovic M, Bradley EJ, et al. Effect of hyperglycemia on gene expression during early organogenesis in mice. *PLoS One*. 2016; 11(7): e0158035.
- Uhde K, van Tol HTA, Stout TAE, Roelen BAJ. Exposure to elevated glucose concentrations alters the metabolomic profile of bovine blastocysts. *PLoS One*. 2018; 13(6): e0199310.
- van Mourik MSM, Macklon NS, Heijnen CJ. Embryonic implantation: cytokines, adhesion molecules, and immune cells in establishing an implantation environment. *J Leukoc Biol*. 2009; 85(1): 4-19.
- Lessey BA, Castelbaum AJ, Wolf L, Greene W, Paulson M, Meyer WR, et al. Use of integrins to date the endometrium. *Fertil Steril*. 2000; 73(4): 779-787.
- Yoshimura Y. Integrins: expression, modulation, and signaling in fertilization, embryogenesis and implantation. *Keio J Med*. 1997; 46(1): 16-24.
- Koot YEM, Teklenburg G, Salker MS, Brosens JJ, Macklon NS. Molecular aspects of implantation failure. *Biochim Biophys Acta*. 2012; 1822(12): 1943-1950.
- Rutherford EJ, Hill ADK, Hopkins AM. Adhesion in physiological, benign and malignant proliferative states of the endometrium: microenvironment and the clinical big picture. *Cells*. 2018; 7(5): 43.
- Zhou X, Zhang J, Haimbach R, Zhu W, Mayer-Ezell R, Garcia-Calvo M, et al. An integrin antagonist (MK-0429) decreases proteinuria and renal fibrosis in the ZSF 1 rat diabetic nephropathy model. *Pharmacol Res Perspect*. 2017; 5(5): e00354.
- Sawada K, Toyoda M, Kaneyama N, Shiraiwa S, Moriya H, Miyatake H, et al. Upregulation of $\alpha 3\beta 1$ -integrin in podocytes in early-stage diabetic nephropathy. *J Diabetes Res*. 2016; 2016: 9265074.

Effects of Exosomes Derived from Kidney Tubular Cells on Diabetic Nephropathy in Rats

Fereshtesadat Fakhredini, Ph.D.^{1,2}, Esrafil Mansouri, Ph.D.^{1,2}, Seyyed Ali Mard, Ph.D.³, Armita Valizadeh Gorji, Ph.D.⁴, Mohammad Rashno, Ph.D.⁵, Mahmoud Orazizadeh, Ph.D.^{1,2*}

1. Cell and Molecular Research Centre, Faculty of Medicine, Ahvaz Jundishapur University of Medical Sciences, Ahvaz, Iran
2. Department of Anatomical Sciences, Faculty of Medicine, Ahvaz Jundishapur University of Medical Sciences, Ahvaz, Iran
3. Department of Physiology, Physiology Research Centre, Research Institute for Infectious Diseases of the Digestive System, School of Medicine, Ahvaz Jundishapur University of Medical Sciences, Ahvaz, Iran
4. Department of Bone Marrow Transplantation, Ahvaz Jundishapur University of Medical Sciences, Ahvaz, Iran
5. Department of Immunology, Faculty of Medicine, Ahvaz Jundishapur University of Medical Sciences, Ahvaz, Iran

*Corresponding Address: P.O.Box: 61335, Department of Anatomical Sciences, Faculty of Medicine, Ahvaz Jundishapur University of Medical Sciences, Ahvaz, Iran
Email: orazizadehm@gmail.com

Received: 25/April/2020, Accepted: 16/August/2020

Abstract

Objective: One of the severe complications and well-known sources of end stage renal disease (ESRD) from diabetes mellitus is diabetic nephropathy (DN). Exosomes secreted from diverse cells are one of the novel encouraging therapies for chronic renal injuries. In this study, we assess whether extracted exosomes from kidney tubular cells (KTCs) could prevent early stage DN *in vivo*.

Materials and Methods: In this experimental, exosomes from conditioned medium of rabbit KTCs (RK13) were purified by ultracentrifuge procedures. The exosomes were assessed in terms of morphology and size, and particular biomarkers were evaluated by transmission electron microscopy (TEM), scanning electron microscopy (SEM), Western blot, atomic force microscopy (AFM) and Zetasizer Nano analysis. The rats were divided into four groups: DN, control, DN treated with exosomes and sham. First, diabetes was induced in the rats by intraperitoneal (i.p.) administration of streptozotocin (STZ, 50 mg/kg body weight). Then, the exosomes were injected each week into their tail vein for six weeks. We measured 24-hour urine protein, blood urea nitrogen (BUN), and serum creatinine (Scr) levels with detection kits. The histopathological effects of the exosomes on kidneys were evaluated by periodic acid-Schiff (PAS) staining and expressions of miRNA-29a and miRNA-377 by quantitative real-time polymerase chain reaction (qRT-PCR).

Results: The KTC-Exos were approximately 50-150 nm and had a spherical morphology. They expressed the CD9 and CD63 specific markers. Intravenous injections of KTC-Exos potentially reduced urine volume ($P<0.0001$), and 24-hour protein ($P<0.01$), BUN ($P<0.001$) and Scr ($P<0.0001$) levels. There was a decrease in miRNA-377 ($P<0.01$) and increase in miRNA-29a ($P<0.001$) in the diabetic rats. KTC-Exos ameliorated the renal histopathology with regulatory changes in microRNAs (miRNA) expressions.

Conclusion: KTC-Exos plays a role in attenuation of kidney injury from diabetes by regulating the miRNAs associated with DN.

Keywords: Diabetic Nephropathy, Exosomes, Kidney, miRNAs

Cell Journal (Yakhteh), Vol 24, No 1, January 2022, Pages: 28-35

Citation: Fakhredini FS, Mansouri E, Mard SA, Valizadeh Gorji A, Rashno M, Orazizadeh M. Effects of exosomes derived from kidney tubular cells on diabetic nephropathy in rats. Cell J. 2022; 24(1): 28-35. doi: 10.22074/cellj.2022.7591.
This open-access article has been published under the terms of the Creative Commons Attribution Non-Commercial 3.0 (CC BY-NC 3.0).

Introduction

It is widely accepted that diabetic nephropathy (DN) is one of the destructive complications of diabetes mellitus and one of the main causes of End-stage renal disease (ESRD) worldwide (1). Statistically, approximately 347 million people suffer from diabetes, and this number is estimated to reach 430 million in 2030. DN is becoming more common and has almost reached epidemic proportions (1, 2). The diverse structural and functional modifications responsible for DN pathogenesis include hemodynamic changes, expression or activation of different proteins and signalling pathways, oxidative stress, mesangial cell expansion, fibrosis development and glomerulosclerosis (GS) (3). Despite common treatments that include ameliorating high blood

pressure and hyperglycaemia, there are no efficient treatment options that counteract and reverse DN (4-6). Over the past decade, cell therapy is increasingly considered to be one of the newly developed regenerative therapies for renal damages (7).

The results of studies show that the effectiveness of treatment on these cells is strongly associated with exosomes, which are membrane-bound extracellular vesicles (8). Exosomes are microvesicles that have a two-layer lipid membrane and are secreted by different cell types. They play an important role as an alternative mechanism for biological transport between distant cells. This transport is characterised by an intracellular packaging process in which various proteins and other gene products are loaded into exosomal carriers and then released into the extracellular environment (9). The two lipid layers of the exosomes protect their contents from destruction

by proteases and nucleases present in the bloodstream. Exosomes also have protein markers on their surface that reflect their endosomal origin. They are considered to be cell-derived vesicles, 30 to 100 nm in diameter, which are discharged into the microenvironment via numerous cell types (10). Exosomes consist of microRNAs (miRNAs), proteins, and mRNAs that can be transferred to target cells and cause epigenetic and genetic changes to the target cells (11). Horizontal transfer of vesicular miRNAs and mRNAs may result in an angiogenic program in endothelial cells or modulate the injured cell phenotypes (12).

Based on the results of studies, miRNAs are considered to be one of the groups of non coding RNAs that are expressed in all tissues. They play important roles in various diseases, including diabetes (13). Increased glucose levels stimulate *miR-377* expression, which results in increased fibronectin production via repression of superoxide dismutase and p21-activated kinase (14). *miR-377* targets hemoxygenase-1 (HO-1) and HO-1 prevents DN through antioxidant effects. The *miR377/HO-1* pathway could be a new pathway where *miR-377* stimulates DN via HO-1 (15, 16). Three members of the *miR-29* family are suppressed under elevated glucose conditions in proximal tubular cells, mesangial cells and podocytes (17). The members of the *miR-29* family are responsible for anti-fibrotic effects in DN. *miR-29a* directly targets the 3'UTR of *COL4a1* and *COL4a2*, and leads to decreased expressions of these two fibrotic genes (18, 19).

The current study aims to evaluate the effects of exosomes derived from kidney tubular cells (KTCs) on DN in a rat model of diabetes. We propose that KTC-Exos could modulate kidney complications from diabetes and they could be a possible new regulator in DN therapy.

Materials and Methods

In this experimental study, male Sprague-Dawley rats (n=40, 220-270 g) were obtained from the Animal House Centre of Ahvaz Jundishapur University of the Medical Sciences (Ahvaz, Iran). The rats were kept in cages on a 12/12-hour light/dark cycle at 21-24°C. Ethical Committee of Ahvaz Jundishapur University of Medical Sciences approved this study (IR.AJUMS.ABHC.REC.1398.008).

Culture of the kidney tubular cell line

The rabbit KTC line (RK13, NCBI code: C523) was purchased from Pasteur Institute of Iran and immediately transferred to Dulbecco's Modified Eagle Medium (DMEM) high glucose (Gibco, UK) that consisted of 2 mM L-glutamine and 100U penicillin/streptomycin (all from Invitrogen, Waltham, MA, USA) and 10% fetal bovine serum (FBS, Gibco, UK). The cells were stored in an incubator at 37°C and 5% CO₂ to enable proliferation. The medium was replaced after five days, and the cells were washed with phosphate buffered saline (PBS, Sigma, USA) in order to remove any non-adherent cells.

The cells were passaged using 0.25 % trypsin when they were ~90% confluent.

Isolation and purification of the kidney tubular cell-derived exosomes

KTC-Exos were prepared and treated according previously published protocols (20, 21). Briefly, the 80-90% confluent cells were washed with PBS, and then cultured at 37°C and 5% CO₂ in DMEM without FBS for an additional 48 hours. The exosomes were isolated from the supernatant of passage-2 cells, 48 hours after cultivation in serum-free DMEM. The conditioned medium was collected and centrifuged at 300 g for 10 minutes, 2000 g for 10 minutes, and 10 000 g for 30 minutes at 4°C to remove the cells, large dead cells, and debris. The resultant supernatant was filtered through a sterile 0.22 µm (Millipore, USA) filter to remove any remaining cells and cellular debris. Afterwards, the supernatant was transferred to an ultra-clear tube (Millipore, USA) and centrifuged with a high-speed centrifuge at 60 000×g at 4°C for 90 minutes to isolate the purified exosomes, as a final pellet (22). The KTC-Exos pellet was resuspended in 200µl of PBS and stored at -80°C. The protein contents of the KTCs-Exos solution were determined by the Bradford assay, according to the manufacturer's instructions (Thermo Fisher Scientific, USA). Absorbance was read at 595 nm using a microplate reader.

Transmission electron microscopy and scanning electron microscopy of kidney tubular cell-derived exosomes

Both transmission electron microscopy (TEM) and scanning electron microscopy (SEM) were used to assess the morphological features of the exosomes. First, the exosomal pellet was fixed with 1% glutaraldehyde (Sigma, USA) and then 20 µl of the fixed exosomes were inserted on a carbon-coated grid and allowed to dry at room temperature for 30 minutes. Then, a LEO 906 TEM (Zeiss, Germany) was used to each the samples were washed twice with PBS for 5 minutes, and stained with 1% uranyl acetate for 10 minutes before they were visualized under a TEM at an accelerating voltage of 80 kV. DigitalMicrograph software (Gatan, Inc., Washington, DC, USA) was used to record the TEM images that were acquired with an Orius 200 camera (Gatan, Inc., Washington, DC, USA). We also assessed the particle surface morphology by SEM. A total of 1 to 5 µl of the dried sample was placed on a silicon chip, fixed with 2% paraformaldehyde and sputter-coated with gold-palladium, then visualised by SEM at 30 kV.

Determination of the distribution and size of the kidney tubular cell-derived exosomes by dynamic light scattering, using a Zetasizer Nano device

Dynamic light scattering (DLS) was used to analyse the solvent nanoparticle (NP), which is capable of measuring particles in a solution quickly, easily, and without sample preparation. For this purpose, the extracted exosomes

were resuspended in PBS (100 µl). After shaking the solution, a Malvern Zetasizer Nano device (Malvern Instruments, Malvern, UK) was used to measure the sizes of the exosomes.

Western blot for characterisation of the kidney tubular cell-derived exosomes surface markers

We used Western blotting to characterise the KTC-Exo surface markers. The presence of two specific surface markers, CD9 and CD63, confirmed the KTC-Exos identity (23). Briefly, the exosomes were lysed with RIPA/PI buffer (Santa Cruz Biotechnology, Inc., Dallas, TX, USA) and the level of protein was estimated by the Bradford protein assay. Then, the KTC-Exos protein was loaded onto a 12% sodium dodecyl sulphate/poly-acrylamide gel electrophoresis (SDS-PAGE). In addition, the protein samples were transferred to the polyvinylidenedifluoride membrane via electroblotting the membrane of polyvinylidenedifluoride (Millipore, USA) at 100 mA for 1.5 hours. Then, the membranes were exposed to the primary rabbit polyclonal anti-CD9 and anti-CD63 antibodies, and the β-actin antibody (Abcam, UK) in order to test for the presence of CD63 and CD9. The membranes were washed three times for 5 minutes each time in 1× tris-HCl buffered saline with Tween (TBST) that consisted of TBS and 0.1% Tween 20. Incubation was done in TBST with the horseradish peroxidase-conjugated goat anti-rabbit secondary antibody (Abcam, UK) for one hour. ECL solution was applied for detection and imaging of the proteins in the membrane. Lumigan PS-3 substrate is catalyzed in ECL solution by a horseradish peroxidase enzyme connected to the secondary antibody. The radiation produced by luminol was released as a result of this reaction and was detected using special films. The protein bands that resulted were compared between groups and statistically analyzed.

Assay of KTC-Exos -Exo by atomic force microscopy

The exosomal pellet was prepared over several rounds of high-speed centrifugation, and then diluted in 5 ml of deionized water and vortexed. The exosomal solution was subsequently transferred to the south-central laboratory of Ahvaz Jundishapur University of Medical Sciences. Distribution, size, NP size, characteristics, morphology, and surface features of the soluble exosomes were analysed by atomic force microscopy (AFM). The two-dimensional images were also analysed.

Diabetes induction

The healthy male rats were allowed to fast for 24 hours before diabetes induction. A single intraperitoneal (i.p.) injection of streptozotocin (STZ, 50 mg/kg body weight, Sigma, USA) (24) that was recently dissolved in citrate buffer (0.1 M at pH=4.5) was used to induce diabetes. The control animals were injected with the vehicle buffer. Blood samples were obtained from the animals' tail veins 72 hours after the STZ injection. Fasting blood glucose levels were measured by a glucose strip test and a glucometer (EasyGlucoBlood Glucose Monitoring System, Infopia, South Korea). Animals with fasting blood glucose levels <250 mg/dl were considered

to have diabetes (24).

Experimental design

A total of 40 animals were selected and placed into four groups (n=10 per group). Group 1 was the control group that injected via the tail veins for six weeks. Group 2 (sham group) received 100 µg of an exosome solution in 100 µl of PBS that was injected through the tail veins once per day for six weeks. Group 3 comprised the diabetes group, where rat received a single i.p. injection of STZ (50 mg/kg). Group 4 was the diabetes+KTC-Exos group that received 100 µg of the exosome solution in 100 µl of PBS by injection (25, 26) into the tail veins once per day for six weeks. The animals were separately placed in metabolic cages for 24 hours with access to drinking water in order to measure the 24-hour urine total protein levels upon the completion of the experiment.

Measurement of 24-hour urine protein, blood urea nitrogen and serum creatinine levels

A Bicinchoninic acid (BCA) kit was used to measure urine that was collected following the 6th week of exosome treatment. A combination of the urine and BCA working solution was incubated at 37°C for 30 minutes, and optical density (OD) was examined at a wavelength of 562 nm. At the end of experimental period, the rats were sacrificed after administration of chloral hydrate anaesthesia. Blood plasma was collected from left ventricles of the rats and centrifuged at 3500 rpm for 5 minutes. Both the serum creatinine (Scr) and blood urea nitrogen (BUN) levels were measured by kits (Scr, C011-1, BUN, C013-2, both purchased from Jiangcheng Bio, Nanjing, China). Then, the kidneys were removed. The left kidneys were washed by PBS and fixed with 10% buffered formalin for sectioning into paraffin sections followed by periodic acid-Schiff (PAS) staining. The right kidneys were rinsed, snap-frozen in liquid nitrogen and stored at -80°C for the *miR-29a* and *miR-377* assays.

Light microscopy examination

We observed the PAS stained sections under a light microscope. Summarily, the mesangial area was counted as mesangial expansion, which was determined in 20 consecutive glomeruli from each rat (26). Finally, the relative mesangial expansion was characterised as the fold change from the normal controls.

Extraction of microRNAs and cDNA synthesis

AnmiRNeasy/Plasma kit (Roche, cat. no.: 05080576001, Germany) was used according to the manufacturer's instructions to extract the miRNAs from the frozen specimens. A spectrophotometer at 260 nm and 280 nm wavelengths (NanoDrop Thermo Fisher Scientific, S.N:D015) was utilized to determine the RNA purity and concentration. Subsequently, cDNA was synthesized from 1 µg of total RNA using amiScript II RT Kit (BONmiR, BON209001, Iran) based on the company's instructions.

Quantitative real-time polymerase chain reaction

Quantitative real-time polymerase chain reaction (qRT-PCR) with a light cycler 96 RT-PCR system (Roche Diagnostics, Indianapolis, IN, USA) was used to measure miRNA expressions. Each PCR amplification was performed in duplicate and the resultant volume of 13 μ L that consisted of 6.5 μ L 2x QuantiTect SYBR Green PCR Master Mix, 1 μ L cDNA, 4.5 μ L RNAase-free water, and 0.5 μ L miRNA-specific forward Primer (miR-29a [ACT GAT TTC TTT TGG TGT] or miR-377 [CGA TCA CAC AAA GGC A]; Bonyakhteh), and 0.5 μ L universal reverse primer ([ACT TAT GTT TTT GCC GTT T] Bonyakhteh). The initial activation phase was conducted at 95°C for two minutes to activate the HotStarTaq DNA polymerase and then for 40 cycles at 95°C for 5 seconds and 60°C for 30 seconds. Additionally, the non-template control (H₂O) was regularly in each PCR. RNU87, as the internal control, was used to normalize miRNA expression levels and the fold change was computed with $2^{-\Delta\Delta Ct}$. Each sample was assayed three times.

Statistical analysis

Statistical analysis was carried out with SPSS 16 software (SPSS Inc., USA). The data were analysed using one-way ANOVA followed by post hoc Least Significant Difference (LSD) test and are presented as mean \pm SD. $P < 0.05$ was considered significant.

Results

Kidney tubular cell phenotype

We observed the KTCs in the cell culture flasks every day after the first day of culture. The morphology and growth of these KTCs were checked by light microscopy to verify an epithelial-like morphology and growth rate. The epithelial-like cells showed high rapid growth and were approximately 95% confluent after 3-4 days (Fig.1).

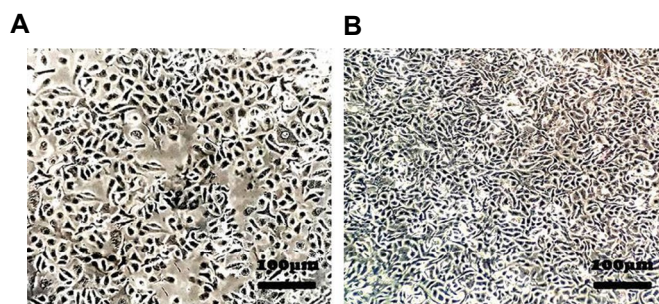


Fig.1: Morphology and growth of kidney tubular cells (KTCs). Growth cells after **A.** Two days and **B.** Four days at $\times 100$ magnification (scale bar: 100 μ m).

Transmission electron microscopy evaluation of the exosomes

The exosomes generated by the KTCs were separated from the culture medium by different centrifuge speeds and evaluated by TEM (Fig.2). Ultrastructural analyses of the exosomes showed considerable reinforcement of the typical

spherical-shaped exosomes with diameters of 50-150 nm. In addition, TEM evaluations showed that the exosomes had an average diameter of ≤ 150 nm with an intact round morphology and they possessed membranes (Fig.2A).

Determination of the exosome protein concentration by the Bradford method

The protein concentration of the isolated exosomes was calculated by the Bradford method and BSA was used as the standard. The protein concentration in the sample was 2512 μ g/ml.

Scanning electron microscopy evaluation of the exosomes

SEM was used to assess the outer surface characteristics of the exosomes. Small vesicles with round morphology were observed. The size of the vesicles was determined to be 70-260 nm based on the vesicle sizes that were seen in several images. The majority of the vesicles were smaller than 100 nm in size (Fig.2B).

Dynamic light scattering analysis

DLS analysis of the exosomes size showed a bell-shaped size distribution with a peak at about 99.4 nm (Fig.2C).

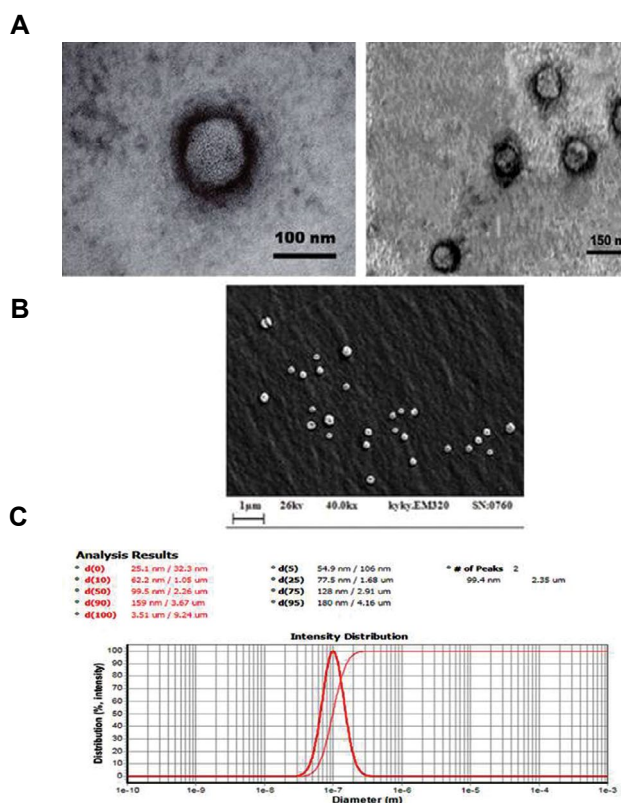


Fig.2: Characterization of exosomes. **A.** Transmission electron microscopy (TEM) observations indicated that the average diameter of the exosomes was ≤ 150 nm. The exosomes had a preserved intact spherical morphology. **B.** Scanning electron microscopy (SEM) analysis showed that the average diameter of the exosomes was ≤ 100 nm and they had a preserved intact spherical morphology. **C.** Dynamic light scattering (DLS) results indicated that almost 50% of the solution ingredients had an average diameter of 99.4 nm.

Western blot analysis

The results of Western blot analysis showed the expressions of two exosome markers, CD63 (25KDa) and CD9 (24-27 KDa), in the KTC-Exos (Fig.3). β -actin (42 KDa) was used as the positive control. Both expression patterns were significant and the results confirmed that the NPs were exosomes.

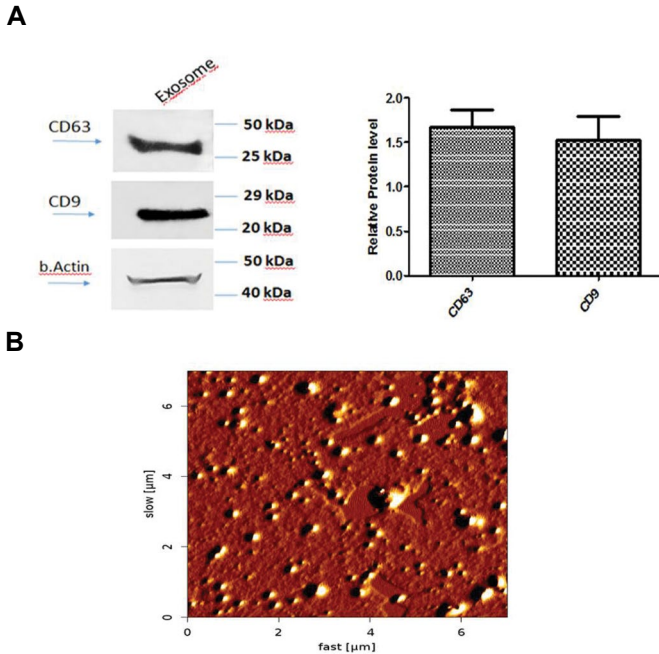


Fig.3: Expression of exosome surface markers by western blotting. **A.** The exosome markers CD9 (24-27 KDa) and CD63 (25 KDa) were expressed in the kidney tubular cell-derived exosomes (KTC-Exos). β -actin (42 KDa) was used as the positive control. **B.** Atomic force microscopy (AFM) image of the KTC-Exos. This showed distinct spherical particles that ranged from 60 to 150 nm.

Atomic force microscopy analysis

AFM obtained from the exosomes showed that the NPs were symmetric, spherical, and without aggregation. The size of the NPs ranged from 60 to 150 nm (Fig.3).

Urine volume in diabetic rats after injection of kidney tubular cell-derived exosomes

Intravenous injection of the KTC-Exos significantly decreased polyuria in the diabetic rats compared with the diabetic group ($P < 0.001$, Fig.4A).

Biochemical analysis

The results showed remarkably elevated Scr, BUN and 24-hour urine protein levels in the diabetic group in comparison to the control group. The KTC-Exos group had significant decreases in Scr ($P < 0.01$), BUN ($P < 0.001$), and 24-hour urine protein ($P < 0.0001$) levels (Fig.4B-D).

Periodic acid-Schiff staining

At the end of the 6th week following the creation of the diabetes model, we observed focal mesangial matrix expansion in the diabetic animals in comparison with the control group (Fig.5A1). Moreover, the section obtained from the diabetic group's kidneys demonstrated partial glomerular hypertrophy and enhanced intra-glomerular cells that were

located mainly in the mesangial region with mesangial expansion (Fig.5BI). In the diabetic animals that received KTC-Exos, there was enhancement in intraglomerular cells and the mesangial matrix. No obvious sign of the rapid growth of the mesangial matrix and glomerular hypertrophy were observed (Fig.5CI). According to quantitative analyses, the KTC-Exos significantly prevented mesangial expansion the mesangial expansion ($P < 0.0001$, Fig.5II).

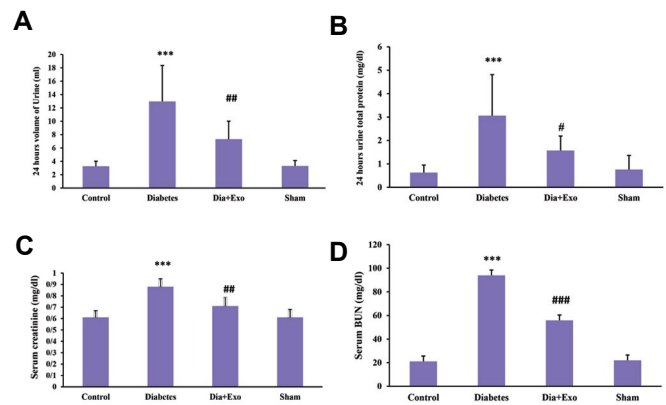


Fig.4: Effects of the kidney tubular cell-derived exosomes (KTC-Exos) on rats with diabetes. **A.** Urine volume, **B.** 24-hour urine protein, **C.** Serum creatinine (Scr), and **D.** Blood urea nitrogen (BUN) levels in the control and diabetes groups before and after treatment with KTC-Exos. Values are expressed as mean \pm SD for eight rats. ***, $P < 0.0001$ (comparison with control), #, $P < 0.01$, ##, $P < 0.001$, and ###, $P < 0.0001$ (comparison with diabetes).

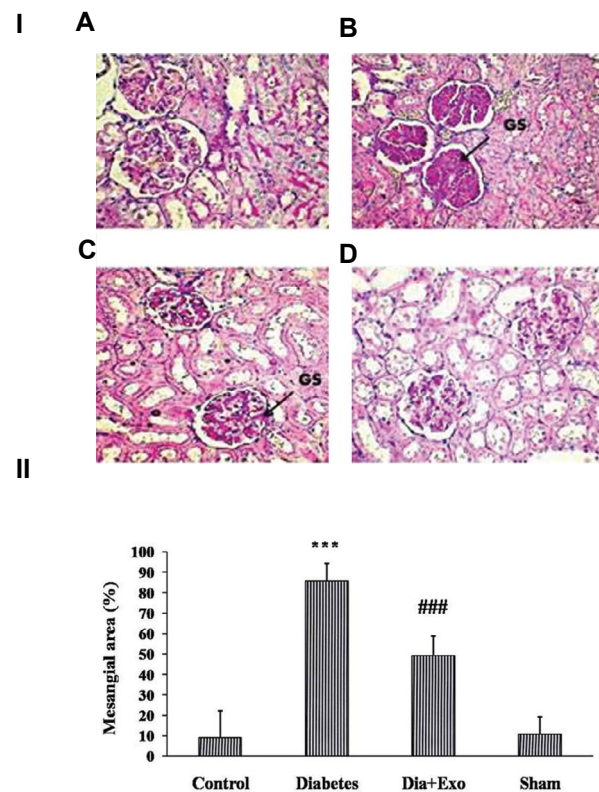


Fig.5: Intravenous injection of the kidney tubular cell-derived exosomes (KTC-Exos) ameliorated the changes in renal histopathology in diabetic rats after six weeks. **1.** Light microscopy examination of tissue sections that were stained by periodic acid-Schiff (PAS) from the different groups. **A.** Control, **B.** Diabetic, **C.** Diabetes treated with KTC-Exos, and **D.** Sham groups. **2.** Quantitative analysis of mean mesangial area from each group of rats. The results are expressed as the means \pm standard deviation for eight rats. ***, $P < 0.0001$, versus control group, ###, $P < 0.0001$, versus diabetic group, and GS; Glomerulosclerosis (magnification: x400).

Effect of kidney tubular cell-derived exosomes on expression levels of miR-377 and miR-29a

As seen in Figure 6, the qRT-PCR results show that *miR-377* expression considerably increased, whereas *miR-29a* expression significantly decreased following DN. In the KTC-Exos group, the level of increased *miR-377* significantly decreased ($P < 0.001$) and *miR-29a* expression significantly ($P < 0.001$). The levels of *miR-377* and *miR-29a* in the sham group were similar to the control group.

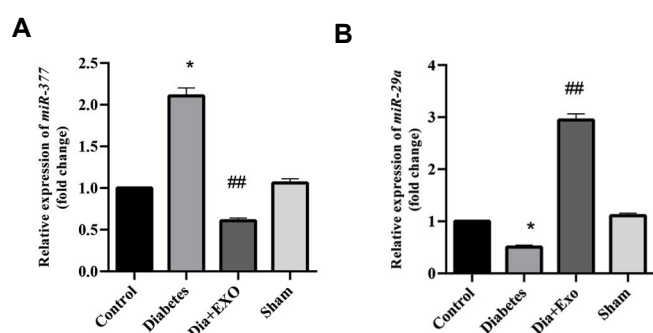


Fig.6: The effect of kidney tubular cell-derived exosomes (KTC-Exos) on the expression levels of **A.** *miR-377* and **B.** *miR-29a* following diabetic nephropathy (DN) injury. The quantitative real-time polymerase chain reaction (qRT-PCR) results showed that *miR-377* expression was significantly increased ($P < 0.01$) whereas *miR-29a* expression significantly decreased ($P < 0.01$) in the DN rats. The expression level of *miR-377* in the Dia+Exo Rats was significantly lower compared to the diabetes group, and the expression level of *miR-29a* in Dia+Exo Rats was significantly higher than the diabetes group. Data are presented as the means \pm standard deviation for eight rats. *, $P < 0.01$ versus the control group and ##, $P < 0.001$ versus the diabetes group.

Discussion

This study was designed to assess exosomes derived from highly differentiated KTCs as treatment for DN. DN is one of the main causes of ESRD and it is characterised by pathological modifications to the kidneys, which results in progressive loss of glomerular filtration rate, tubule-interstitial fibrosis, and proteinuria. Current treatments include precise monitoring of blood pressure and glucose levels, as well as blockage of the rennin-angiotensin mechanism in order to stop DN progression (27). However, novel treatment options for DM should be devised by experts in this field. Notably, several parameters could influence DN expansion after the onset of proteinuria (28).

The present study focused on the main factors involved in DN - endothelial cells and podocytes, both of which have tremendous contributions to the creation of filtration barriers. Increased glucose may decrease density and the numbers of podocytes, eliminate integrity of glomerular filtration membranes, modify its selective permeability, and enhance the development of glomerular sclerosis that can increase DN. Both loss and injury of the interacting proteins of the podocytes can promote apoptosis and destroy slit membrane integrity, thereby aggravating proteinuria and accelerating development of DN (29).

The potential use for exosomes in various research and

clinical practices has made it one of the probable therapeutic options for improving DN. In comparison to stem cells, KTCs also have advantages, especially in regenerative medicine. Some important studies have focused on the effects of exogenous kidney-derived exosomes on renal failure, such as ischemia-reperfusion (30). It is hypothesized that differentiated kidney cells may present more advanced developmental and cell differentiation impacts in comparison with undifferentiated cells; the contents of their exosomes may be different and more effective in treating renal injuries.

We isolated the exosomes by performing sequential and differential centrifugation procedures, as a general strategy, which resulted in the successful generation of KTC-Exos. Next, we assessed the ability of these KTC-Exos to control or reverse DN. The rats that received the KTC-Exos showed significant suppression of polyuria, proteinuria, Scr, and BUN expression levels. One of the main purposes of the present study was to evaluate the impact of KTC-Exos on *miR-29a* and *miR-377* expression in DN progression and pathogenesis in diabetic rats. We observed a considerable increase in mean *miR-377* expression and a significant decrease in mean *miR-29a* expression in the DN animals compared to the control group. This study showed that KTC-Exos administration led to significant downregulation of *miR-377* and upregulation of *miR-29a* in kidney cells of the treated rats. These results suggested that KTC-Exos had a protective function in high glucose-induced miRNA and growth factors (31).

miRNA dysregulations have been identified in many research areas, including DN (32). miRNAs are pivotal regulators of cellular and molecular pathways; therefore, identifying the targets of DN-associated miRNAs can provide further insights into the pathogenesis of DN (33).

In addition, miRNAs in extracellular environments are the essential modulators in renal fibrosis, DN, progressive kidney diseases, and acute kidney injuries. The miRNAs packed in extracellular vesicles, like exosomes, have shown modifications in concentrations related to the incidence of DN and are considered to be potent non-invasive biomarkers that can be used to diagnose and treat DN in patients (34).

There was high expression of *miR-377* in the increased glucose-treated cultured cells, Transforming growth factor beta (*TGF- β*) treated humans, and mice mesangial cells. Increased expression of *miR-377* led to suppression of *p21*-activated kinases and superoxide dismutase, which promoted fibronectin expression. The results of previous studies have shown that *miR-377* caused a decrease in the activities of some target genes, *PAK1* and *SOD1/2*. This led to increased vulnerability to the oxidant stresses and fibronectin accumulation in the extracellular matrix (ECM) (35). Therefore, this miRNA could pivotally contribute to the response of the mesangial cells to diabetic medium and may be a target miRNA for therapy.

Other miRNAs, such as the *miR-29* family (*miR-29a*, *miR-29b*, *miR-29c*), are responsible for anti-fibrotic effects in DN. *miR-29a* directly targets the 3'UTR of *COL4a1* and *COL4a2*, leading to decreased expressions of these two fibrotic genes (36). The *miR-29* family targets a group of mRNAs that encode the proteins implicated in fibrosis, as numerous collagens, elastin and fibrillin. Consequently, decreased *miR-29* expression activates such mRNAs expressions and promotes fibrotic responses (37). In cultured human proximal tubular epithelial cells, increased glucose and *TGF-β1* decrease *miR-29a* expression. Collagen IV is reported to be a target of *miR-29a*, and *miR-29a* regulates collagen expression. Decreased *miR-29a* levels in diabetes may increase collagen deposition, thus mediating the DN pathogenesis (38).

Recent studies have focused on exosomes as treatments for chronic disease models. Exosomes provide protection against the development of chronic kidney damage via suppression of GS, tubulointerstitial fibrosis and capillary rarefaction. For example, researchers examined exosomes with six months following an ischaemia-reperfusion injury (IRI) kidney model and reported that renal microvascular density rarefaction in the presence of sustained hypoxia had a correlation with acceleration of development towards chronic kidney diseases. Microvesicles can reduce tubule-interstitial fibrosis, microvascular rarefaction, and GS, which maintain renal functions (39). Furthermore, the obtained histopathological results showed the ability of exosomes decrease kidney damage, including GS, in a diabetic model.

Based on the literature and the present study results, exosomes extracted from the KTCs may prevent kidney impairments in diabetic patients. Therefore, the combination of exosomes and KTCs would be an encouraging treatment approach in regenerative medicine that would have less immune rejection, increased stability and more acceptable differentiation.

Conclusion

The present findings showed that exosomes derived from KTCs can ameliorate kidney damages in animals with diabetes. Several miRNAs are involved in the pathogenesis and development of DN, where as other miRNAs prevent this disease. Restoration of miRNAs expression to a normal level may be a therapeutic potential for stopping or attenuating disease progression. We have shown that administration of KTC-Exos resulted in upregulation of *miR-377* and downregulation of *miR-29a* in DN, and significantly modulated and improved the symptoms of this disease. These miRNAs present a notable capacity for acting as biomarkers for diagnosing, treating, and prognosis of DN. One of the newly developed treatment approaches would be to apply KTC-Exos for treatment of DN. The effects of exosomes on abnormal regression, damage to podocyte cells, and thickening of the glomerular basement membrane, which are complications of DN, should be taken into consideration in future studies.

Acknowledgments

This manuscript was extracted from the Ph.D. thesis of Fereshtesadat Fakhredini and supported by a grant (CMRC-9805) from the Research Council of Ahvaz Jundishapur University of Medical Sciences in 2019. The authors declare that there are no conflicts of interest.

Authors' Contributions

F.S.F., M.O., E.M.; Contributed to the study conception and design, performed all of the experiments, data and statistical analysis, and interpreted the data. F.S.F., S.A.M., M.R.; Performed western blot and real-time PCR techniques. A.V.G.; Contributed to the cell culture work. M.O., E.M.; Supervised the research. F.S.F.; Drafted the manuscript, which was revised by M.O. and E.M. All authors read and approved the final manuscript.

References

- Martínez-Castelao A, Navarro-González JF, Górriz JL, de Alvaro F. The concept and the epidemiology of diabetic nephropathy have changed in recent years. *J Clin Med*. 2015; 4(6): 1207-1216.
- Saran R, Robinson B, Abbott KC, Agodoa LYC, Albertus P, Ayanian J, et al. US renal data system 2016 annual data report: epidemiology of kidney disease in the United States. *Am J Kidney Dis*. 2017; 69(3Suppl 1): A7-A8.
- Sagoo MK, Gnudi L. Diabetic nephropathy: is there a role for oxidative stress? *Free Radic Biol Med*. 2018; 116: 50-63.
- Cao Q, Chen XM, Huang C, Pollock CA. MicroRNA as novel biomarkers and therapeutic targets in diabetic kidney disease: an update. *FASEB Bioadv*. 2019; 1(6): 375-388.
- Kim MK. Treatment of diabetic kidney disease: current and future targets. *Korean J Intern Med*. 2017; 32(4): 622-630.
- Ahmad J. Management of diabetic nephropathy: recent progress and future perspective. *Diabetes MetabSyndr*. 2015; 9(4): 343-358.
- Nagaishi K, Mizue Y, Chikenji T, Otani M, Nakano M, Konari N, et al. Mesenchymal stem cell therapy ameliorates diabetic nephropathy via the paracrine effect of renal trophic factors including exosomes. *Sci Rep*. 2016; 6: 34842.
- Dominguez JH, Liu Y, Gao H, Dominguez JM 2nd, Xie D, Kelly KJ. Renal tubular cell-derived extracellular vesicles accelerate the recovery of established renal ischemia reperfusion injury. *J Am Soc Nephrol*. 2017; 28(12): 3533-3544.
- Roy S, Hochberg FH, Jones PS. Extracellular vesicles: the growth as diagnostics and therapeutics; a survey. *J Extracell Vesicles*. 2018; 7(1): 1438720.
- Li JS, Li B. Renal injury repair: how about the role of stem cells. *Adv Exp Med Biol*. 2019; 1165: 661-670.
- Wang SY, Hong Q, Zhang CY, Yang YJ, Cai GY, Chen XM. miRNAs in stem cell-derived extracellular vesicles for acute kidney injury treatment: comprehensive review of preclinical studies. *Stem Cell Res Ther*. 2019; 10(1): 281.
- Keshkar S, Azarpira N, Ghahremani MH. Mesenchymal stem cell-derived extracellular vesicles: novel frontiers in regenerative medicine. *Stem Cell Res Ther*. 2018; 9(1): 63.
- Kato M. Noncoding RNAs as therapeutic targets in early stage diabetic kidney disease. *Kidney Res Clin Pract*. 2018; 37(3): 197-209.
- Yang H, Lian D, Zhang X, Li H, Xin G. Key genes and signaling pathways contribute to the pathogenesis of diabetic nephropathy. *Iran J Kidney Dis*. 2019; 13(2): 87-97.
- Ma N, Xiang Y, Zhang Y, Zhao X, Zhou L, Gao X. The balance mediated by miRNAs and the hemeoxygenase 1 feedback loop contributes to biological effects. *J Cell Biochem*. 2013; 114(12): 2637-2642.
- Li H, Zhang L, Wang F, Shi Y, Ren Y, Liu Q, et al. Attenuation of glomerular injury in diabetic mice with tert-butylhydroquinone through nuclear factor erythroid 2-related factor 2-dependent antioxidant gene activation. *Am J Nephrol*. 2011; 33(4): 289-297.
- Tung CW, Ho C, Hsu YC, Huang SC, Shih YH, Lin CL. MicroRNA-29a Attenuates diabetic glomerular injury through modulating cannabinoid receptor 1 signaling. *Molecules*. 2019; 24(2): 264.

18. Ebadi Z, Moradi N, Kazemi Fard T, Balochnejadmojarrad T, Chamani E, Fadaei R, et al. Captopril and spironolactone can attenuate diabetic nephropathy in wistar rats by targeting microRNA-192 and microRNA-29a/b/c. *DNA Cell Biol.* 2019; 38(10): 1134-1142.
19. Kelly KJ, Zhang J, Han L, Kamocka M, Miller C, Gattone VH 2nd, et al. Improved structure and function in autosomal recessive polycystic rat kidneys with renal tubular cell therapy. *PLoS One.* 2015; 10(7): e0131677.
20. Bär C, Thum T, de Gonzalo-Calvo D. Circulating miRNAs as mediators in cell-to-cell communication. *Epigenomics.* 2019; 11(2): 111-113.
21. Wu R, Huang C, Wu Q, Jia X, Liu M, Xue Z, et al. Exosomes secreted by urine-derived stem cells improve stress urinary incontinence by promoting repair of pubococcygeus muscle injury in rats. *Stem Cell Res Ther.* 2019; 10(1): 80.
22. Nojehdehi Sh, Hashemi SM, Hesampour A. Isolation and characterization of exosomes separated from stem cells by ultra-centrifuge method. *Research in Medicine.* 2018; 41(4): 422-405.
23. Mao F, Wu Y, Tang X, Kang J, Zhang B, Yan Y, et al. Exosomes derived from human umbilical cord mesenchymal stem cells relieve inflammatory bowel disease in mice. *Biomed Res Int.* 2017; 2017: 5356760.
24. Jelodar Gh, Mohammadi M, Akbari A, Nazifi S. Cyclohexane extract of walnut leaves improves indices of oxidative stress, total homocysteine and lipids profiles in streptozotocin-induced diabetic rats. *Physiol Rep.* 2020; 8(1): e14348.
25. Ebrahim N, Ahmed IA, Hussien NI, Dessouky AA, Farid AS, Elshazly AM, et al. Mesenchymal stem cell-derived exosomes ameliorated diabetic nephropathy by autophagy induction through the mTOR signaling pathway. *Cells.* 2018; 7(12): 226.
26. Jiang ZZ, Liu YM, Niu X, Yin JY, Hu B, Guo SC, et al. Exosomes secreted by human urine-derived stem cells could prevent kidney complications from type I diabetes in rats. *Stem Cell Res Ther.* 2016; 7: 24.
27. Sun ZJ, Li XQ, Chang DY, Wang SX, Liu G, Chen M, et al. Complement deposition on renal histopathology of patients with diabetic nephropathy. *Diabetes Metab.* 2019; 45(4): 363-368.
28. Shi JX, Huang Q. Glucagon-like peptide-1 protects mouse podocytes against high glucose-induced apoptosis, and suppresses reactive oxygen species production and proinflammatory cytokine secretion, through sirtuin 1 activation in vitro. *Mol Med Rep.* 2018; 18(2): 1789-1797.
29. Zhan X, Yan C, Chen Y, Wei X, Xiao J, Deng L, et al. Celastrol antagonizes high glucose-evoked podocyte injury, inflammation and insulin resistance by restoring the HO-1-mediated autophagy pathway. *Mol Immunol.* 2018; 104: 61-68.
30. Dominguez JH, Liu Y, Gao H, Dominguez JM, Xie D, Kelly KJ. Renal Tubular cell-derived extracellular vesicles accelerate the recovery of established renal ischemia reperfusion injury. *J Am Soc Nephrol.* 2017; 28(12): 3533-3544.
31. Nargesi AA, Lerman LO, Eirin A. Mesenchymal stem cell-derived extracellular vesicles for renal repair. *Curr Gene Ther.* 2017; 17(1): 29-42.
32. Fan B, Luk AOY, Chan JCN, Ma RCW. MicroRNA and diabetic complications: a clinical perspective. *Antioxid Redox Signal.* 2018; 29(11): 1041-1063.
33. Simpson K, Wonnacott A, Fraser DJ, and Bowen T. MicroRNAs in diabetic nephropathy: from biomarkers to therapy. *Curr Diab Rep.* 2016; 16(3): 35.
34. Petrillo F, Iervolino A, Zacchia M, Simeoni A, Masella C, Capolongo G, et al. MicroRNAs in Renal diseases: a potential novel therapeutic target. *Kidney Dis (Basel).* 2017; 3(3): 111-119.
35. Al-Kafaji G, Al-Muhtareh HA. Expression of microRNA-377 and microRNA-192 and their potential as blood-based biomarkers for early detection of type 2 diabetic nephropathy. *Mol Med Rep.* 2018; 18(1): 1171-1180.
36. Wang B, Wang J, He W, Zhao Y, Zhang A, Liu Y, et al. Exogenous miR-29a attenuates muscle atrophy and kidney fibrosis in unilateral ureteral obstruction mice. *Hum Gene Ther.* 2020; 31(5-6): 367-375.
37. Wang B, Komers R, Carew R, Winbanks CE, Xu B, Herman-Edelstein M, et al. Suppression of microRNA-29 expression by TGF- β 1 promotes collagen expression and renal fibrosis. *J Am Soc Nephrol.* 2012; 23(2): 252-265.
38. Du B, Ma LM, Huang MB, Zhou H, Huang HL, Shao P, et al. High glucose down-regulates miR-29a to increase collagen IV production in HK-2 cells. *FEBS Lett.* 2010; 584(4): 811-816.
39. Meng W, He C, Hao Y, Wang L, Li L, Zhu G. Prospects and challenges of extracellular vesicle-based drug delivery system: considering cell source. *Drug Deliv.* 2020; 27(1): 585-598.

Fabrication and *In Vitro* Evaluation of A Chondroitin Sulphate-Polycaprolactone Composite Nanofibrous Scaffold for Potential Use in Dermal Tissue Engineering

Mohamad Pezeshki-Modaress, Ph.D.¹, Mohadeseh Akbarzadeh, M.Sc.², Dariush Ebrahimibagha, M.Sc.³,
Mojgan Zandi, Ph.D.², Tayyeb Ghadimi, M.D.¹, Amin Sadeghi, M.Sc.⁴, Sarah Rajabi, Ph.D.^{5*}

1. Burn Research Centre, Iran University of Medical Sciences, Tehran, Iran

2. Department of Biomaterials, Iran Polymer and Petrochemical Institute, Tehran, Iran

3. Hard Tissue Engineering Research Centre, Tissue Engineering and Regenerative Medicine Institute, Central Tehran Branch, Islamic Azad University, Tehran, Iran

4. Soft Tissue Engineering Research Centre, Tissue Engineering and Regenerative Medicine Institute, Central Tehran Branch, Islamic Azad University, Tehran, Iran

5. Department of Cell Engineering, Cell Science Research Centre, Royan Institute for Stem Cell Biology and Technology, ACECR, Tehran, Iran

*Corresponding Address: P.O. Box: 16635-148, Department of Cell Engineering, Cell Science Research Centre, Royan Institute for Stem Cell Biology and Technology, ACECR, Tehran, Iran
Email: srajabi@royaninstitute.org

Received: 05/June/2020, Accepted: 06/September/2020

Abstract

Objective: Poly(ϵ -caprolactone) (PCL) has considerable mechanical and biological properties that make it a good candidate for tissue engineering applications. PCL alongside proteins and polysaccharides, like gelatin (GEL) and chondroitin sulphate (CS), can be used to fabricate composite scaffolds that provide mechanical and biological requirements for skin tissue engineering scaffolds. The aim of this study was fabricating novel composite nanofibrous scaffold containing various ratios of GEL/CS and PCL using co-electrospinning process.

Materials and Methods: In this experimental study, PCL mixed with a GEL/CS blend has limitations in miscibility and the lack of a common solvent. Here, we electrospun PCL and GEL/CS coincide separately on the same drum by using different nozzles to create composite nanofibrous scaffolds with different ratios (2:1, 1:1 and 1:2) of GEL to CS-PCL, and we mixed them at the micro/nanoscale. Morphology, porosity, phosphate-buffered saline (PBS) absorption, chemical structure, mechanical property and *in vitro* bioactivity of the prepared composite scaffolds were analysed.

Results: Scanning electron microscopy (SEM) images showed beadless nanofibres at all ratios of GEL to CS-PCL. The composite scaffolds (2:1, 1:1 and 1:2) had increased porosity compared to the PCL nanofibrous scaffolds, in addition to a significant increase in PBS absorption. The mechanical properties of the composite scaffolds were investigated under different conditions. The results demonstrated that all of the composite specimens had better strength when compared with the GEL/CS nanofibres. The increase in PCL ratio led to an increase in tensile strength of the nanofibres. Human dermal fibroblasts (HDF) were cultured on the fabricated composite scaffolds and evaluated by 3-(4,5-dimethylthiazol-2-yl)-5-(3-carboxymethoxyphenyl)-2-(4-sulfophenyl)-2H-tetrazolium (MTS) analysis and SEM. The results showed the bioactivity of these nanofibres and the potential for these scaffolds to be used for skin tissue engineering applications.

Conclusion: The fabricated co-electrospun composite scaffolds had higher porosity and PBS absorption in comparison with the PCL nanofibrous scaffolds, in addition to significant improvements in mechanical properties under wet and dry conditions compared to the GEL/CS scaffold.

Keywords: Chondroitin Sulphate, Co-electrospinning, Nanofibres, Polycaprolactone, Tissue Engineering

Cell Journal (Yakhteh), Vol 24, No 1, January 2022, Pages: 36-43

Citation: Pezeshki-Modaress M, Akbarzadeh M, Ebrahimibagha D, Zandi M, Ghadimi T, Sadeghi A, Rajabi S. Fabrication and in vitro evaluation of a chondroitin Fabrication and in vitro evaluation of a chondroitin Sulphate-polycaprolactone composite nanofibrous Scaffold for potential use in dermal tissue engineering. Cell J. 2022; 24(1): 36-43. doi: 10.22074/cellj.2022.7655.

This open-access article has been published under the terms of the Creative Commons Attribution Non-Commercial 3.0 (CC BY-NC 3.0).

Introduction

Polymeric nanofibrous scaffolds simulate the native extracellular matrix (ECM) in skin tissue and offer compelling advantages (1, 2). Selection of scaffold architecture is important because the dimensions of the ECM protein fibre (collagen) are smaller than the cell dimensions, and they can easily contact the cells directly in three dimensions. The micro-environmental features of a tissue-engineered scaffold should be considered in order to restore tissue function and exchange proper signals between cells and other cells or environments (3). Therefore, preparation of nanoscale fibres that resemble the environmental conditions of a tissue could be of benefit when developing tissue-engineered scaffolds that have nanoscale structures (4-6).

Electrospinning is a flexible, reliable method to produce nanofibres that have various applications for tissue engineering (7). Both natural and synthetic polymers are good candidates for production of electrospun nanofibres. Natural polymers have good biocompatibility and biological properties because their structure mimics native cellular environments; however, they often have low mechanical properties when compared to synthetic polymers (8, 9). Therefore, the combination of natural and synthetic polymers is considered a promising option when preparing nanofibrous scaffolds for tissue engineering applications. Access to a range of polymers could be beneficial for improving special properties such as mechanical or biological features; however, there are limitations. For example, natural polymers mostly have

polar structures and are easily soluble in polar solvents like water, whereas synthetic hydrophobic polymers are soluble in nonpolar organic solvents. Finding a common solvent is difficult; otherwise, researchers must use toxic or aggressive solvents (10). Poly(ϵ -caprolactone) (PCL)/chitosan blends, for instance, are dissolved in trifluoroethanol (TFE), hexafluoro-2-propanol and trifluoroacetic acid (11-13). In order to overcome these solvent problems, natural and synthetic polymers can be fabricated separately on the same collector by a co-electrospinning process.

Widespread use of GAGs and gelatin (GEL) for preparation of scaffolds is an effective approach used to replace natural ECM components (14, 15). GEL is derived from collagen and can improve the wound healing process by inducing cell migration, adhesion, growth and organization (16, 17). Chondroitin sulphate (CS) plays an important role in tissue regeneration and wound healing, and is one of the main components of the ECM. CS supports cell proliferation, attachment and migration. Therefore, GEL/CS is a suitable biomaterial for tissue engineering and wound healing applications, and its nanofibrous structure has tremendous potential to mimic the ECM in tissue engineering (18, 19). The results of different studies show that both mechanical properties and cellular activities of proteins, like collagen and GEL, can be improved by incorporation of polysaccharides such as CS or chitosan (15, 20). Furthermore, PCL is a biodegradable and a biocompatible material that has noticeable mechanical properties and spinnability. PCL has been used to fabricate nanofibrous scaffolds by electrospinning (21, 22). There are many reports about the use of natural polymeric nanofibres for tissue engineering applications; however, low mechanical performance, particularly under wet conditions, has limited their clinical applications. Skin is usually subjected to tensile stresses. Moreover, the scaffolds used as substitutes for skin tissue regeneration have high area/thickness ratios; therefore, the tensile mechanical performances of scaffolds are important factors that can influence both the clinical operations and wound healing processes (8, 9, 16). The co-electrospinning process can be a promising technique for fabrication of nanoscale/microscale composite scaffolds that have enhanced physical properties. In this study, we intend to fabricate a new composite nanofibrous scaffold that contains various ratios of GEL/CS and PCL by co-electrospinning. The fabricated composite nanofibrous scaffolds were crosslinked using N-(3-dimethylaminopropyl)-N'-ethyl carbodiimide hydrochloride (EDC) as a zero-length crosslinker. The effect of PCL ratio on physical, chemical and biological properties of these composite scaffolds was investigated. To the best of our knowledge, there is no published study about composite scaffolds that contain CS and PCL, and crosslinked using EDC for skin tissue engineering applications.

Materials and Methods

Fabrication of electrospun nanofibres

In this experimental study, we prepared a PCL solution (MW: 80 000, Sigma Aldrich, USA) in a co-solvent system of formic/acetic acid (9:1 ratio, Merck, Germany) with a concentration of 12.5% (w/v) for fabrication of the PCL. The GEL solution that contained CS was prepared as previously reported (20, 23). Briefly, GEL type B (Sigma Aldrich, USA) and CS type A from bovine trachea (Sigma Aldrich, USA) blend solutions were prepared in a solvent system of TFE: water (equal volume ratio, Merck, Germany) and mixed overnight at room temperature in order to have a homogeneous blend solution with a GEL/CS ratio of 85:15. We prepared five samples that consisted of neat PCL, GEL/CS and three different composite nanofibres (GEL/CS-PCL). The composite scaffolds consisted of the following ratios: one syringe of GEL/CS to one syringe of PCL (1:1); two syringes of GEL/CS to one syringe of PCL (2:1); and one syringe of GEL/CS to two syringes of PCL (1:2). The prepared solutions were subjected to electrospinning using a 5 ml syringe and a cylindrical collector covered with aluminum foil in a horizontal system (Co881007 NYI, ANSTCO, Iran). The electrospinning process was performed at a process condition of 0.6 ml/h flow rate and 19 kV applied voltage for the GEL/CS samples. PCL was electrospun at a 0.9 ml/h flow rate and 25 kV applied voltage. The collector was placed 100 mm of the needle tips. Table 1 summarizes the compositions of the electrospun scaffolds.

Table 1: Different combinations of GEL/CS- PCL composite electrospun scaffolds

Scaffold	Number of nozzles and feeding rate (ml/h) for GEL-CS	Number of nozzles and feeding rate (ml/h) for PCL
GEL/CS	1 (0.6 ml/h)	0 (0.9 ml/h)
GEL/CS-PCL (2:1)	2 (0.6 ml/h)	1 (0.9 ml/h)
GEL/CS-PCL (1:1)	1 (0.6 ml/h)	1 (0.9 ml/h)
GEL/CS-/PCL (1:2)	1 (0.6 ml/h)	2 (0.9 ml/h)
PCL	0 (0.6 ml/h)	1 (0.9 ml/h)

PCL; Poly(ϵ -caprolactone), GEL/CS; Gelatin/chondroitin sulphate, and h; Hour.

Crosslinking and sterilization

The chemical crosslinking agent to the nanofibrous scaffolds consisted of 0.02 g EDC (Merck, Germany) in which 10 ml ethanol (Merck, Germany) was added for 24 hours, followed by sterilization in 70% ethanol for 4 hours. The scaffolds were washed several times in phosphate-buffered saline (PBS) to remove any residual ethanol.

Morphology of the fibres

A scanning electron microscope (VEGA, TESCAN, Czech), at an operating voltage of 15 kV, was used to investigate the morphology of the GEL/CS-PCL electrospun nanofibres. The samples were mounted on aluminum stubs and coated with a thin layer of gold.

Measurement of porosity and phosphate-buffered saline absorption

Dry scaffolds (W_d) were plunged in ethanol for two hours and the weights of the samples in ethanol were noted as W_l . The ethanol was removed from the surface of scaffolds by a filter paper and the wet scaffold weights were measured as W_w . The porosity of the electrospun nanofibres was calculated by following formula (8, 24):

$$\text{Porosity (\%)} = (W_w - W_d) / (W_w - W_l) \times 100$$

The PBS solution absorbed of prepared composite nanofibres was calculated by placing the crosslinked electrospun composite scaffolds in PBS (pH=7.4) at 37°C for 24 hours as reported previously (24, 25):

$$\text{PBS absorption (\%)} = (w_1 - w_0) / w_0 \times 100$$

Where: w_0 and w_1 are the weights of the scaffolds before and after soaking in PBS, respectively. The values are shown as the mean \pm standard error (n=3).

Mechanical properties

Mechanical performance of the prepared composite nanofibres was analysed as previously reported using a mechanical tester STM-20 (SANTAM, Iran) and rectangular shape ($3 \times 1 \text{ cm}^2$) with an approximate thickness of 50 μm under a 10 mm/min deformation rate at room temperature (8, 26, 27). The tensile strength and elongation at the break of the composite scaffolds were expressed as the mean \pm standard error (n=3). The tensile strength of samples was investigated under three conditions: non-crosslinked (as spun) dry state, crosslinked dry state and wet state. For the wet conditions, the nanofibres were immersed in 50 ml of PBS (pH=7.4) for two hours at room temperature.

Fourier transform infrared analysis

The GEL/CS-PCL nanofibrous scaffolds were analysed by infrared spectroscopy to identify their chemical structures (EQUINOX 55, Bruker, Germany). Fourier transform infrared (FTIR) spectra were scanned in the spectral range of 400-4000 cm^{-1} .

Cell culture study

Human dermal fibroblasts (HDF) were purchased from Royan Cell Bank Services (code no: RSCB0179, Ethics Code: IR.IUMS.REC.1396.32153). The medium consisted of DMEM/F12 (Gibco, Canada) with 1% L-glutamine (Gibco, Canada), 10% foetal bovine serum (FBS, Gibco, Canada) and 1% penicillin/streptomycin (Gibco, Canada). A flask tissue culture (T-75) was used

to culture the HDF. In all of the experiments, we used cells that were between four and six passages. The cells were maintained at 37°C, 5% CO_2 and 95% humidity. The culture medium was refreshed every two days. Prior to cell seeding, 0.05% trypsin/EDTA (Gibco, Canada) was used to dissociate the cells, which were subsequently centrifuged and resuspended in medium.

Analysis of cell proliferation and morphology on the composite scaffolds

The scaffolds were sterilized and the samples were incubated overnight in culture medium. The HDF were resuspended in culture medium (1×10^4 cells/ cm^2) with 10% FBS which loaded on the scaffolds in 24-well culture plates. The medium was changed every two days. All experiments were performed in triplicate. 4'-6-diamidino-2-phenylindole (DAPI, Sigma Aldrich, USA) staining, 3-(4,5-dimethylthiazol-2-yl)-5-(3-carboxymethoxyphenyl)-2-(4-sulfophenyl)-2H-tetrazolium (MTS) assay and scanning electron microscopy (SEM) were used to analyse the samples. The MTS assay is a standard method to evaluate cell proliferation and metabolic activity on scaffolds. The MTS (Promega, G5421) assay was performed according to the manufacturer's instructions. Briefly, HDF cells were seeded on the scaffolds in medium, at a density of 1×10^4 cells/ cm^2 (n=3). The medium was replaced every two days. At 1, 3, 7 and 14 days after seeding, we added the MTS solution to each well. Then, the plates were incubated in the dark at 37°C for three hours. Absorption of the solution was measured at 490 nm.

On days 1 and 7, the samples were fixed with 10% formaldehyde for two hours, stained with DAPI and washed with PBS in order to assess the amount of cells that adhered to the nanofibres and to visualise their nuclei. The images were taken using a fluorescence microscope (Olympus, IX71, Japan) to determine the location and distribution of the cell nuclei.

SEM was used to study the morphological characteristics of the cells cultured on the nanofibres. The samples were cultured for one and seven days, and then the scaffolds were harvested. The samples were washed with PBS and fixed overnight with 2.5% glutaraldehyde at 4°C to remove any non-adherent cells. These samples were then dehydrated by a graded series of alcohol (30, 50, 70, 80, 90, 96 and 100%) and subsequently vacuum-dried overnight. The scaffolds were coated with gold and observed by SEM at 15 kV.

Statistical analysis

All of the experimental data are presented as mean \pm standard error. Statistical analysis for elucidation of differences in the measured properties between the groups was accomplished using one-way analysis of variance (ANOVA) in SPSS 16.0 software (America, IBM) followed by Tukey's HSD post hoc test.

Results

Morphology of the nanofibres

Figure 1 shows the SEM micrographs of the electrospun GEL/CS, PCL and GEL/CS-PCL composite scaffolds with different ratios of PCL. Nanofibrous structures were attained in all of the scaffolds and no beads were observed.

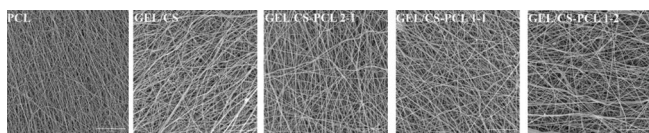


Fig.1: SEM micrographs of the PCL, GEL/CS and composite scaffolds with different ratios of PCL (GEL/CS-PCL 2:1, GEL/CS-PCL 1:1 and GEL/CS-PCL 1:2). SEM; Scanning electron microscopy, PCL; Poly(ϵ -caprolactone), and GEL/CS; Gelatin/chondroitin sulphate (scale bar: 10 μ m).

Porosity and phosphate-buffered saline absorption

Figure 2A shows the physical and chemical properties of the PCL, GEL/CS and GEL/CS-PCL hybrid nanofibrous scaffolds. The GEL/CS nanofibrous scaffolds had the highest value ($96 \pm 0.5\%$), whereas the PCL scaffold was $82 \pm 2\%$. Co-electrospinning with different ratios of PCL and GEL/CS (2:1, 1:1 and 1:2) led to an increase in porosity compared to pure PCL.

PBS absorption of all specimens was performed to evaluate the exudate drainage ability of the nanofibrous scaffolds (Fig.2B). It is important that wound exudate can be steadily captured by the scaffold during the dermis regeneration process. Therefore, one of the effective dermal scaffold properties should be the ability to have high water absorption, which helps with better cell activity.

Hydrophilicity of the scaffold's components (e.g., GEL) can help to absorb the wound exudates (28). As shown in Figure 2, the GEL/CS scaffold had the highest absorption (around $900 \pm 100\%$) compared to the composite scaffolds. By taking into consideration the higher feeding rate of PCL, in comparison with GEL/CS, the composite GEL/CS-PCL 1:2 scaffold displayed the lowest PBS absorption among the co-electrospun samples because of the high mass ratio of PCL and hydrophobicity of the final composite.

Mechanical properties

Figure 2C, D show tensile strength and elongation at the break of the composite scaffolds. The GEL/CS based hybrid scaffolds with different concentrations of PCL were fabricated in three ratios (2:1, 1:1, 1:2). Mechanical performance of the prepared composite scaffolds was analysed under three different conditions: spun dry state, crosslinked dry state, and crosslinked wet state. Figure 2C shows that pure PCL has significant mechanical properties compared to pure GEL/CS; therefore, by increasing the proportion of PCL in the composite, the amount of stress needed to break the sample increased for the specimens under all conditions. The highest level was observed

in the GEL/CS-PCL 1:2 in the crosslinked dry state. Furthermore, we observed that the composite scaffolds containing PCL fibres, had higher elongation at break and more capability to resist rupturing (Fig.2D).

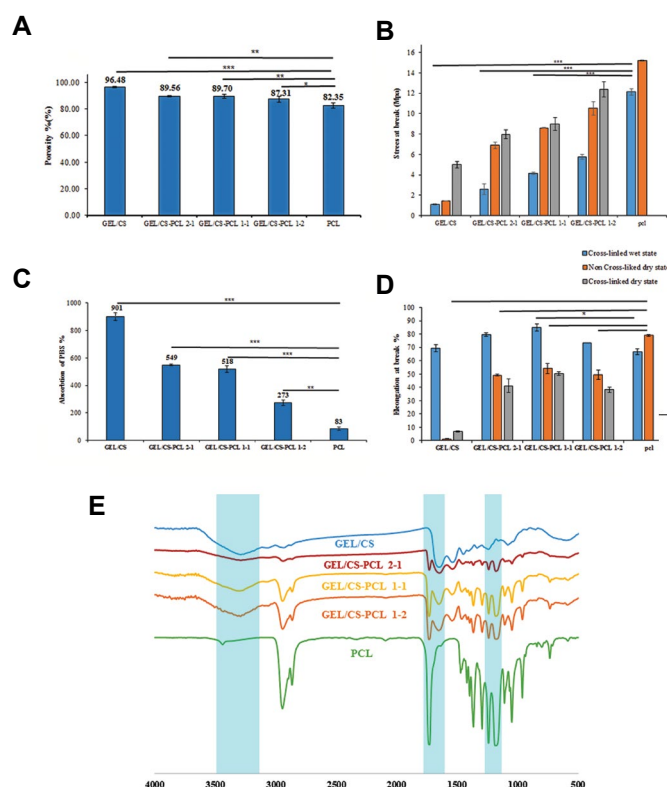


Fig.2: Physical and chemical properties of electrospun PCL, GEL/CS and composite scaffolds with different ratios of PCL (GEL/CS-PCL 2:1, GEL/CS-PCL 1:1 and GEL/CS-PCL 1:2). The values are presented as mean \pm standard error (n=3). **A.** Porosity analysis, **B.** Swelling ratio, **C.** **D.** Mechanical analysis and **E.** FTIR spectra (the X-axis of the spectrum is the wavenumber [cm^{-1}]). *, $P < 0.05$, **, $P < 0.01$, ***, $P < 0.001$, ****, $P < 0.0001$ indicate statistical significance, PCL; Poly(ϵ -caprolactone), GEL/CS; Gelatin/chondroitin sulphate, and FTIR; Fourier transform infrared spectra.

Fourier transform infrared analysis

Chemical structure analysis of the specimens was carried out by FTIR at 400-4000 cm^{-1} (Fig.2E). Carbonyl stretching of C=O is the dominant peak of PCL (1727 cm^{-1}). Moreover, peaks at 2942 and 2865 cm^{-1} are ascribed to C-H stretching vibration. The C=O and C-C had stretching peaks at 1293 cm^{-1} and 1240 cm^{-1} , respectively, while symmetric C-O-C stretching peaked at 1170 cm^{-1} (29). Because GEL/CS has alcoholic groups in its structure, 3460 cm^{-1} was the stretching vibration of OH. The C-O-C stretching vibration at 1070 cm^{-1} was related to the saccharide structure of GEL/CS. The peaks at 1430, 1400 and 1427 cm^{-1} resulted from coupling C-O stretching and O-H variable angle and the S=O stretching vibration (SO_4 -groups of GEL/CS), respectively. Other peaks at 750 cm^{-1} , 860 cm^{-1} and 940 cm^{-1} were related to C-O-S vibration (30-32).

In vitro cell adhesion and proliferation

In order to assess the biocompatibility of these GEL/CS-PCL scaffolds, we investigated proliferation, distribution

and adhesion of the HDF onto the composite nanofibres. Figure 3 shows the DAPI staining results. The cell nuclei remained intact during seven days of cell culture.

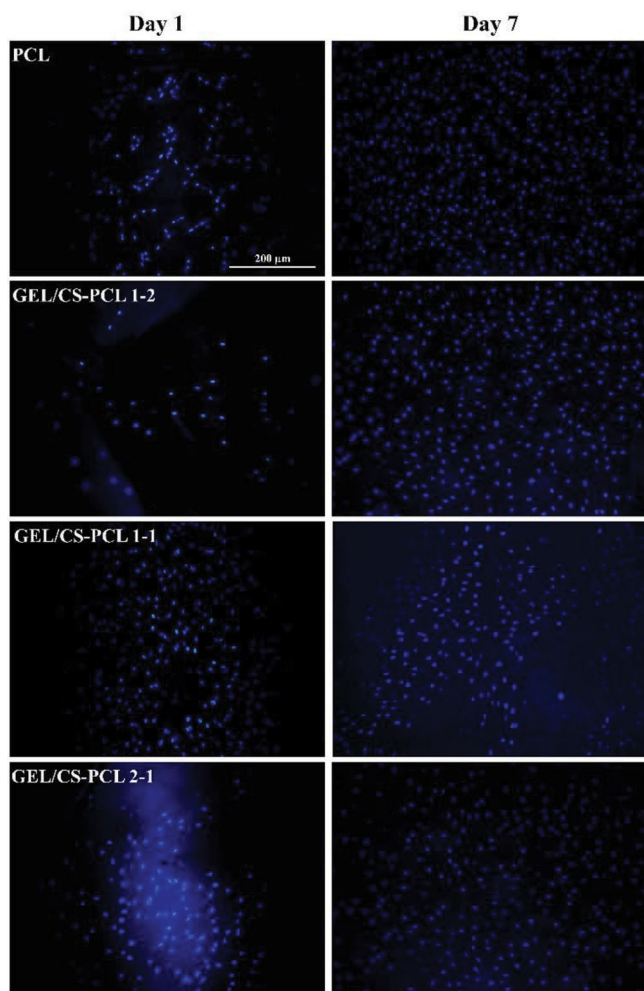


Fig.3: DAPI staining of HDF cells on electrospun PCL and composite scaffolds (GEL/CS-PCL 2:1, GEL/CS-PCL 1:1 and GEL/CS-PCL 1:2) after one and seven days of cell culture (scale bar: 200 μm for all DAPI images). DAPI; 4'-6-diamidino-2-phenylindole, PCL; Poly(ε-caprolactone), GEL/CS; Gelatin/chondroitin sulphate, and HDF; Human dermal fibroblasts.

Suitable cell attachment and proliferative behaviour were seen for all composite scaffolds. SEM analysis was performed on days 1 and 7 to obtain adequate precision in assessing cell adhesion and distribution, and their interactions with the composite scaffolds. Figure 4 depicts the different magnifications of the SEM results for the HDF cells cultured on prepared composite scaffolds that contained different ratios of PCL. We observed spreading and attachment of the cells on all of the composite scaffolds. DAPI staining images, by comparing the population of cells at days 1 and 7, indicated that the cells had high proliferation and proper distribution on the nanofibrous substrates. This finding confirmed the SEM results.

The results of the MTS assay for HDF cell viability for 14 days in cells cultured on scaffolds is shown in Figure 5. The absorbances of the composite GEL/CS-PCL scaffolds

compared to the PCL and GEL/CS nanofibres showed that co-electrospinning these polymers improved cell proliferation during 14 days. According to the MTS assay, the best proliferation for HDF cells was noted in the GEL/CS-PCL 1:1 and 2:1 composite nanofibrous scaffolds (Fig.5). Fibroblast cells in scaffolds that contained high ratios of GEL/CS in their composition (GEL/CS-PCL 1:1 and 2:1) had accelerated adhesion and proliferation.

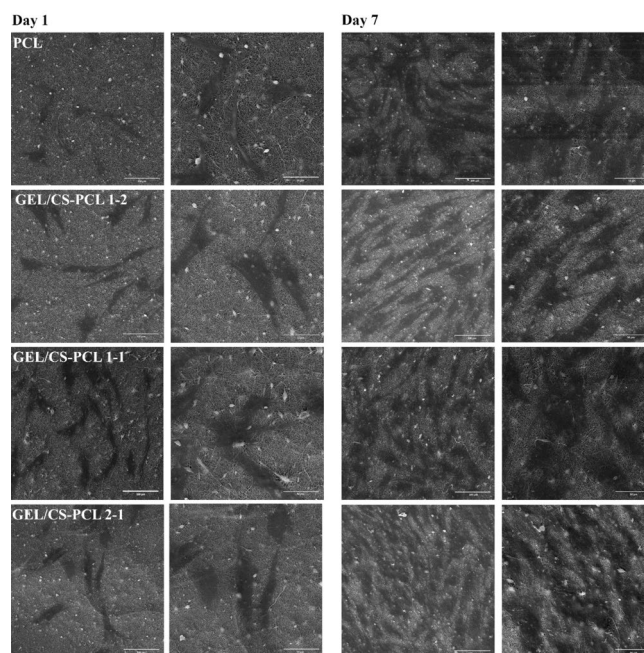


Fig.4: SEM micrographs of HDF cells on electrospun PCL and composite scaffolds (GEL/CS-PCL 2:1, GEL/CS-PCL 1:1 and GEL/CS-PCL 1:2) after one and seven days of culture visualised at different magnifications [scale bar:100 μm (left) and 50 μm (right)]. SEM; Scanning electron microscopy, PCL; Poly(ε-caprolactone), GEL/CS; Gelatin/chondroitin sulphate, and HDF; Human dermal fibroblasts.

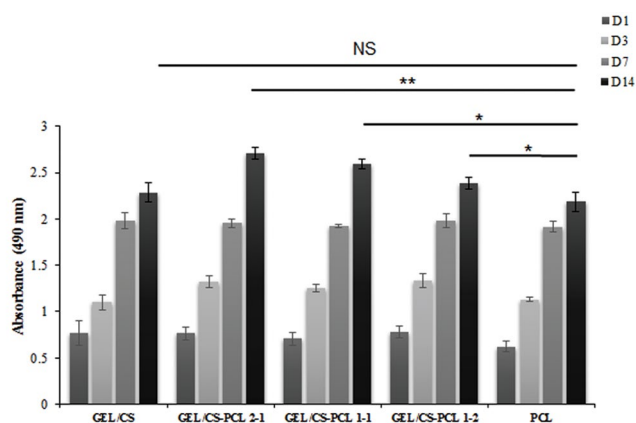


Fig.5: 3-(4,5-dimethylthiazol-2-yl)-5-(3 carboxymethoxyphenyl)-2-(4-sulfophenyl)-2H-tetrazolium (MTS) assay after 1, 3, 7 and 14 days for PCL, GEL/CS and composite scaffolds (GEL/CS-PCL 2:1, GEL/CS-PCL 1:1 and GEL/CS-PCL 1:2). The values are presented as the mean ± standard error (n=3). *, P<0.05, **, P<0.01 indicate statistical significance, NS; Not significant, PCL; Poly(ε-caprolactone), and GEL/CS; Gelatin/chondroitin sulphate.

Discussion

Co-electrospinning is a fascinating technique used to fabricate nanofibrous structures from completely different polymers and solvent systems. In this study, we took into consideration the bioactivity of a GEL/CS blend and the remarkable mechanical properties of PCL to prepare nanofibrous composite scaffolds that contained different ratios of PCL and GEL/CS by co-electrospinning. Two different solvent systems were used for the electrospinning process because PCL is a hydrophobic polymer and the GEL/CS blend are hydrophilic polymers.

In order to investigate the effect of PCL in the scaffold in terms of mechanical, chemical and biological properties, we assessed various ratios of PCL simultaneously combined with GEL/CS on one collector. In order to control the deposition of PCL and GEL/CS on the surface of the collector, three nozzles were used simultaneously. For example, in the GEL/CS-PCL 2:1 scaffold, two nozzles injected the GEL/CS solution and the third nozzle injected the PCL solution toward the collector.

SEM micrographs revealed that all of the prepared composite nanofibrous scaffolds were bead-free, and had uniform and highly porous morphologies. Scaffold porosity plays a key role in the penetration of nutrients and oxygen, waste removal, and drainage of wound exudate during dermis regeneration. Our results revealed that all of the GEL/CS- PCL composite electrospun scaffolds were similar in terms of porosity. Changing the PCL ratio, at the range used in this study, had no significant effect on composite scaffold porosity. Different ranges of porosity (between 60% and 90%) are often used for tissue engineering applications (9, 33, 34). In this study, prepared GEL/CS-PCL composite scaffolds had more than 80% porosity, which was comparable with different scaffolding methods like salt leaching, phase separation, fibre bonding, and three-dimensional printing (33, 35). Electrospun scaffolds have both high porosity and interconnected pore morphology; therefore, the efficient mass transfer of oxygen and nutrients would enable better migration and ECM formation of cells (34, 36, 37).

PBS absorption by the scaffolds was evaluated as an indication for exudate drainage ability of the composite scaffolds. Hydrophilicity of scaffold components like GEL and CS can help to absorb wound exudates (24, 28). We observed that all composite specimens were approximately equal in terms of porosity; therefore, the effect of using a hydrophilic material in the final electrospun scaffold is significant. Increasing the proportion of GEL/CS in the composite nanofibres (e.g., comparing GEL/CS-PCL 2:1 and 1:2) resulted in enhanced PBS absorption, whereas PCL, because of its hydrophobic structure, had the least PBS absorption. Co-electrospinning of GEL/CS with PCL at an equal number of nozzles (1:1) could improve PBS absorption to 524%.

Skin is usually exposed to tensile stresses; therefore, significant factors such as elongation at break and

tensile strength of scaffolds for dermal regeneration applications with high area and thickness ratios can impact only wound healing and the clinical operation. PCL is a common material with high tensile strength and elongation at break, and it is used to fabricate different kinds of scaffolds. We previously demonstrated (23, 24) that GEL and CS blend nanofibres have good potential for tissue engineering applications. We added PCL and used the co-electrospinning technique to enhance the mechanical properties of our GEL/CS nanofibres. The mechanical properties of these composite scaffolds were analysed under three different conditions: spun dry state, crosslinked dry state, and crosslinked wet state. The crosslinked wet state showed the effect of hydrated conditions on the mechanical property of the scaffold and simulated physiological conditions of the body. A comparison of GEL/CS and GEL/CS-PCL 1:1 in the crosslinked wet state showed that co-electrospinning of PCL with GEL/CS at equal nozzles (1:1) improved the tensile strength to 283% and elongation at break to 23%.

Crosslinking, as well as the addition of PCL to specimens, can improve the mechanical properties of scaffolds. In the absence of PCL fibres, crosslinking plays an important role in enhancing mechanical properties. Stress at break increased in the pure GEL/CS from 1.44 ± 0.02 MPa to 4.98 ± 0.31 MPa (245%) in the non-crosslinked dry state and crosslinked dry state, respectively. This boosting effect in the hybrid composition was less compared to pure GEL/CS. Under wet situations, although PBS can act as a plasticizer and lead to a longer elongation at break and lower tensile strength, compared to the dry states. Composite scaffolds that have a higher ratio of GEL/CS show less stress at break, which could be due to increased absorption of PBS. The results in this study demonstrated a significant effect of PCL in improving the GEL/CS mechanical properties under all conditions.

The biocompatibility of the composite nanofibres were evaluated using the MTS assay, SEM and DAPI staining. SEM micrographs of growing HDF cells demonstrated a good interaction that surrounded the fibres and attachment to the surface by filopodia. Cells stretched completely on the nanofibres by a spindle-like shape. The cells had a good adhesion and a characteristic spindle shape, as HDF cells, in which the scaffolds maintained the phenotype of the fibroblast cells. The SEM images also showed interconnection of neighbouring cells, which secreted filopodia. Different cellular activities were expected with the electrospun GEL/CS- PCL scaffolds that had different ratios of PCL because of the differences in chemical compositions in terms of hydrophobicity and functional groups of the natural and synthetic polymers. Absorbances of the composite GEL/CS- PCL scaffolds with PCL and GEL/CS nanofibres according to the MTS assay revealed that co-electrospinning of these polymers improved both the mechanical properties and cell proliferation during 14 days. Although HDF cell adhesion and proliferation were considerable in all specimens, both the GEL/CS-PCL 1:1 and GEL/CS-PCL 2:1 scaffolds had the best performance

for culturing HDF. Fibroblast cells in scaffolds that contain high ratios of GEL/CS in their composition have accelerated adhesion and proliferation.

Conclusion

The high mechanical performance of PCL was used to significantly improve the mechanical properties of GEL/CS nanofibrous scaffolds, as a bioactive structure for tissue engineering applications, by co-electrospinning. SEM images showed beadless nanofibrous structures for all PCL ratios. The fabricated co-electrospun composite scaffolds had better porosity and PBS absorption (524%) in comparison with the PCL nanofibrous scaffolds. Mechanical properties of the composite nanofibrous GEL/CS-PCL scaffolds were also investigated under wet and dry conditions. The results demonstrated that all composite specimens had better strength and elongation at break in comparison with GEL/CS nanofibres; increasing the PCL ratios led to increased tensile strength of the nanofibres. We compared the mechanical properties of the scaffolds in the crosslinked wet state and noted that co-electrospinning of PCL with GEL/CS at equal nozzles (1:1) improved both tensile strength and elongation at break in the GEL/CS to 283% and 23%, respectively. HDF cells cultured on fabricated composite scaffolds, along with MTS analyses and SEM micrographs, showed bioactivity of all the composite scaffolds; however, the GEL/CS-PCL 1:1 scaffold appeared to have the most potential for skin tissue engineering applications.

Acknowledgments

This study was supported by a grant from Iran University of Medical Science (grant no. 96-03-129-32153). There is no conflict of interest in this study.

Authors' Contributions

M.P.-M.; Supervision, conceptualization, and writing the original draft. M.A., D.E., A.S.; Methodology, investigation, validation, and writing the original draft. M.Z.; Design, methodology, and validation. T.G.; Methodology and validation. S.R.; Supervision, methodology, and statistical analysis. All authors performed editing and approved the final version of this manuscript for submission.

References

- Calderon MAR, Zhao W. Applications of polymer nanofibers in biomaterials, biotechnology and biomedicine: a review. *Appl Biochem Biotechnol.* 2014; 125: 401-414.
- Pal P, Srivas PK, Dadhich P, Das B, Maulik D, Dhara S. Nano-/microfibrous cotton-wool-like 3D Scaffold with core-shell architecture by emulsion electrospinning for skin tissue regeneration. *ACS Biomater Sci Eng.* 2017; 3(12): 3563-3575.
- Barnes CP, Sell SA, Boland ED, Simpson DG, Bowlin GL. Nanofiber technology: designing the next generation of tissue engineering scaffolds. *Adv Drug Deliv Rev.* 2007; 59(14): 1413-1433.
- Li D, Sun H, Jiang L, Zhang K, Liu W, Zhu Y, et al. Enhanced biocompatibility of PLGA nanofibers with gelatin/nano-hydroxyapatite bone biomimetics incorporation. *ACS Appl Mater Interfaces.* 2014; 6(12): 9402-9410.
- Heydarkhan-Hagvall S, Schenke-Layland K, Dhanasopon AP, Rofail F, Smith H, Wu BM, et al. Three-dimensional electrospun ECM-based hybrid scaffolds for cardiovascular tissue engineering. *Biomaterials.* 2008; 29(19): 2907-2914.
- Amini F, Semnani D, Karbasi S, Banitaba SN. A novel bilayer drug-loaded wound dressing of PVDF and PHB/Chitosan nanofibers applicable for post-surgical ulcers. *Int J Polym Mater Polym Biomater.* 2019; 68(13): 772-777.
- Bazmandeh AZ, Mirzaei E, Fadaie M, Shirian S, Ghasemi Y. Dual spinneret electrospun nanofibrous/gel structure of chitosan-gelatin/chitosan-hyaluronic acid as a wound dressing: In-vitro and in-vivo studies. *Int J Biol Macromol.* 2020; 162: 359-373.
- Akbarzadeh M, Pezeshki-Modaress M, Zandi M. Biphasic, tough composite core/shell PCL/PVA-GEL nanofibers for biomedical application. *J Appl Polym Sci.* 2019;137(4): 1-12.
- Sadeghi-Avalshahr A, Nokhasteh S, Molavi AM, Khorsand-Ghayeni M, Mahdavi-Shahri M. Synthesis and characterization of collagen/ PLGA biodegradable skin scaffold fibers. *Regen Biomater.* 2017; 4(5): 309-314.
- Valente T, Ferreira JL, Henriques C, Borges JP, Silva JC. Polymer blending or fiber blending: A comparative study using chitosan and poly (ϵ -caprolactone) electrospun fibers. *J Appl Polym Sci.* 2019; 136(11): 47191.
- Wan YY, Wu H, Cao X, Jeson S. Compressive mechanical properties and biodegradability of porous poly (caprolactone)/chitosan scaffolds. *Polym Degrad Stab.* 2008; 93(10): 1736-1741.
- Prabhakaran MP, Venugopal JR, Chyan TT, Hai LB, Chan CK, Lim AY, et al. Electrospun biocomposite nanofibrous scaffolds for neural tissue engineering. *Tissue Eng Part A.* 2008; 14(11): 1787-1797.
- He Y, Wang W, Tang X, Liu X. Osteogenic induction of bone marrow mesenchymal cells on electrospun polycaprolactone/chitosan nanofibrous membrane. *Dent Mater J.* 2017; 36(3): 325-332.
- Torres-Giner S, Gimeno-Alcaniz JV, Ocio MJ, Lagaron JM. Comparative performance of electrospun collagen nanofibers cross-linked by means of different methods. *ACS Appl Mater Interfaces.* 2008; 1(1): 218-223.
- Zhong S, Teo WE, Zhu X, Beuerman R, Ramakrishna S, Yung LYL. Formation of collagen- glycosaminoglycan blended nanofibrous scaffolds and their biological properties. *Biomacromolecules.* 2005; 6(6): 2998-3004.
- Pezeshki M, Mojgan M, Rajabi S. Tailoring the gelatin/chitosan electrospun scaffold for application in skin tissue engineering : an in vitro study. *Prog Biomater.* 2018; 7(3): 207-218.
- Meghdadi M, Atyabi SM, Pezeshki-Modaress M, Irani S, Noormohammadi Z, Zandi M. Cold atmospheric plasma as a promising approach for gelatin immobilization on poly (ϵ -caprolactone) electrospun scaffolds. *Prog Biomater.* 2019; 8(2): 65-75.
- Zou XH, Jiang YZ, Zhang GR, Jin HM, Hieu TM, Ouyang HW. Specific interactions between human fibroblasts and particular chondroitin sulfate molecules for wound healing. *Acta Biomater.* 2009; 5(5): 1588-1595.
- Serrano MC, Nardecchia S, Garcia-Rama C, Ferrer ML, Collazos-Castro JE, del Monte F, et al. Chondroitin sulphate-based 3D scaffolds containing MWCNTs for nervous tissue repair. *Biomaterials.* 2014; 35(5): 1543-1551.
- Sharifi F, Irani S, Azadegan G, Pezeshki-Modaress M, Zandi M, Saeed M. Co-electrospun gelatin-chondroitin sulfate/polycaprolactone nanofibrous scaffolds for cartilage tissue engineering. *Bioact Carbohydrates Diet Fibre.* 2020; 22: 100215.
- Saeed M, Mirzadeh H, Zandi M, Irani S, Barzin J. Rationalization of specific structure formation in electrospinning process: Study on nano-fibrous PCL-and PLGA-based scaffolds. *J Biomed Mater Res Part A.* 2015; 103(12): 3927-3939.
- Zamanlui S, Mahmoudifard M, Soleimani M, Bakhshandeh B, Vasei M, Faghihi S. Enhanced chondrogenic differentiation of human bone marrow mesenchymal stem cells on PCL/PLGA electrospun with different alignments and compositions. *Int J Polym Mater Polym Biomater.* 2018; 67(1): 50-60.
- Honarpardaz A, Irani S, Pezeshki-Modaress M, Zandi M, Sadeghi A. Enhanced chondrogenic differentiation of bone marrow mesenchymal stem cells on gelatin/glycosaminoglycan electrospun nanofibers with different amount of glycosaminoglycan. *J Biomed Mater Res A.* 2019; 107(1): 38-48.
- Sadeghi A, Zandi M, Pezeshki-Modaress M, Rajabi S. Tough, hybrid chondroitin sulfate nanofibers as a promising scaffold for skin tissue engineering. *Int J Biol Macromol.* 2019; 132: 63-75.
- Shi Y, Ma L, Zhou J, Mao Z, Gao C. Collagen/chitosan-silicone membrane bilayer scaffold as a dermal equivalent. *Polym Adv Technol.* 2005; 16(11-12): 789-794.
- Mao JS, Zhao LG, Yin YJ, De Yao K. Structure and properties of

- bilayer chitosan–gelatin scaffolds. *Biomaterials*. 2003; 24(6): 1067-1074.
27. Mahboudi S, Pezeshki-Modaress M, Akbari Noghabi K. The study of fibroblast cell growth on the porous scaffold of gelatin–starch blend using the salt-leaching and lyophilization method. *Int J Polym Mater*. 2015; 64(12): 653-659.
 28. Norouzi M, Shabani I, Ahvaz HH, Soleimani M. PLGA/gelatin hybrid nanofibrous scaffolds encapsulating EGF for skin regeneration. *J Biomed Mater Res Part A*. 2015; 103(7): 2225-2235.
 29. Gautam S, Dinda AK, Mishra NC. Fabrication and characterization of PCL/gelatin composite nanofibrous scaffold for tissue engineering applications by electrospinning method. *Mater Sci Eng C Mater Biol Appl*. 2013; 33(3): 1228-1235.
 30. Lai JY, Li YT, Cho CH, Yu TC. Nanoscale modification of porous gelatin scaffolds with chondroitin sulfate for corneal stromal tissue engineering. *Int J Nanomedicine*. 2012; 7: 1101-1114.
 31. Sarkar S, Lightfoot-Vidal SE, Schauer CL, Vresilovic E, Marcolongo M. Terminal-end functionalization of chondroitin sulfate for the synthesis of biomimetic proteoglycans. *Carbohydr Polym*. 2012; 90(1): 431-440.
 32. Silva JM, Georgi N, Costa R, Sher P, Reis RL, Van Blitterswijk CA, et al. Nanostructured 3D constructs based on chitosan and chondroitin sulphate multilayers for cartilage tissue engineering. *PLoS One*. 2013; 8(2): e55451.
 33. Chong EJ, Phan TT, Lim IJ, Zhang YZ, Bay BH, Ramakrishna S, et al. Evaluation of electrospun PCL/gelatin nanofibrous scaffold for wound healing and layered dermal reconstitution. *Acta Biomater*. 2007; 3(3): 321-330.
 34. Khorshidi S, Solouk A, Mirzadeh H, Mazinani S, Lagaron JM, Sharifi S, et al. A review of key challenges of electrospun scaffolds for tissue-engineering applications. *J Tissue Eng Regen Med*. 2016; 10(9): 715-738.
 35. Chandrasekaran AR, Venugopal J, Sundarajan S, Ramakrishna S. Fabrication of a nanofibrous scaffold with improved bioactivity for culture of human dermal fibroblasts for skin regeneration. *Biomater*. 2011; 6(1): 15001.
 36. Jun I, Han HS, Edwards JR, Jeon H. Electrospun fibrous scaffolds for tissue engineering: Viewpoints on architecture and fabrication. *Int J Mol Sci*. 2018; 19(3): 745.
 37. Rnjak-kovacina J, Weiss AS. Increasing the pore size of electrospun scaffolds. *Tissue Eng Part B Rev*. 2011; 17(5): 365-372.
-

The Inhibitory Effect of Sulforaphane on The Proliferation of Acute Myeloid Leukemia Cell Lines through Controlling miR-181a

Mohsen Koolivand, M.Sc.¹, Maryam Ansari, M.Sc.^{2,3}, Soheila Moein, Ph.D.^{4*}, Masoomeh Afsa, M.D.³, Kianoosh Malekzadeh, Ph.D.^{2,4*}

1. Royan Stem Cell Technology Company, Tehran, Iran

2. Department of Medical Genetics, Faculty of Medicine, Hormozgan University of Medical Sciences, Bandar Abbas, Iran

3. Hormozgan Institute of Health, Hormozgan University of Medical Sciences, Bandar Abbas, Iran

4. Department of Biochemistry, Faculty of Medicine, Hormozgan University of Medical Sciences, Bandar Abbas, Hormozgan, Iran

*Corresponding Addresses: P.O.Box: 79196-93116, Department of Biochemistry, Faculty of Medicine, Hormozgan University of Medical Sciences, Bandar Abbas, Hormozgan, Iran

P.O.Box: 79196-93116, Department of Medical Genetics, Faculty of Medicine, Hormozgan University of Medical Sciences, Bandar Abbas, Iran
Emails: smoein@sums.ac.ir, kianoosh.malekzadeh@hums.ac.ir

Received: 17/March/2020, Accepted: 22/July/2020

Abstract

Objective: The present study investigated the role of miR-181a as a small non-coding RNA molecule in acute myeloid leukemia (AML) pathogenesis and reflected on the effects of Sulforaphane (SFN) on AML progression.

Materials and Methods: This experimental study had two parts. *In vivo* study, the miR-181a levels was measured in patients with symptoms of AML and compared to healthy controls (HCs) to investigate its role in AML pathogenesis. Afterward, an *in vitro* study was performed to examine the effects of SFN on the growth, apoptosis and proliferation rate of AML cell lines. Finally, the effect of SFN on miR-181a was evaluated as a major miRNA involved in hematopoiesis.

Results: The results of this study showed an increasing trend (2.9-fold, P=0.0019) in miR-181a expression levels in AML patients as compared with HCs. The data associated with MTT assay and flow cytometry (FCM) additionally demonstrated the anti-proliferative effects of SFN against AML cell lines, with a reduction in miR-181a levels. As well, no significant difference was noted between 24 hours and 48 hours treatments by SFN. It was deduced that modulation of miR-181a expression levels could be one of the mechanisms associated with the anti-proliferative effects of SFN against AML.

Conclusion: MiR-181a levels contribute to AML pathogenesis and thus they can be considered as a strategy in controlling AML progression in patients. Accordingly, SFN can arrest cell proliferation and induce apoptosis in AML cell lines through retardation expression of miR-181a and affecting miR-181a pathway, which already clarified its role in the differentiation of hematopoietic stem cells and indicates another mode of anti-cancer action of sulforaphane.

Keywords: Acute Myeloid Leukemia, miR-181a, Sulforaphane

Cell Journal (Yakhteh), Vol 24, No 1, January 2022, Pages: 44–50

Citation: Koolivand M, Ansari M, Moein S, Afsa M, Malekzadeh K. The inhibitory effect of sulforaphane on the proliferation of acute myeloid leukemia cell lines through controlling miR-181a. Cell J. 2022; 24(1): 44-50. doi: 10.22074/cellj.2022.7508.

This open-access article has been published under the terms of the Creative Commons Attribution Non-Commercial 3.0 (CC BY-NC 3.0).

Introduction

Acute myeloid leukemia (AML) is known as an invasive malignancy of the precursor cells of the blood (1-3). It is also the most common type of cancer resulting from genetic mutations, which can disturb differentiation and apoptosis (4, 5). Disturbance in molecular pathways as well as regulation by some biomarkers such as microRNAs (miRNAs), is thus one cause of this disease (6). These sections or transcripts are referred to as non-coding RNAs, with a length of 19-25 nucleotides, playing several roles in the cells produced by RNA polymerase II or III (7).

MiRNAs show different physiological behaviors and pathological conditions. In addition to tumor suppressor genes, oncogenes, and chromosomal changes, considered to be the main causes of cancer, miRNAs can also play a role in the cancer process (2, 8). Evidence suggests that miRNAs can be diagnostic and therapeutic biomarkers due to their role in pathogens. Studies have further demonstrated the key role of miR-181a in the maintenance

of cells and their pathological effects in hematopoietic neoplasms (9). Moreover, miR-181a can directly inhibit the differentiation of granulocytes and quasi-macrophages by protein kinase C delta (PRKCD), calcium/calmodulin-dependent protein kinase kinase 1 (CAMKK1), and CTD small phosphatase-like (CTDSPL) mRNAs. PRKCD is also required for phorbol myristate acetate (PMA) or all-trans retinoic acid (ATRA) induction for the differentiation of myeloid leukemia, and it is a regulator of p38 upstream, which can lead to the phosphorylation of p38 (10).

Today, with the growing use of natural antioxidant compounds, their beneficial effects are being examined by many clinical studies. In addition to the importance of auxiliary compounds (including antioxidants) in reducing chemotherapy side effects, they may be also important in cellular pathways and have an effective new role in cancer treatment strategies (11). Sulforaphane (SFN), as a natural antioxidant, is an alternative product derived from the metabolism of cabbage, and its photochemical activity is high (12). The anti-cancer effects of isothiocyanate

in cabbage are attributed to the N=C=S group. These vegetables are rich in SFN, and are respected as anti-cancer drugs (13).

SFN can reduce existing leukemia cells by arresting the G/M phase in the cell cycle and induction of apoptosis through escalating reactive oxygen species (ROS) and calcium ions (Ca^{2+}) as well as activating some caspase proteins (14). In addition, in previous studies, SFN has been reported to moderate the development and severity of AML by controlling some miRNAs by altering their expressions (2).

Some studies have further shown that SFN has various protective functions against cell damage and tumor processes (15). Overall, SFN has an inhibitory effect on the growth and development of tumors. In addition, SFN can affect the epigenetic control of some key cancer genes resulting in reducing the progression and recurrence of cancer and thus improve patient survival (16). Although many studies have investigated the anti-cancer activities of this antioxidant (17, 18), few investigations have so far examined the effects of SFN on leukemia cells and miRNA expression levels (2). The main objective of this study was to evaluate the effects of SFN on the expression levels of miR-181a in AML cell lines, and AML patients and healthy individuals. The results of the present study may illustrate a new function for the anti-cancer potential of SFN.

Materials and Methods

Human specimens

The experimental part of this research (*in vivo* study) was to evaluate the pathologically changes in level of miR-181a in AML patients. For this purpose, the blood samples of the cases infected with AML were gained from the Hematology and Oncology Department of Shahid Mohammadi Hospital based in the city of Bandar Abbas. The study was confirmed by the Ethics and Human Rights Committee affiliated with Hormozgan University of Medical Sciences (HUMS), Bandar Abbas, Iran (HUMS.REC.1394.84). The informed consent form was distributed and signed by all the subjects before their participation.

Cell-lines

Based on numerous previous studies and upon determining the features of each cell line (16), four well-known AML cell lines were selected for *in vitro* part of our study. The selected cell lines are mostly promyelocytes and poorly differentiated cells. The selected AML cell lines were U937 (AML-M4/M5 monoblasts) (NCBI code, C130), HL-60 (AML-M2 myeloblasts) (NCBI code, C217), NB-4 (AML-M3 promyelocytes) (NCBI code, C 515), and KG-1 (myeloblast or promyelocyte stage of maturation) (NCBI code, C119), obtained from Pasteur Institute of Iran (<http://pasteur.ac.ir>). Less than 12 hours after being obtained, each of the four cell lines was passaged in the Roswell Park Memorial Institute (RPMI)-1640 medium (Invitrogen, Germany), consisting of 10% fetal bovine serum (FBS, Gibco, Germany) and 1% penicillin-streptomycin (pen-strep) solution (Invitrogen, Germany), maintained at 95% humidity, a temperature of

37°C, and 5% carbon dioxide (CO_2). The growth rate was calculated in base of the No. of viable cells [$(\frac{\text{The No. of viable cells each time of measuring} \times 100}{\text{The No. of viable cells in previous measuring}}) - 100$] and stated in percentage.

Cell proliferation assay

The effects of D, L-SFN (S4441) on the proliferation of the AML cell lines were evaluated by MTT (3-(4,5-dimethylthiazol-2-yl) -2,5-diphenyltetrazolium bromide) (Sigma-Aldrich, USA) assay.

To perform the MTT assay, the number of U-937, NB-4, HL-60, as well as KG-1 cells were counted by a hemocytometer, and then they were cultured in a 96-well plate (U-937: 8000; NB-4: 20000; HL-60: 15000; KG-1: 10000 cells in base of IC_{50}), and incubated for 2 hours under standard conditions. According to previous studies (2, 19), 15, 30, 45, and 60 μM concentrations of SFN (Sigma-Aldrich, USA) were selected. However, the given doses were evaluated independently and their toxicity was assessed according to the half-maximal inhibitory concentration (IC_{50}) measurement. Then, the cells were treated with the selected SFN concentration for 24 and 48 hours. After incubation for 24 hours, 20 μl of MTT solution was added at the final concentration of 0.5 mg/ml to each well and incubated at 37°C for 4 hours (2). They were subsequently centrifuged for 10 minutes at 4000 g and the crystals formed were dissolved in 150 μl dimethyl sulfoxide (DMSO). Finally, absorption of each well was measured at 495 nm using a micro-plate reader (Anthos 2020, England).

RNA extraction

RNA was extracted from the blood samples with ZR Whole Blood RNA MiniPrep™ kit (ZYMO RESEARCH, Irvine, CA), and then exposed to miScript II RT Kit (Qiagen, Germany) to synthesize cDNA followed by a real-time polymerase chain reaction (RT-PCR) (miScript SYBR Green PCR kit from Qiagen, Germany). To determine the total RNA of the cell lines after an interval (24 hours and 48 hours), TriPure Isolation Reagent (Roche, Germany) kit was applied as per the manufacturer's instructions.

RNA quantity and quality analysis

A NanoDrop® ND-1000 Spectrophotometer (Thermo Scientific, Germany) was used to determine the purity and the quantity of RNA and cDNA. It should be noted that pure RNA has a photoconductivity ratio of 280/260, 1.9 to 2 times, which could refer to suitable purity of extracted total RNAs. To evaluate quality, the extracted RNAs were run on 1% agarose gel. The quality of the extracted RNA is considered acceptable when the gel had three bands of 28S, 18S, and 5S, and the intensity of 28S band was two times higher than that of the 18S band. All of the extracted samples had good quality in this research.

Real time-polymerase chain reaction

To detect the miR-181a expression levels in AML cell

lines, the entire extracted RNA of the cell lines and the patients were exposed to miScript II RT Kit (Qiagen, Germany) for cDNA synthesis. Then, 1 ng of this extracted RNA was used to prepare the reverse transcription reaction mixer with a volume of 20 μ l. The cDNA samples were subsequently stored at -20°C until use. The miR-181a and the RNU6 (as housekeeping) primers were also utilized from Qiagen (Cat.No. MS00008827 for miR-181a and MS00033740 for RNU6). RT-PCR was further used and the miScript SYBR® Green PCR Kit (Qiagen, Germany) was applied in accordance with the company's directions. Briefly, the RT-PCR program was as follows: the primary shock was at 95°C for 5 minutes accompanied by 40 cycles at 94°C for 15 s (denaturation), at 55°C for 30 s (annealing), and finally 70°C for 30 seconds (extension) (2). After amplification, the relationship between miR-181a expression levels was obtained by dividing the miR-181a mRNA values by the *U-6* gene mRNA values in each sample. Each experiment was repeated at least two times and done on three repeats for each time.

Apoptosis analysis

The fluorescein isothiocyanate (FITC) Annexin-V kit (Cat No. 640922, BioLegend, UK) was utilized to measure the effects of SFN on cell apoptosis. The two AML cell lines, KG-1 and HL-60, were evaluated after being treated with SFN.

The doses of SFN used in this study (15, 30, 45, and 60 μ M) were evaluated over two time intervals (24 hours and 48 hours). The cells were collected and suspended in 2 ml phosphate-buffered saline (PBS, Cat No. 10010049, Gibco, Thermo Fisher Scientific, Inc.). After that according to manufactures' instructions,

FITC (5 μ L), Annexin V (5 μ L), and 7-AAD (10 μ L) were added to cell suspension (900 μ l) in each tube, and incubated in the dark condition for 15 min at room temperature (25°C). Then, 300 μ l of the binding buffer was added to each tube, and analysis was performed by flow cytometry (FACS, Becton Dickinson, Franklin Lakes, NJ, USA). The Flow Jo software was used to analyze the data.

Statistical analysis

The IBM SPSS Statistics software (version 21, IMB, USA), Microsoft Excel software and GraphPad Prism-5 were used for statistical analyses and $P \leq 0.05$ were considered to be statistically significant. Kolmogorov-Smirnov test was applied to check data distribution and normality. Expression of miR-181a was evaluated by $2^{-\Delta\Delta C_t}$. Accordingly, Wilcoxon two-sample test, Mann-Whitney U test, and finally Student's t test were utilized for detecting significant differences between expression levels.

Results

Demographic results

The patients and the controls were matched in terms of gender, age, and ethnicity as much as possible (2) (Table 1).

Cytotoxic effects of SFN on various cell types

The effects of SFN on the growth rate were evaluated by incubation of AML cell lines with various its concentrations for 24 hours and 48 hours. Results were shown as changes in percentages as compared with non-treated cells (SFN concentration was zero), that were randomly assigned as 100% viability.

Table 1: Demographic characteristics of AML patients and HC groups

Variables	AML patient (n=25)	Healthy control (n=25)	P value
Age (Min-Max) (Y)	52.5 (\pm 22.51) (3-79)	52.4 (\pm 22.40) (4-77)	0.981
\leq 50	12 (48)	12 (48)	
$>$ 50	13(52)	13(52)	
Gender			0.642
Female	10 (40)	10 (40)	
Male	15 (60)	15 (60)	
% blast cells (Min-Max)	71.2% (\pm 20.8) (28-94)	0	
% Blast \leq 70	9 (36.0)	0	
% Blast $>$ 70	16 (64.0)	0	
AML stage			
M1	4 (16.0)	0	
M2	12 (48.0)	0	
M4	5 (20.0)	0	
M5	5 (20.0)	0	

Data are presented as mean \pm SD or n (%). AML; Acute myeloid leukemia and HC; Healthy control.

Quantification of the number of cells in all cell lines treated with SFN revealed that the cell viability decreased at higher concentrations of SFN in both tested time points (24 and 48 hours). The growth rate of the cell lines also declined in plates treated with SFN, indicating an inverse relationship between SFN concentration and the growth rate of the cells. The highest and the lowest number of living cells were observed at 15 and 60 μM SFN; respectively. The number of dead cells correspondingly increased as SFN concentration multiplied (Fig.1).

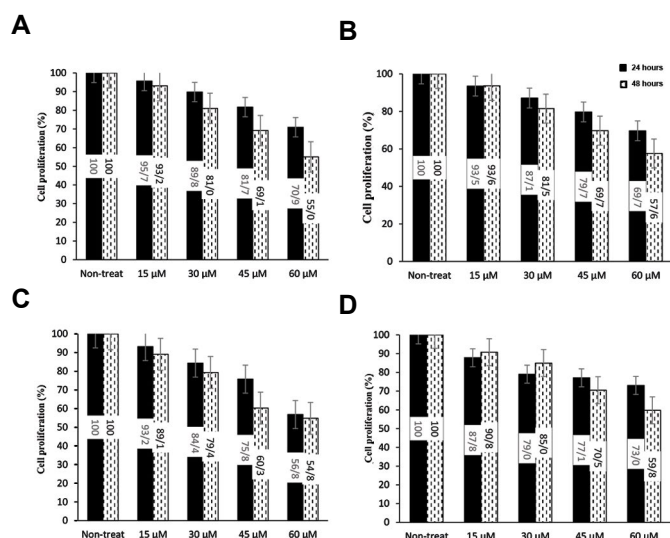


Fig.1: Effects of concentration and exposure duration of SFN on growth rates of AML cell lines. **A.** HL60, **B.** KG-1, **C.** U-937, and **D.** NB-4 were evaluated. Each datum was expressed as changes in the percentages of treated cells as compared with non-treated ones. The data were obtained from the number of viable cells based on the MTT assay. The Y-axis shows cell proliferation (changes in percentages of HC group). SFN; Sulforaphane, AML; Acute myeloid leukemia, and HC; Healthy controls.

Apoptosis assays of different SFN concentrations for KG-1 and HL-60 cell-lines

To evaluate the effects of SFN on inducing apoptosis, HL-60 and KG-1 cell lines (representing aggressive and mild AML cell lines, respectively) were treated with different SFN concentrations (15, 30, 45, and 60 μM) for 48 hours. The HC groups (non-treated cells) and cell lines treated with doxorubicin (DOX) (as an anti-cancerous apoptotic agent) were also considered as the negative and positive controls; respectively. The results showed that treatment of HL-60 and KG-1 cells with 60 μM of SFN could induce the highest apoptosis rate (17.9% and 46.6%, respectively), and the lowest apoptosis rate had similarly occurred when HL-60 (4.5%) and KG-1 cells (6.7%) were treated by 15 μM SFN.

Respectively, 12.3 and 5.6 % of cells were engaged in early and late apoptosis at the presence of 60 μM SFN. The lowest initial apoptosis rate (3%) was observed in the treatment with 15 and 30 μM SFN (Fig.2) in the KG-1 cell-

line. The apoptosis percentage at different doses of SFN demonstrated that the highest apoptosis rate appeared at a dose of 60 μM (46.6%), followed by 45, 30, and 15 μM , showing the highest apoptosis rate with ratios of 20.7%, 10.58%, and 6.59%; respectively. The highest early (26.3%) and late (20.3%) apoptosis rates also happened at 60 μM SFN, and the lowest early (4.7%) and late apoptosis (1.9%) rates were arisen at 15 μM SFN, respectively, for KG-1 cell-lines. The necrosis rate at the mentioned doses was roughly low. Increasing early apoptosis converged with rising doses of SFN in both HL-60 and KG-1 cell lines indicated the anti-proliferative effects of SFN.

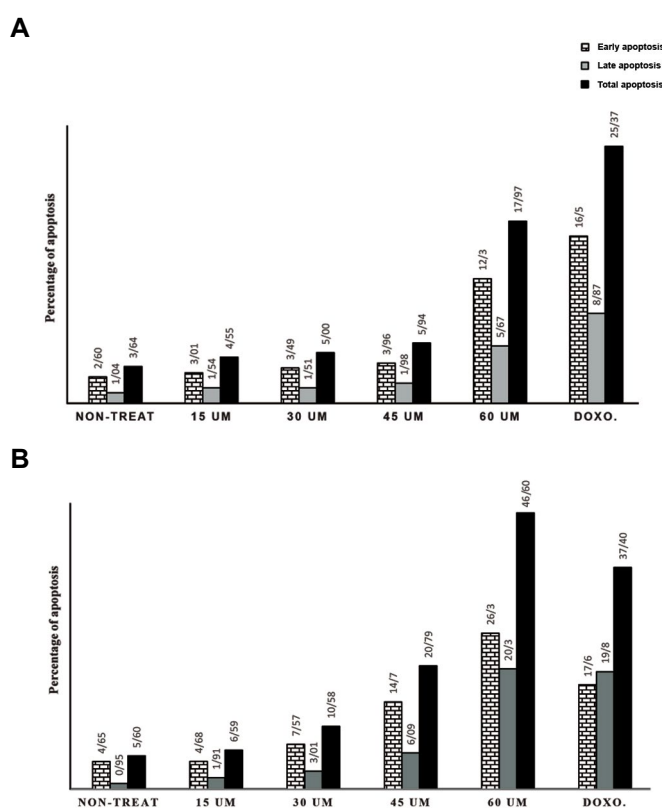


Fig.2: Effects of different concentrations of sulforaphane to induce apoptosis in cell lines after 48 hours treatment. The obtained data of flow-cytometry in cell lines **A.** HL60 and **B.** KG1 were shown.

Disruption of MiR-181a expression level in human samples

Comparison of miR-181a expression levels between patients and HC samples showed that miR-181a expression levels were considerably enhanced (Fig.3A) in the patients ($P=0.0019$). In the M1 stage of the disease, miR-181a expression level in the patient group were increased 2.21-fold and in the M2 stage, 2.9-fold that of the HC group, whereas, no significant changes were observed ($M4=0.94$ and $M5=1.03$) in higher stages in comparison with HCs. In other words, gene expression levels were more greatly increased in the first stages (*i.e.*, M1 and M2) than in the higher stages (namely, M3 and M4). This difference of changes in miR-181a expression levels between lower stages (M1 and M2) in comparison with higher stages

(M3 and M4) was significant ($P=0.0318$, Fig.3B).

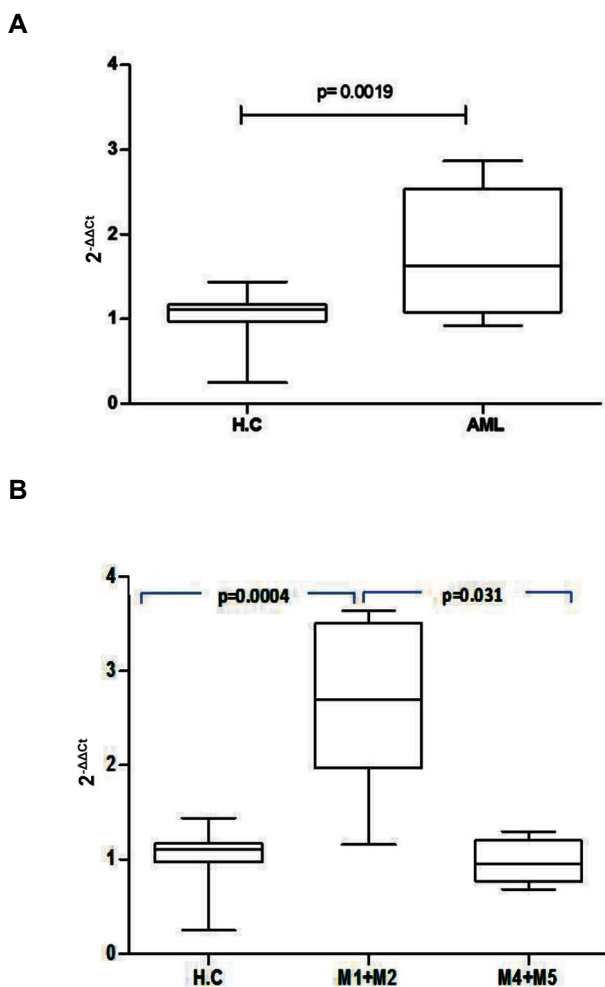


Fig.3: The level of miR-181a in blood of patients suffered from AML compared to HC. **A.** Comparison with AML patients and HCs and **B.** Comparison between lower sub-types (AML and M1+M2) and higher sub-types (AML and M3+M4). AML; Acute myeloid leukemia, HC; Healthy control, and M1-M4; Subtypes of acute myeloid leukemia 1 to 4.

Reduction of MiR-181a expression levels in different cell lines by increasing concentration and duration of treatment with SFN

Our data demonstrated that miR-181a expression levels significantly reduced in all treated cell lines compared with the untreated ones (Fig.4). The decline in miR-181a expression levels was also observed following a rise in SFN concentrations in the treated cells. Moreover, miR-181a expression levels gradually diminished during the 24 and 48 hours intervals, though the decline was much more pronounced at the end of the 24 hours period than the 48 hours. At the end of 24 hours, miR-181a expression levels decreased by 0.96-, 0.64-, and 0.41-folds in the HL-60 cell-lines treated with 15, 30, and 45 μM of SFN; respectively.

This pattern was 0.49-, 0.26-, and 0.06-folds for the KG-1 cell line; 0.66-, 0.46-, and 0.11-folds for the U-937

cell line; and 0.26-, 0.16-, and 0.12-folds for the NB4 cell line ($P<0.001$); respectively. The same descending trend in miR-181a expression level was further observed after 48h treatment with different concentrations of SFN, but no significant difference was notable between 24 and 48 hours treatments (Fig.4). At the end of the 48 hours treatment with 15, 30 and, 45 μM of SFN, the miR-181a expression levels decreased by 0.87-, 0.38-, and 0.11-folds for HL-60. As well the given levels reduced by 0.53-, 0.22-, and 0.03-folds for the KG1 cell line; 0.51-, 0.22-, and 0.09-folds for the U-937 cell line; and 0.31-, 0.21-, and 0.15-folds for the NB-4 cell-line; respectively ($P<0.001$, Fig.4).

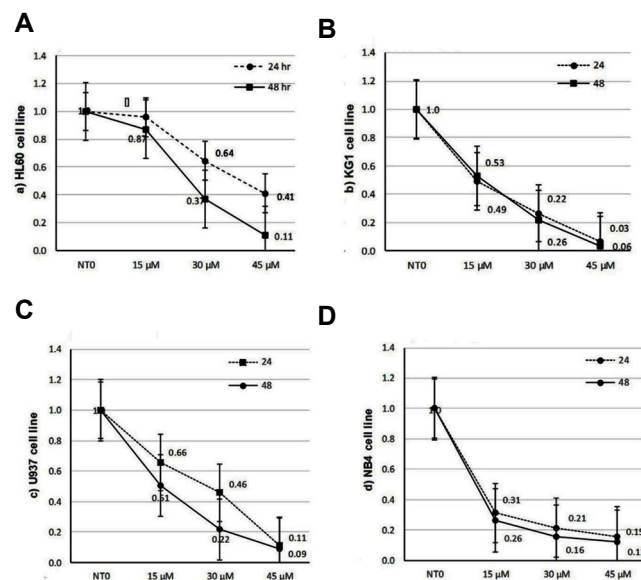


Fig.4: The level of miR-181a under 24 and 48 hours treatments with various SFN doses compared in all four studied AML cell lines **A.** HL60, **B.** KG-1, **C.** U-937 and **D.** NB-4. Y-axis represents relative expression ($2^{-\Delta\Delta\text{CT}}$). NT0; Zero concentration of SFN, SFN; Sulforaphane, and AML; Acute myeloid leukemia

Discussion

AML is caused by the accumulation of myeloid precursors in the bone marrow for a variety of reasons. In addition to recent routine treatments, some complementary therapies have been thus far suggested. Some of the advocated compounds are antioxidant-based supplements that may eliminate several side effects of chemical treatments. One of these compounds is the antioxidant SFN, whose effects have been studied in cancers including apoptosis, angiogenesis, and metastasis, chromatin structure and DNA stability, cell cycle and checkpoints, inflammation and oxidative stress, and cell signaling (20). Mechanisms associated with AML are still being debated.

MiRNAs can significantly contribute to AML and consequently control the differentiation of hematopoietic and tumor cells. On the other hand, any disturbance in their expression levels can cause hematopoietic malignancies, including AML (21-23). In this respect, Liu et al. (24) have revealed that miR-181a expression levels increased

in AML patients, accompanied by a rise in proliferation in AML cell lines as well as regulation of transition from stage S to G1 by this miRNA. It has been further shown that miR-181a leads to inhibition of macrophage-like and granulocyte differentiation in HL-60 cells (10). What has been reported in a previous study was the relationship between high expression levels of miR-181a and higher French-American-British (FAB) system percentage of AML M1/M2, higher blood blasts, and better treatment responses (25).

In the present research, miR-181a expression levels were first assessed *in vivo* and AML patients and HC samples. Our findings suggested that SFN has anti-cancer effects. In addition, a few investigations had been conducted on the effects of SFN on the expression levels. Therefore, the present study aimed to reflect on the effects of SFN on miR-181a expression levels in AML cell lines. According to this study, expression levels in patients with AML samples were significantly higher than those in HC.

The results of the present study were consistent with some previous studies (9, 26). Debernardi et al. (26) have highlighted an association between miR-181a and AML subtypes. Moreover, miR-181a expression levels were higher in AML-M1 or AML-M2 compared with samples with the above morphology, AML-M4 or AML-M5. The miR-181a expression levels were further high in AML subtypes. Nonetheless, overexpression of miR-181a in AML cells could lead to inhibition of cell growth and metabolic activity (9).

Here we showed that the antioxidant SFN increased mortality in AML cells and even apoptosis. Where the growth rate and the number of AML cells diminished as concentration and exposure time of SFN increased. Koolivand et al. (2) have previously reported that SFN use could reduce miRNA expression levels. They found that miR-155 expression levels could be dependent on SFN doses. In another study, Suppipat et al. (27) demonstrated that SFN in leukemic cells could initiate apoptosis and arrest of the cell cycle in G2/M by activating caspases (3, 8, and 9) and inactivating poly ADP-ribose polymerase (PARP). SFN has been also indicated to induce toxicity to HL-60 cells (28). Other studies also reported that SFN act as a potent compound to arrest cell-cycle and induce apoptosis in cancer cells and suggested its contributing factor to combination cancer therapy (29, 30).

In this study, significant pathological changes of miR-181a were observed in AML patients that is likely involved in AML progression. Increasing apoptosis of AML cell lines was also accompanied by decreasing miR-181a expression levels. Higher miR-181a expression levels were interestingly observed at the presence of higher concentration of SFN and longer exposure time to it.

It can be deduced that control of miR-181a expression levels is probably one of the goals associated with SFN use for its anti-proliferative effects against AML. Analyzing the anti-leukemia activity of miR-181a in AML, Huang et al. (31), have also found that suppressing miR-181a

expression levels by anti-miR-181a could activate certain pathways such as Kirsten rat sarcoma 2 viral oncogene homolog) gene (KRAS), NRAS proto-oncogene, GTPase (NRAS), and mitogen-activated protein kinase 1 (MAPK1). This property indicated that miR-181a had tumor-suppressing and oncogenic functions.

To conclude, our results show that miR-181a can be affected by SFN. It seems that SFN may have inhibitory effects on AML progression by altering miR-181a expression levels. However, further studies are needed in the future to estimate the contribution of the changes in miR-181a expression levels with relative improvements in AML patients' conditions.

Conclusion

MiR-181a can be suggested as a candidate prognostic marker for the evaluation of AML progression as well as the effectiveness of treatments. In this study, the anti-proliferative effects of SFN against AML cells were also observed, which converged with decreasing levels of miR-181a. Also, it seems that SFN induced its anti-cancer effects against AML cell lines through the miR-181a pathway involved in the differentiation of hematopoietic stem cells.

Acknowledgments

The authors express their appreciation to Hormozgan University of Medical Sciences (HUMS) for providing Grant No. 94-07-0480. This manuscript was based on the results of a Master's thesis fulfilled by Mohsen Koolivand. The authors hereby declared no conflict of interest.

Authors' Contributions

M.K.; Investigation, sample collection, Lab. work and experimental work, writing-original draft, and editing. M.A.; Sample collection, Lab. work and experimental work. S.M.; Supervision, data curation, and writing-original draft. M.A.; Data curation and writing-original draft. K.M.; Conceptualization, data curation and analyzing, investigation, project administration, supervision, writing-original draft, writing review and editing. All authors read and approved the final manuscript.

References

1. Estey E, Döhner H. Acute myeloid leukaemia. *Lancet*. 2006; 368(9550): 1894-1907.
2. Koolivand M, Ansari M, Piroozian F, Moein S, MalekZadeh K. Alleviating the progression of acute myeloid leukemia (AML) by sulforaphane through controlling miR-155 levels. *Mol Biol Rep*. 2018; 45(6): 2491-2499.
3. Yang X, Xu X, Liu Y, Gong A, Wang D, Liao X, et al. Advances in acute myeloid leukemia stem cells. *Advances in hematologic malignancies: IntechOpen*; 2019.
4. Koolivand M, Moein S, MalekZadeh K. The relationship of miR-181a expression level and AML: a systematic review protocol. *Int J Surg Protoc*. 2019; 13: 1-4.
5. Rubnitz JE, Gibson B, Smith FO. Acute myeloid leukemia. *Pediatr Clin North Am*. 2008; 55(1): 21-51, ix.
6. Hickey CJ, Schwind S, Radoska HS, Dorrance AM, Santhanam R, Mishra A, et al. Lenalidomide-mediated enhanced translation of

- C/EBP α -p30 protein up-regulates expression of the antileukemic microRNA-181a in acute myeloid leukemia. *Blood*. 2013; 121(1): 159-169.
7. Berindan-Neagoe I, Monroig Pdel C, Pasculli B, Calin GA. MicroRNAome genome: a treasure for cancer diagnosis and therapy. *CA Cancer J Clin*. 2014; 64(5): 311-336.
 8. Zhang B, Pan X, Cobb GP, Anderson TA. microRNAs as oncogenes and tumor suppressors. *Dev Biol*. 2007; 302(1): 1-12.
 9. Dahlhaus M, Schult C, Lange S, Freund M, Junghanss C. MicroRNA 181a influences the expression of HMGB1 and CD4 in acute Leukemias. *Anticancer Res*. 2013; 33(2): 445-452.
 10. Su R, Lin HS, Zhang XH, Yin XL, Ning HM, Liu B, et al. MiR-181 family: regulators of myeloid differentiation and acute myeloid leukemia as well as potential therapeutic targets. *Oncogene*. 2015; 34(25): 3226-3239.
 11. Mut-Salud N, Álvarez PJ, Garrido JM, Carrasco E, Aránega A, Rodríguez-Serrano F. Antioxidant intake and antitumor therapy: toward nutritional recommendations for optimal results. *Oxid Med Cell Longev*. 2016; 2016: 6719534.
 12. Amjad AI, Parikh RA, Appleman LJ, Hahm ER, Singh K, Singh SV. Broccoli-derived sulforaphane and chemoprevention of prostate cancer: from bench to bedside. *Curr Pharmacol Rep*. 2015; 1(6): 382-390.
 13. Singh SV, Singh K. Cancer chemoprevention with dietary isothiocyanates mature for clinical translational research. *Carcinogenesis*. 2012; 33(10): 1833-1842.
 14. Shang HS, Shih YL, Lee CH, Hsueh SC, Liu JY, Liao NC, et al. Sulforaphane-induced apoptosis in human leukemia HL-60 cells through extrinsic and intrinsic signal pathways and altering associated genes expression assayed by c DNA microarray. *Environ Toxicol*. 2017; 32(1): 311-328.
 15. Pham N-A, Jacobberger JW, Schimmer AD, Cao P, Gronda M, Hedley DW. The dietary isothiocyanate sulforaphane targets pathways of apoptosis, cell cycle arrest, and oxidative stress in human pancreatic cancer cells and inhibits tumor growth in severe combined immunodeficient mice. *Mol Cancer Ther*. 2004; 3(10): 1239-1248.
 16. Jiang X, Liu Y, Ma L, Ji R, Qu Y, Xin Y, et al. Chemopreventive activity of sulforaphane. *Drug Des Devel Ther*. 2018; 12: 2905-2913.
 17. Burnett JP, Lim G, Li Y, Shah RB, Lim R, Paholak HJ, et al. Sulforaphane enhances the anticancer activity of taxanes against triple negative breast cancer by killing cancer stem cells. *Cancer Lett*. 2017; 394: 52-64.
 18. Mielczarek L, Krug P, Mazur M, Milczarek M, Chilmonczyk Z, Wiktorska K. In the triple-negative breast cancer MDA-MB-231 cell line, sulforaphane enhances the intracellular accumulation and anticancer action of doxorubicin encapsulated in liposomes. *Int J Pharm*. 2019; 558: 311-318.
 19. Wu S, Zhou Y, Yang G, Tian H, Geng Y, Hu Y, et al. Sulforaphane-cysteine induces apoptosis by sustained activation of ERK1/2 and caspase 3 in human glioblastoma U373MG and U87MG cells. *Oncol Rep*. 2017; 37(5): 2829-2838.
 20. Jabbarzadeh Kaboli P, Afzalipour Khoshkbejari M, Mohammadi M, Abiri A, Mokhtarian R, Vazifemand R, et al. Targets and mechanisms of sulforaphane derivatives obtained from cruciferous plants with special focus on breast cancer—contradictory effects and future perspectives. *Biomed Pharmacother*. 2020; 121: 109635.
 21. Liao Q, Wang B, Li X, Jiang G. miRNAs in acute myeloid leukemia. *Oncotarget*. 2017; 8(2): 3666-3682.
 22. Gaur V, Chaudhary S, Tyagi A, Agarwal S, Sharawat SK, Sarkar S, et al. Dysregulation of miRNA expression and their prognostic significance in paediatric cytogenetically normal acute myeloid leukaemia. *Br J Haematol*. 2020; 188(6): e90-e94.
 23. Mafra ACP, Calin GA. MicroRNAs in haematological diseases. In Peplow PV, Martinez B, Calin GA, Esquela-Kerscher A, editors. *MicroRNAs in diseases and disorders: emerging therapeutic targets*. UK: Royal Society of Chemistry; 2019; 293-322.
 24. Liu X, Liao W, Peng H, Luo X, Luo Z, Jiang H, et al. miR-181a promotes G1/S transition and cell proliferation in pediatric acute myeloid leukemia by targeting ATM. *J Cancer Res Clin Oncol*. 2016; 142(1): 77-87.
 25. Schwind S, Marcucci G, Maharry K, Radmacher MD, Whitman SP, Paschka P, et al. MicroRNA 181a (miR-181a) expression as a prognosticator in cytogenetically normal acute myeloid leukemia (CN AML). *J Clin Oncol*. 2009; 27 (15 suppl): 7001.
 26. Debernardi S, Skoulakis S, Molloy G, Chaplin T, Dixon-McIver A, Young BD. MicroRNA miR-181a correlates with morphological sub-class of acute myeloid leukaemia and the expression of its target genes in global genome-wide analysis. *Leukemia*. 2007; 21(5): 912-916.
 27. Suppipat K, Park CS, Shen Y, Zhu X, Lacorazza HD. Sulforaphane induces cell cycle arrest and apoptosis in acute lymphoblastic leukemia cells. *PLoS One*. 2012; 7(12): e51251.
 28. Lehner K, Feliciano O, O'Donnell RW. Using carboxyfluorescein succinimidyl ester (CFSE) to measure the effects of sulforaphane on cell division in a human leukemia cell line. *FASEB J*. 2013; 27 Suppl 1: 1028.
 29. Chen H, Landen CN, Li Y, Alvarez RD, Tollefsbol TO. Epigallocatechin gallate and sulforaphane combination treatment induce apoptosis in paclitaxel-resistant ovarian cancer cells through hTERT and Bcl-2 down-regulation. *Exp Cell Res*. 2013; 319(5): 697-706.
 30. Choi YH. ROS-mediated activation of AMPK plays a critical role in sulforaphane-induced apoptosis and mitotic arrest in AGS human gastric cancer cells. *Gen Physiol Biophys*. 2018; 37(2): 129-140.
 31. Huang X, Schwind S, Santhanam R, Eisfeld AK, Chiang CL, Lankenau M, et al. Targeting the RAS/MAPK pathway with miR-181a in acute myeloid leukemia. *Oncotarget*. 2016; 7(37): 59273-59286.

Akt1 Decreases Gcn5 Protein Stability through Regulating The Ubiquitin-Proteasome Pathway in Mouse Embryonic Fibroblasts

Da Som Jeong, B.Sc.^{1,2}, Yu Cheon Kim, B.Sc.^{1,2}, Ji Hoon Oh, Ph.D.^{1*}, Myoung Hee Kim, Ph.D.^{1*}

1. Department of Anatomy, Embryology Laboratory, Yonsei University College of Medicine, Seoul, Korea
2. Brain Korea 21 PLUS Project for Medical Science, Yonsei University College of Medicine, Seoul, Korea

*Corresponding Address: Department of Anatomy, Embryology Laboratory, Yonsei University College of Medicine, Seoul, Korea
Emails: rednovember@yuhs.ac, mhkim1@yuhs.ac

Received: 02/February/2021, Accepted: 2/May/2021

Abstract

General control non-derepressible 5 (Gcn5) is a member of histone acetyltransferase (HAT) that plays key roles during embryogenesis as well as in the development of various human cancers. Gcn5, an epigenetic regulator of *Hoxc11*, has been reported to be negatively regulated by Akt1 in the mouse embryonic fibroblasts (MEFs). However, the exact mechanism by which Akt1 regulates Gcn5 is not well understood. Using protein stability chase assay, we observed that Gcn5 is negatively regulated by Akt1 at the post-translational level in MEFs. The stability of Gcn5 protein is determined by the competitive binding with the protein partner that interacts with Gcn5. The interaction of Gcn5 and Cul4a-Ddb1 complex predominates and promotes ubiquitination of Gcn5 in the wild-type MEFs. On the other hand, in the Akt1-null MEFs, the interaction of Gcn5 and And-1 inhibits binding of Gcn5 and Cul4a-Ddb1 E3 ubiquitin ligase complex, thereby increasing the stability of the Gcn5 protein. Taken together, our study indicates that Akt1 negatively controls Gcn5 via the proteasomal degradation pathway, suggesting a potential mechanism that regulates the expression of *Hox* genes.

Keywords: Akt1, Gcn5, Proteasome Endopeptidase Complex, Ubiquitin

Cell Journal(yakhteh), Vol 24, No 1, January 2022, Pages: 51-54

Citation: Jeong DS, Kim YC, Oh JH, Kim MH. Akt1 decreases Gcn5 protein stability through regulating the ubiquitin-proteasome pathway in mouse embryonic fibroblasts. Cell J. 2022; 24(1): 51-54. doi: 10.22074/cellj.2022.7961.

This open-access article has been published under the terms of the Creative Commons Attribution Non-Commercial 3.0 (CC BY-NC 3.0).

The *Hox* genes are transcription factors that have a pivotal role in the anteroposterior axis determining during embryogenesis (1, 2). In addition, *Hox* genes are expressed in adult tissues and abnormal expression of those genes is associated with the development, progression, and metastasis of various cancers (3-5). This means that the expression of *Hox* genes should be precisely controlled in a specific spatiotemporal manner. Dynamic gene expression regulation is achieved by epigenetic changes by various histone modifying and chromatin remodeling enzymes, such as histone deacetylase (HDAC) and acetyltransferase (HAT) (6-8). General control non-derepressible 5 (Gcn5) is a member of the GCN5-related N-acetyltransferase (*GNAT*) superfamily of HAT (9). Histone acetylation by Gcn5, along with other types of histone modifications, has been reported as an important epigenetic factor regulating *Hox* gene expression during embryonic development (10).

Akt, a serine/threonine kinase, is required to regulate various biological responses (11). Interestingly, we have previously identified Akt1 as a *Hox* modulator (12, 13). Along with a long history of research on Akt, recent epigenetic studies have unveiled novel Akt substrates such as p300, EZH2, and BMI1, indicating a critical role of Akt in regulating epigenetic processes (14). According to our previous results, Gcn5 also binds directly to Akt1 and the protein level of Gcn5 is dependent on whether Akt1 is expressed (15, 16). This strongly suggests the Akt1 functions as a Gcn5 regulator, but the precise mechanism of this action has not yet been elucidated.

Therefore, we conducted a follow-up study to find out how Akt1 regulates the protein stability of Gcn5 in the mouse embryonic fibroblasts (MEFs). We observed that degradation of Gcn5 is mediated by Cul4a-Ddb1 E3 ligase complex, which is regulated by Akt1 expression. These results help us to understand how Akt1 and Gcn5 regulate *Hox* gene expression during embryonic development. Revealing that Akt1 acts as an epigenetic regulator of *Hox* gene expression further implicates a possible mechanism how PI3K/Akt pathway, which plays an important role in cancer, can affect the regulation of *HOX* gene expression in various human cancers.

The wild-type MEFs and Akt1-null MEFs were generated as described previously (17, 18). For preparation of embryonic fibroblast cells, embryos were dissected to remove the head and other viscera. Remaining tissues were finely minced and washed with phosphate buffered saline (PBS). Then, cells were trypsinized (LS 015-10, WelGENE Inc., Daegu, Korea) and plated in the Dulbecco's modified Eagle's medium (DMEM, LS 001-05, WelGENE Inc., Daegu, Korea) which is containing 10% fetal bovine serum (S 001-01, WelGENE Inc., Daegu, Korea) and 1% of penicillin-streptomycin (LS 203-01, WelGENE Inc., Daegu, Korea). The Akt1-null MEFs were generated to have neomycin insertion between exon 3 and exon 8 by homologous recombination. The procedure for preparation of Akt1-null MEFs are same as wild-type MEFs. Cells were grown in a humidified incubator of 5% CO₂ at 37°C.

For Western blotting, cell lysates were extracted using NP40 and protein contents were determined using the Pierce BCA Protein Assay Kit (23227, Thermo Scientific, Rockford, IL, USA). Protein samples were run on the 8-10% sodium dodecyl sulfate (SDS) poly-acrylamide gel, immobilized onto PVDF transfer membranes (IPVH00010, Bio-Rad, Hercules, CA, USA), and probed with appropriate antibodies. Anti-Gcn5I2 (#3305, Cell Signaling Technology, Danvers, MA, USA), anti-Akt1 (#2938, Cell Signaling Technology), anti-Cul4a (A300-739A, Bethyl, Montgomery, Texas, USA), anti-Ddb-1 (A300-462A, Sigma, St. Louis, MO, USA), anti-And1 (630301, BioLegend, San Diego, CA, USA), anti-Ubiquitin (#3936, Abcam, Cambridge, UK), and anti- β -actin (ab6276, Abcam, Cambridge, UK) were used to detect each protein.

Coimmunoprecipitation (Co-IP) assay, harvested cells were lysed with NP40 lysis buffer, containing protease inhibitor cocktail (11697498001, Roche, Darmstadt, Germany). The lysate was precleared with Protein A/G plus-agarose beads (sc-2003, Santa Cruz Biotechnology, Dallas, TX, USA) for 1 hour at 4°C. Anti-Gcn5 (A-11) (sc-365321, Santa Cruz Biotechnology) primary antibody or normal IgG (sc-2025, Santa Cruz Biotechnology, Dallas, TX, USA) was incubated at 4°C for overnight with gentle rotation. The following day, target protein-antibody complexes were precipitated with Protein A/G plus-agarose beads for 3 hours. Target complexes were detached from the Protein A/G plus-agarose beads by heating at 95°C for 5 minutes. Protein samples were resolved by SDS-PAGE and used for immunoblotting.

Using Trizol reagent (15596018, Invitrogen, Carlsbad, CA, USA), total RNA was isolated from wild-type MEFs and Akt1^{-/-} MEFs. Reverse transcription was conducted to synthesize cDNA with RNA (2 μ g) using ImProm-II™ Reverse Transcriptase. Quantitative PCR was carried out using StepOnePlus™ Real-Time PCR System (4376600, Applied Biosystems, Foster City, CA, USA) and Power SYBR Green PCR Master Mix (4367659, Applied Biosystems, Foster City, CA, USA). Quantitative real-time PCR results were analyzed by comparative cycle threshold (Ct) values and relative expression levels for target genes were normalized to that of β -actin. Primers for quantitative polymerase chain reaction (qPCR) were as follows: Mouse

Gcn5-F: 5'-ATTCCTGTCCATGCTTGAGG-3'
R: 5'-TCCAGGGTCAGGTTCTCAGG-3' (195 bp)

β -actin-F: 5'-CATGTTGAGACCTTCAACACCCC-3'
R: 5'-GCCATCTCCTGCTCGAAGTCTAG-3' (318 bp)

For protein stability chase assay, wild-type MEFs and Akt1-null MEFs were treated with cycloheximide (CHX; 66-81-9, Sigma, St. Louis, MO, USA) at a concentration of 10 μ g/ml for 1 to 8 hours or MG132 (1211877-36-9,

Sigma, St. Louis, MO, USA) at a concentration of 20 μ g/ml for 2 hours, followed by cell lysates isolation for western blot analysis. Quantification of protein bands was performed by using the ImageJ software v.1.8.0 (Wisconsin, U.S) according to the manufacturer's instructions and the measured values were displayed as a bar graph.

Data are represented as the mean values with the standard error of the mean (SEM). Statistically significant differences were determined by Student's t test. P<0.05 was considered statistically significant.

The *Gcn5* gene expression level was not significantly different between wild-type MEFs and Akt1-null MEFs, while the protein level was increased in the Akt1-null MEFs than in wild-type MEFs (Fig.1A, B). In addition, the results of the CHX (an inhibitor of de novo protein synthesis) chase assay showed that the Gcn5 protein half-life was about 4 hours in wild-type MEFs, whereas Gcn5 was stable for more than 8 hours in the Akt1-null MEFs (Fig.1C). Western blotting results of the CHX chase experiment were quantified (Fig.1D). These data suggest that Akt1 may deteriorate Gcn5 protein stability in the MEFs.

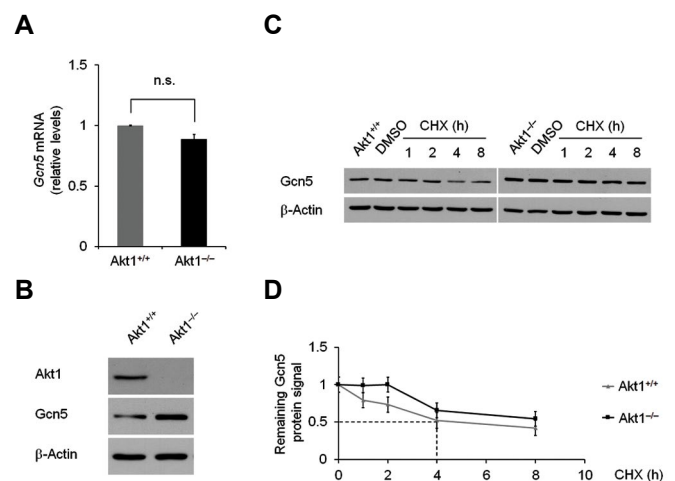


Fig.1: Gcn5 is post-translationally down-regulated by Akt1 in the MEFs. **A.** Real-time qPCR analysis for *Gcn5* transcription level detection in the wild-type and Akt1-null MEFs (P=0.0658). **B.** Western blotting analysis for detection of Gcn5 protein level in the wild-type and Akt1-null MEFs. Mouse β -actin was used as an internal control. **C.** Western blotting analysis of Gcn5 in the wild-type and Akt1-null MEFs after 10 μ g/ml of cycloheximide treatment for 1, 2, 4, and 8 hours for Gcn5 protein stability. DMSO was used as a negative control. **D.** Quantification of immunoblotting results of cycloheximide chase which is calculated by using Image J software. MEFs; Mouse embryonic fibroblasts, qPCR; Quantitative polymerase chain reaction, DMSO; Dimethyl sulfoxide, and n.s.; Not significant.

To demonstrate that the degradation of Gcn5 occurs via the ubiquitin/proteasome pathway, we examined the effects of the proteasome inhibitor MG132 in the MEF cells. The stability of endogenous Gcn5 protein of wild-type MEFs was recovered by MG132 treatment (Fig.2). These results showed that the level of Gcn5 protein in the MEFs is controlled at the post-translational level through the ubiquitin/proteasome

pathway and Akt1 is involved in this process.

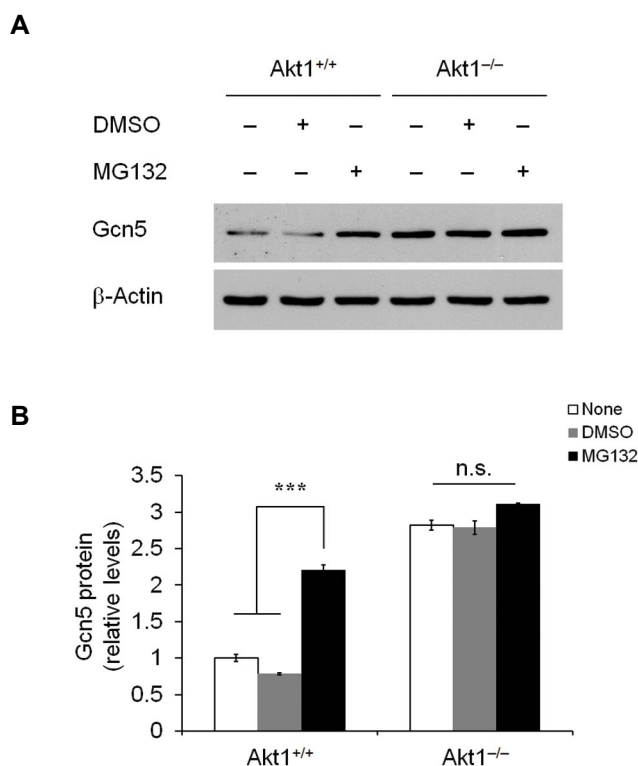


Fig.2: Gcn5 proteins are degraded in a proteasome-dependent manner in the MEFs. **A.** Western blotting analysis of Gcn5 in wild-type and Akt1-null MEFs after 20 μ M of MG132 treatment for 2 hours for Gcn5 protein stability. DMSO was used as a negative control. **B.** Quantification of immunoblotting results of MG132 treatment which is measured by using Image J software. ***; $P=7.28E-06$, n.s.; Not significant, MEFs; Mouse embryonic fibroblasts, and DMSO; Dimethyl sulfoxide.

Cul4a mediates ubiquitination and degradation of specific substrates by constructing complexes with Ddb1 and ubiquitin ligase E3 (19). And-1, an HMG domain-containing protein, is known as a factor that associates with the Gcn5 protein stability in the cancer cells. So, we hypothesized that these protein complexes would be involved in the Gcn5 protein stability regulation in the MEFs. To figure out this hypothesis, we first examined the protein level of this complex in the MEF cells, wild-type and Akt1-null MEFs. The protein level of Cul4a-Ddb1 E3 ubiquitin ligase was decreased in the Akt1-null MEFs than the wild-type MEFs. Conversely, the And-1 was found to be elevated in the Akt1-null MEFs in compared with the wild-type MEFs (Fig.3A). Next, we performed co-immunoprecipitation experiments with anti-Gcn5 antibody to identify protein interactions between Gcn5 and these complexes in the wild-type and Akt1-null MEFs. The interaction between Gcn5 and Cul4a-Ddb1 complex was stronger than the wild-type MEFs in comparison with the Akt1-null MEFs. On the other hand, the interaction of Gcn5 with And-1 was inversely related to the Cul4a-Ddb1 complex. More interestingly, the ubiquitination of Gcn5 was only observed in the Akt1 wild-type MEFs, suggesting rapid Gcn5 protein degradation (Fig.3B).

These observations demonstrated that And-1 contributes to Gcn5 protein stability via blocking the binding of Gcn5/Cul4a-Ddb1 complexes in the MEFs and is consistent with the previous report (20).

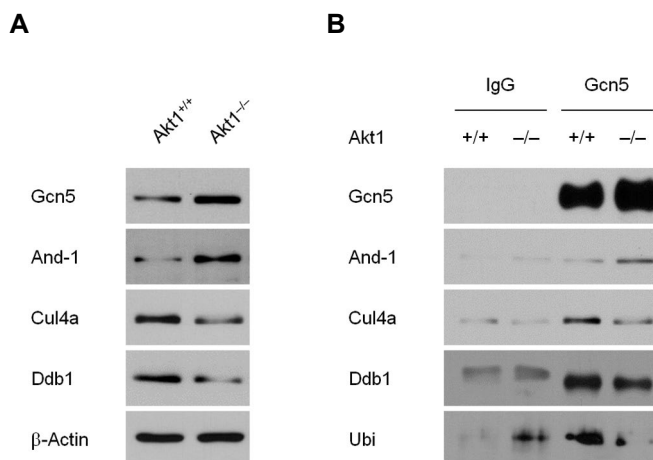


Fig.3: Degradation of Gcn5 protein is mediated by Cul4a-Ddb1 E3 ligase complex in the mouse embryonic fibroblasts (MEFs). **A.** The protein levels of Cul4a-Ddb1 E3 ubiquitin ligases and And-1 in the wild-type and Akt1-null MEFs. **B.** Co-immunoprecipitation of Gcn5 and Cul4a-Ddb1 E3 ubiquitin ligases in the wild-type and Akt1-null MEFs.

Recently, AKT has been shown to be directly involved in the ubiquitin-specific protease 4 (USP4) phosphorylation (21, 22). Zhang et al. (22) reported that USP4 contained the AKT consensus RXXXXpT phosphorylated site at Ser 445 through sequencing analysis. AKT-mediated phosphorylation of this motif resulted in increased USP4 stability and deubiquitylating enzymatic activity and also, relocated nuclear USP4 to the cytoplasm. On the other hand, previous reports revealed that phosphorylation on RXXXXpS/T Akt consensus motifs by Akt reduces HAT activity (23). More specifically, our previous study showed that mouse Gcn5 contains Akt consensus sequences [one RXXXXpS/T and several RXXpS/T sites] (15). Given these results, further investigation of phosphorylation may affect the Gcn5 protein regulation with Akt1 is suggested. In order to fully understand, Gcn5 regulation mechanism by Akt1 under specific conditions and its effect on downstream genes is important.

In conclusion, our data demonstrate the mechanism by which Akt1 regulates Gcn5 stability through the ubiquitin-proteasome pathway in MEFs.

Acknowledgements

This work was financially supported by the Brain Korea 21 PLUS Project for Medical Science, Yonsei University; the Basic Science Research Program through the National Research Foundation (NRF) funded by the Ministry of Education, Science, and Technology (2019R1I1A1A01050780 and 2016R1A2B2011821). There is no conflict of interest in this study.

Authors' Contributions

D.S.J., J.H.O.; Experiments design, data analysis, and manuscript writing. D.S.J., Y.C.K.; *In vitro* studies performance. J.H.O., M.H.K.; Study management, supervision, and manuscript finalization. All authors discussed the results and commented on the manuscript and approved the final version.

References

- Mallo M. Reassessing the role of Hox genes during vertebrate development and evolution. *Trends Genet.* 2018; 34(3): 209-217.
- Saito S, Suzuki T. How do signaling and transcription factors regulate both axis elongation and Hox gene expression along the anteroposterior axis? *Dev Growth Differ.* 2020; 62(5): 363-375.
- Li B, Huang Q, Wei GH. The role of HOX transcription factors in cancer predisposition and progression. *Cancers (Basel).* 2019; 11(4): 528.
- Luo Z, Rhee SK, Farnham PJ. The enigmatic HOX genes: can we crack their code? *Cancers (Basel).* 2019; 11(3): 323.
- Shah N, Sukumar S. The Hox genes and their roles in oncogenesis. *Nat Rev Cancer.* 2010; 10(5): 361-371.
- Javaid N, Choi S. Acetylation- and methylation-related epigenetic proteins in the context of their targets. *Genes (Basel).* 2017; 8(8): 196.
- Neganova ME, Klochov SG, Aleksandrova YR, Aliev G. Histone modifications in epigenetic regulation of cancer: perspectives and achieved progress. *Semin Cancer Biol.* 2020; S1044-579X(20)30176-0.
- Palli SR. Epigenetic regulation of post-embryonic development. *Curr Opin Insect Sci.* 2021; 43: 63-69.
- Salah Ud-Din AI, Tikhomirova A, Roujeinikova A. Structure and functional diversity of GCN5-related n-acetyltransferases (GNAT). *Int J Mol Sci.* 2016; 17(7): 1018.
- Lin W, Zhang Z, Chen CH, Behringer RR, Dent SY. Proper Gcn5 histone acetyltransferase expression is required for normal anteroposterior patterning of the mouse skeleton. *Dev Growth Differ.* 2008; 50(5): 321-330.
- Manning BD, Toker A. AKT/PKB signaling: navigating the network. *Cell.* 2017; 169(3): 381-405.
- Kong KA, Lee JY, Oh JH, Lee Y, Kim MH. Akt1 mediates the posterior Hoxc gene expression through epigenetic modifications in mouse embryonic fibroblasts. *Biochim Biophys Acta.* 2014; 1839(9): 793-799.
- Kong KA, Yoon H, Kim MH. Akt1 as a putative regulator of Hox genes. *Gene.* 2013; 513(2): 287-291.
- Molina-Serrano D, Kyriakou D, Kirmizis A. Histone modifications as an intersection between diet and longevity. *Front Genet.* 2019; 10: 192.
- Oh JH, Lee Y, Kong KA, Kim MH. Direct interaction between Akt1 and Gcn5 and its plausible function on hox gene expression in mouse embryonic fibroblast cells. *Biomed Sci Lett.* 2013; 19(3): 266-269.
- Lee YR, Oh JH, Kong KA, Kim MH. Post-transcriptional regulation of Gcn5, a putative regulator of Hox in mouse embryonic fibroblast cells. *Biomed Sci Lett.* 2012; 18(2): 165-168.
- Bae SS, Cho H, Mu J, Birnbaum MJ. Isoform-specific regulation of insulin-dependent glucose uptake by Akt/protein kinase B. *J Biol Chem.* 2003; 278(49): 49530-49536.
- Cho H, Thorvaldsen JL, Chu Q, Feng F, Birnbaum MJ. Akt1/PKB α is required for normal growth but dispensable for maintenance of glucose homeostasis in mice. *J Biol Chem.* 2001; 276(42): 38349-38352.
- Pan Y, Wang B, Yang X, Bai F, Xu Q, Li X, et al. CUL4A facilitates hepatocarcinogenesis by promoting cell cycle progression and epithelial-mesenchymal transition. *Sci Rep.* 2015; 5: 17006.
- Li Y, Jaramillo-Lambert AN, Yang Y, Williams R, Lee NH, Zhu W. And-1 is required for the stability of histone acetyltransferase Gcn5. *Oncogene.* 2012; 31(5): 643-652.
- Hu B, Zhang D, Zhao K, Wang Y, Pei L, Fu Q, et al. Spotlight on USP4: structure, function, and regulation. *Front Cell Dev Biol.* 2021; 9: 595159.
- Zhang L, Zhou F, Drabsch Y, Gao R, Snaar-Jagalska BE, Mickanin C, et al. USP4 is regulated by AKT phosphorylation and directly deubiquitylates TGF- β type I receptor. *Nat Cell Biol.* 2012; 14(7): 717-726.
- Liu Y, Xing ZB, Zhang JH, Fang Y. Akt kinase targets the association of CBP with histone H3 to regulate the acetylation of lysine K18. *FEBS Lett.* 2013; 587(7): 847-853.